ANALYTICAL AND EXPERIMENTAL STUDY OF

CONCENTRICALLY BRACED FRAMES WITH ZIPPER STRUTS

A Dissertation
Presented to
The Academic Faculty

by

Chuang-Sheng Yang

In Partial Fulfillment
of the Requirements for the Degree
Doctor of Philosophy in the
School of Civil and Environmental Engineering

Georgia Institute of Technology
December 2006

ANALYTICAL AND EXPERIMENTAL STUDY OF

CONCENTRICALLY BRACED FRAMES WITH ZIPPER STRUTS

Approved by:

Dr. Roberto T. Leon, Advisor
School of Civil and Environmental Engineering
Georgia Institute of Technology

Dr. Reginald DesRoches, Co-Advisor
School of Civil and Environmental Engineering
Georgia Institute of Technology

Dr. Abdul Hamid Zureick
School of Civil and Environmental Engineering
Georgia Institute of Technology

Dr. Don White
School of Civil and Environmental Engineering
Georgia Institute of Technology

Dr. James I. Craig
School of Aerospace Engineering
Georgia Institute of Technology

Date Approved: August 29, 2006

ACKNOWLEDGEMENTS

The author would like to express his sincere gratitude to his advisor Dr. Roberto T. Leon for his continuous guidance and encouragement throughout this study. His invaluable support and care made possible the completion of this study. It has been a real pleasure and privilege to work with him. Appreciation is also extended to his co-advisor Dr. Reginald DesRoches for his guidance, technical expertise, and continuous support throughout this research. The author is indebted to them for the education, direction, and example they have provided, and looks forward to a continued relationship with them in the future. The assistance provided by the dissertation advisory committee is also gratefully acknowledged. Thank you Dr. Abdul Hamid Zureick, Dr. Don White, and Dr. James Craig.

The author would like to extend his sincere appreciation to his good friends and colleagues, Tony Yang, Macarena Schachter, and Andreas Stavridis for their invaluable contributions throughout all phases of this research. The laboratory assistance of John Bunya, Murat Engendinez, Jason McCormick, and Tiziano Perea is gratefully acknowledged. The author would also like to acknowledge Dr. Andrei Reinhorn (University at Buffalo), Dr. B. Stojadinovic (University of California at Berkeley), and Dr. P. Benson Shing (UCSD) for their contributions to this research.

This research was supported by the National Science Foundation through the NEESR program Grant NEES-2005-0024. (NSF Grant 0324542). The findings and conclusions reported herein are those of the author and do not necessarily represent the

opinions, conclusions, or recommendations of the National Science Foundation or any other sponsoring or cooperating organization.

The author would like to thank his parents, Meng-Hung Yang and Hsiu-Lan Hsiao for their loving support and encouragement. Finally, to my wife, Wan-Yu Lu, thank you for your patience, love, and encouragement.

TABLE OF CONTENTS

LIST OF TABLES

LIST OF FIGURES

SUMMARY

This thesis investigates the performance of concentrically braced zipper frames through complementary experimental and numerical simulation approaches and proposes a design methodology for an innovative bracing scheme labeled as the suspended zipper frame. The suspended zipper frame intends to ensure that the top-story hat truss remains elastic, resulting in very ductile behavior of the structure. In the first part of the work, a three-story prototype frame was designed based on a preliminary design method. Three tests were conducted on one-third scale models of this prototype to verify the design procedure and assess the system performance under very different load histories. Comparisons of the results between analyses and experiments validated the partial-height zipper mechanism envisioned, and led to refinements of the design procedure and establishment of appropriate design details for these frames. The design and performance of this structural system are illustrated with three-, nine-, and twenty-story buildings designed for the same masses as those used in the SAC studies for the Los Angeles area. The proposed design strategy results in suspended zipper frames having more ductile behavior and higher strength than typical zipper frames. In addition, the suspended zipper frames also appear to reduce the tendency of chevron-braced frames to form soft stories and to improve seismic performance without having to use overly stiff beams. Finally, an explanation of the design philosophy as well as code language format of the design procedure is given.

CHAPTER 1

INTRODUCTION

1.1 Background and Motivation

Inverted-V-braced frames (IVBF or chevron frames) are one type of Ordinary Concentrically Braced Frame (OCBF), in which the centerlines of members form a vertical truss system to resist lateral forces such as those produced by earthquakes. The behavior of such a system is controlled by the buckling of the first story braces in compression, resulting in a localization of the failure and loss of lateral resistance (Figure 1.1). In general, this system does not exhibit much force redistribution capability and has not performed well in past earthquakes.

As more emphasis has been placed in the last 20 years on increasing both the ductility and energy dissipation capability of structures in seismic areas, design provisions for a new type of braced frame, labeled the Special Concentrically Braced Frame (SCBF), were developed (Goel 1992, Bruneau et al. 1998). Within these provisions, the performance of Special Inverted-V-Braced Frames (SIVBF) was improved from that of Ordinary Inverted-V-Braced Frames (OIVBF) by limiting width-to-thickness ratio of the bracing members, requiring closer spacing of stitches of the bracing members, and providing special design and detailing of end connections (gusset plates) for the bracing members. However, SIVBFs still exhibit a typical braced frame design problem. Upon continued lateral displacement, the compression brace buckles and its axial capacity decreases while that of the tension brace continues to increase until it reaches yield. This creates a large unbalanced vertical force on the intersecting beam. In order to prevent undesirable deterioration of the lateral strength of the frame, current design provisions require that the beam shall possess adequate strength to resist this

potentially significant post-buckling force in combination with appropriate gravity loads (AISC 2005), resulting in very large beams.

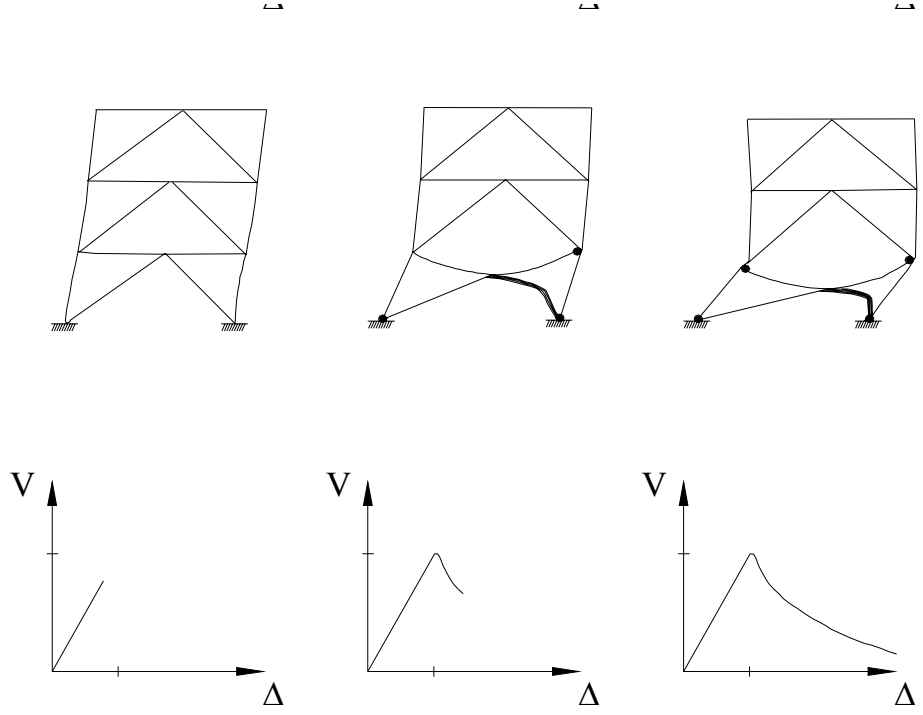

Figure 1.1 Inverted-V-braced mechanism and corresponding lateral force vs. displacement behavior.

The adverse effect of this unbalanced force can be mitigated by adding zipper columns, as proposed by Khatib et al. (1988) and shown in Figure 1.2. The intent of SIVBFs with zipper columns is to tie all brace-to-beam intersection points together, and force all compression braces in a braced bay to buckle simultaneously. This results in a better distribution of energy dissipation over the height of the building. For instance, consider a SIVBF with zipper columns subjected to severe lateral loads. If the compression brace in the first story buckles while all other braces remain elastic, a vertical unbalanced force is then applied at the middle span of the first floor beam [Figure 1.2(b)]. The zipper columns mobilize the stiffness of all beams and remaining braces to

resist this unbalance. The unbalanced force transmitted through the zipper columns increases the compression of the second story compression brace, eventually causing it to buckle [Figure 1.2(c)]. If the excitation is still forcing the structure in the same direction, the large unbalanced force will propagate up in the structure such that all compression braces buckle. Near simultaneous brace buckling over the height of a building will result in a more uniform distribution of damage, a desirable goal. However, instability and collapse can occur once the full-height zipper mechanism forms [Figure 1.2(d)] due to the reduced lateral capacity of the frame after a full mechanism has formed (Tremblay and Tirca, 2003), and this drawback has limited the applicability of this system. In addition to this stability issue, a capacity design approach for these zipper frames will require that assumptions be made as to whether the zipper column and/or the tension braces should be allowed to yield. The development of a design methodology for these frames and the resolution of a number of these behavior and performance issues constitute the original technical contributions of this dissertation.

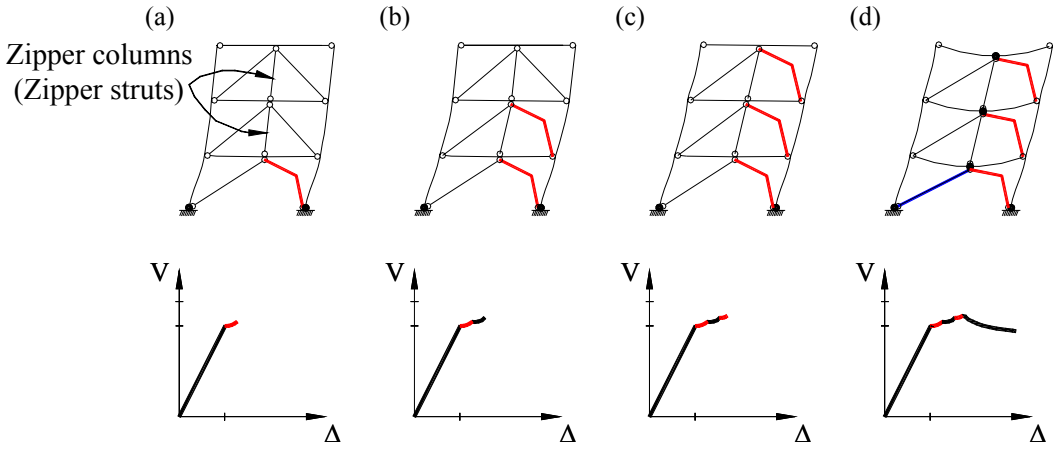

Figure 1.2 Full-height zipper mechanism.

The disadvantages of a full-height zipper mechanism (Figure 1.2) can be overcome by introducing a suspension system, labeled the "suspended zipper frame" as shown in Figure 1.3. In a suspended zipper frame, the top story bracing members are designed to remain elastic when all other compression braces have buckled and the zipper columns have yielded. Since the primary function of the suspended zipper struts is to sustain tension forces, and the suspended zipper struts support the beams at the midspan, the beams can be designed to be flexible. This results in significant savings in the amount of steel for the beams in SIVBFs with suspended zipper struts. Moreover, the force path is also so evident that a capacity design for all structural members is straightforward. The performance of one such well-detailed system could be far superior, as shown in Figure 1.3. Beginning with Chapter 3 of this thesis, this system will be simply labeled the "zipper frame," as only this configuration of the system was the only one extensively investigated as part of this work.

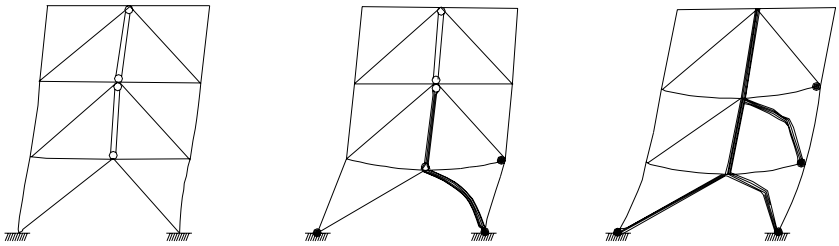

Note: The thick straight line means the member yields.
The thick curve means the brace buckles.

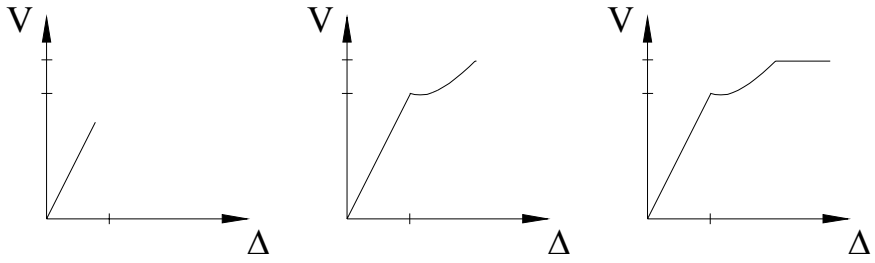

Figure 1.3 Partial-height zipper mechanism.

1.2 Objectives and Research Tasks

The main objective of this study was to develop design provisions for an alternative form of braced frames labeled the zipper frame.

This research is comprised of five tasks (phases):

1. Introduction of a 'hat truss system,' or 'suspension system,' for the partial-height zipper mechanism in zipper-braced frames.
2. Development of a preliminary design procedure for zipper-braced frames.
3. Validation of the preliminary design procedure by a pushover test.
4. Investigation of the seismic behavior of zipper-braced frames through analytical studies and cyclic tests.
5. Establishment and validation of the new design procedure for zipper-braced frames.

In Phase 1, the introduction of a 'hat truss system' into the zipper-braced frames is hypothesized to lead to a stable tri-linear pushover curve [Figure 1.3(c)]. The result is a stable deformation mechanism with large ductility, which prevents overall collapse from appearing in the form of a full-height zipper mechanism.

In Phase 2, a preliminary design procedure for zipper-braced frames was developed to achieve the partial-height zipper mechanism. The procedure subdivides the design into two parts. One is a typical strength design to determine the brace sizes and the other is a capacity design to determine the sizes of the remaining elements.

In Phase 3, following the preliminary design procedure and similitude requirements, a reduced-scale model zipper-braced frame was established. This model was then tested quasi-statically using both pushover and cyclic displacement histories to confirm the loading path envisioned in the process of design.

To investigate the seismic behavior of zipper-braced frames, two more frames were subjected to two very different displacement histories in Phase 4. The first displacement history is the LA22 earthquake (actually the 1995 Kobe Takatori record)

with near fault characteristics (single strong impulse at the load history). The other is the 1985 Llolleo (Chile) earthquake, a far field ground motion that features a large number of cycles and long duration of vibration. This phase incorporated a strong analytical component.

In the final phase (Phase 5), a new design procedure was proposed based on the results of the tests. Three zipper-braced frames were designed and analyzed to validate the new design procedure.

1.3 Organization of the Thesis

This dissertation is comprised of eight chapters and two appendices:

Chapter 1 provides the motivation, objectives, scope, and organization of the thesis, and includes a description of the collaborative nature of the work.

Chapter 2 presents an introduction to concentrically braced frames, including the detailed cyclic response of an axially loaded member as well as the behavior of conventional chevron frames. A preliminary design methodology for zipper-braced frames aiming at mitigating soft story mechanism is proposed. A prototype zipper frame designed in accordance with this design procedure is established for later study.

Chapter 3 describes the pushover test and analysis of the 1/3-scale zipper frame. Section 3.2 gives the details of the experimental pushover test program. In Section 3.3, test results are examined in with emphasis on three aspects: the individual behavior of the braces and zipper struts, the overall behavior of the zipper frame, and the out-of-plane buckling trajectories of the first-story braces. Section 3.4 establishes analytical models for simulating the experimental results, and compares the partial-height zipper mechanism and the full-height zipper mechanism.

Chapter 4 examines the seismic behavior of the 1/3-scale zipper frame in terms of two quasi-static test programs using the LA22 record and 1985 Chile record, respectively. The two parts of this Chapter are organized along the same lines as Chapter 3.

Chapter 5 proposes a refined design methodology for zipper frames incorporating the lessons learned in the experimental tests described in Chapters 3 and 4.

In Chapter 6, three design examples of zipper frames (3, 9, and 20 stories) conforming to the refined design methodology are used to illustrate the performance of the zipper system.

Chapter 7 presents the verification of the three zipper model buildings using the eigenvalue, pushover, and nonlinear dynamic analyses.

Chapter 8 presents the summary and conclusions of this study. Some suggestions for future study are also presented.

CHAPTER 2

BACKGROUND AND PRELIMINARY DESIGN PROCEDURE FOR ZIPPER FRAMES

2.1 Introduction

This chapter first discusses the limited amount of work available on zipper-type frames in the technical literature. It then proposes the preliminary design procedure that served as the basis of the method used to design the zipper frames that were tested in the experimental portion of this work. This design procedure was later modified and refined as a result of the experimental work, as described in Chapter 5. However, since an established design procedure for zipper frames was not available in the literature, the early development of such a method was an essential first step in this project.

2.2 Background

2.2.1 General

Braced framing systems resist lateral loads primarily by developing high axial forces in selected framing members. These systems are extensively described in Bruneau et al., 1998, from which the discussion in Sections 2.2.1 to 2.2.3 is abstracted. Braced framing systems have proved popular in regions of high seismicity because materials savings can be achieved with respect to moment-resisting frames. In addition, braced frames can efficiently control frame drift due to high earthquake-induced inertial forces.

Unlike the moment-resisting frame, the concentrically braced frame (CBF) is a lateral force-resisting system that resists lateral forces on the structural frame by developing internal axial actions and relatively small flexural actions. Figure 2.1 shows

common CBF configurations, in which both inverted V- and V-braced frames in Figures 2.lb and 2.lc are also known as chevron-braced frames.

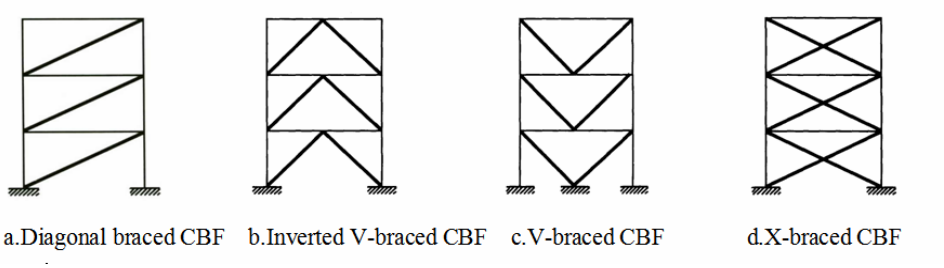

Figure 2.1 Common CBF configurations (Bruneau et al., *Ductile Design of Steel Structures*).

Seismic provisions for the design and detailing of CBFs can be found in the AISC Seismic Provisions for Structural Steel Buildings (AISC 2005). The rules carrying out the analyses and the determinations of the seismic loads for CBFs typically conduct according to Chapters 11 and 12 of Minimum Design Loads for Buildings and Other Structures (ASCE 7-05), as well as the seismic response history procedures in Chapter 16 of ASCE 7-05.

2.2.2 Cyclic Axial Load Response of a Bracing Member[1]

A sample hysteretic curve for a brace under cyclic axial loading is shown in Figure 2.2 with the axes showing the axial load *(P)* vs. axial deformation (δ). Typically, the tension yielding force (Point E) is larger than the compression buckling strength. The first buckling occurrence (Point A) is at a greater load than the subsequent buckling points (Point G). After buckling, the strength decreases towards a minimum post-

[1] Sections 2.2.1 to 2.2.3 are taken from Bruneau et al., 1998.

buckling strength as shown by segment ABC. The behavior of axially loaded members can also be expressed in terms of the transverse displacement at midlength (Δ). Each segment in the hysteresis loop corresponds to a variation in the transverse displacement of a brace, as shown in Figure 2.2. A plastic kink (CD) is evident at the midlength of the brace after the formation of a plastic hinge (BC).

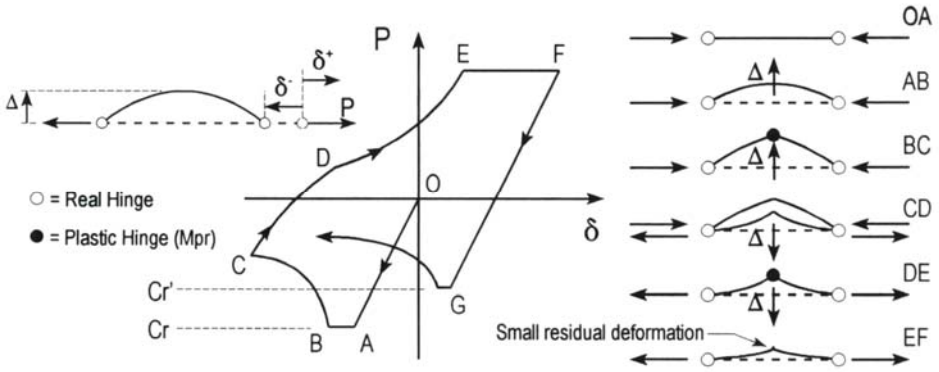

Figure 2.2 Sample hysteresis of a brace under cyclic axial loading.

(Bruneau et al., *Ductile Design of Steel Structures*)

2.2.3 Post-Buckling Behavior of Inverted-V-Braced Frames

Khatib et al. (1988) conducted an exhaustive study on the post-buckling characteristics of inverted-V-braced frames. For the frame considered, shown in Figure 2.3a, it was assumed that the beams were pin-connected to the columns and no vertical loads were applied. The beams and columns were assumed to be axially inextensible. The kinematics of the brace-to-beam intersection point is shown in Figure 2.3b.

2.2.3.1 Story Lateral Stiffness and Classification of Beams

In the elastic range, the tension force *(T)* in brace B1 and the compression force *(C)* in brace B2 are equal in magnitude. The lateral strength of the braced bay at the onset of buckling in brace B2 is $F_c = 2P_c \cos\theta$, where P_c is the elastic buckling load of brace

B2. The corresponding unbalanced vertical load *(P_{un})* applied to the beam at the brace-to-beam intersection point is $P_{un} = (T - C)\sin\theta$, and equal to zero. The lateral stiffness of the story is equal to:

$$K_s = 2\left(\frac{AE}{L}\right)_{br} \cos^2\theta = 2k_e \cos^2\theta$$

where k_e is the elastic axial stiffness of one brace. In loading the frame from $F = 0$ to $F=F_c$, the brace-to-beam intersection point translates from point *A* to point *A'* in Figure 2.3b.

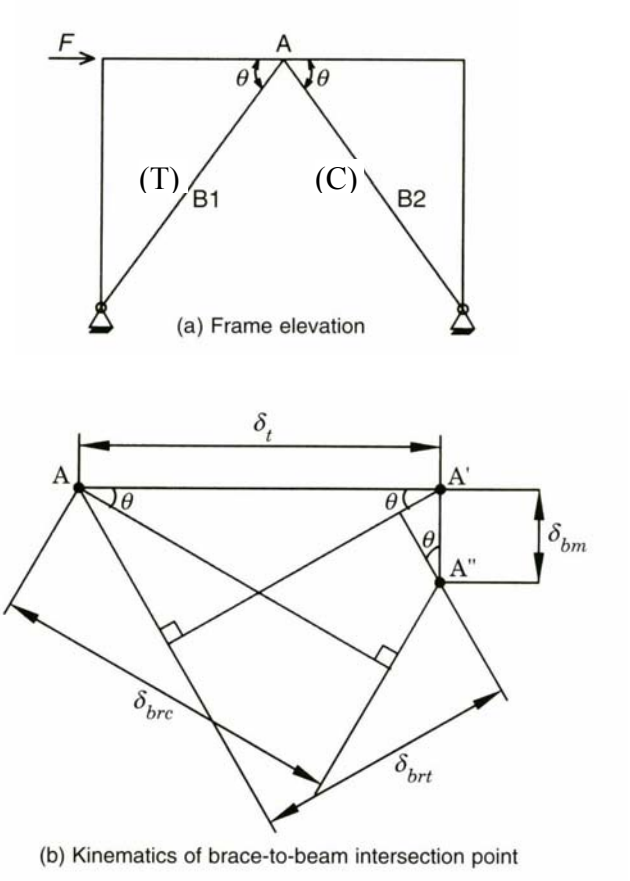

Figure 2.3 Frame geometry and kinematics of an inverted-V-braced frame (Khatib et al. 1988)

Following buckling of brace B2, the forces in the tension and compression braces will generally be unequal, an unbalanced vertical load will be applied to the beam, and the beam will deflect by an amount δ_{bm}, from point A' to point A" in Figure 2.3b. From Figure 2.3b, the displacements δ_{brc} and δ_{brt} can be calculated as:

$$\delta_{brc} = \delta_t \cos\theta + \delta_{bm} \sin\theta \tag{2.1}$$

$$\delta_{brt} = \delta_t \cos\theta - \delta_{bm} \sin\theta \tag{2.2}$$

The increase in the tension force in brace B1 is given by:

$$\Delta T = \delta_{brt} k_{br}$$

and the increase in the compression force in brace B2 is:

$$\Delta C = \delta_{brc} k_{bb}$$

where k_{br} and k_{bb} are the tangent tensile stiffness of brace B1 and the tangent post buckling stiffness of brace B2, respectively. The unbalanced vertical load applied to the beam is equal to:

$$P_{un} = (\Delta T - \Delta C)\sin\theta$$

and the increase in lateral resistance ΔF is equal to:

$$\Delta F = (\Delta T + \Delta C)\cos\theta$$

For positive δ_t and positive δ_{bm}, both δ_{brc} and δ_{brt} will generally be positive. Given that k_{bb} is generally negative following buckling, and k_{br} is positive up to yielding in the tension brace, the compression force in brace B2 will decrease by ΔC, the tension force in brace B1 will increase by ΔT, and the unbalanced vertical load will be equal to:

$$P_{un} = (\Delta T - |\Delta C|)\sin\theta$$

The tangent stiffness of the story *(K_{st})* following buckling of brace B2 is equal to:

$$K_{st} = \frac{\Delta F}{\delta_t} = \cos^2\theta[(k_{br} + k_{bb}) - \frac{(k_{br} - k_{bb})^2 \sin^2\theta}{k_{bm} + (k_{br} + k_{bb})\sin^2\theta}]$$

where k_{bm} (>0) is the stiffness of the beam associated with a vertical degree of freedom at the brace-to-beam intersection point. For the design objective of positive story tangent stiffness, that is, $K_{st} > 0$, the minimum required stiffness of the beam is a function of the brace tangent stiffness values. If k_{br} and k_{bb} are both positive, K_{st} will be positive. If k_{br} is positive and k_{bb} is negative, the beam stiffness required to ensure that $K_{st} > 0$ is:

$$k_{bm} = \frac{-4k_{br}k_{bb}\sin^2\theta}{\left(k_{br} + k_{bb}\right)} \qquad (2.3)$$

To avoid having to consider column stiffness, it is possible to establish a beam classification based on flexural stiffness. Khatib classified beams as either flexible, intermediate, or stiff. Since the flexural stiffness of a beam is a function of its second moment of area and its boundary conditions, flexible beams were those that did not satisfy Equation 2.3 even if they had fixed ends, stiff beams were those that satisfied Equation 2.3 even if they were simply supported, and intermediate beams were all those beams not classified as either flexible or stiff. In order to consider the variation of the unbalance force with brace slenderness and relative beam stiffness, the classification of beam strength, which is independent of the stiffness classification previously described, was established. A beam will be considered as strong if it can sustain the maximum vertical unbalanced force in addition to its normal gravity loading. A weak beam develops plastic hinges prior to the yielding of the tension braces. However, in the remainder of this chapter all beams, stiff and flexible, will be assumed to be strong.

2.2.3.2 Flexible Beam Collapse Mechanism (Figure 2.4)

For stocky braces, the tension yield force P_y **(**$= P_4$**)** is equal to or slightly larger than the elastic buckling load P_c *(*$= P_3$*)* in Figure 2.4a. The maximum unbalanced force applied to the beam is equal to $(P_y - P_c)\sin\theta$ and approximately equal to zero. If the beam is flexible, the tensile force in brace B1 remains practically constant and axial

deformations in the compression brace (δ_{brc}) increase more quickly than the axial deformations in the tension brace (δ_{brt}). This relationship is identified in Figure 2.4a by the dashed lines joining the force-displacement relations for braces B1 and B2. The beam displacements δ_{bm} increase δ_{brc} and decrease δ_{brt} . The resulting story shear force versus lateral displacement relation is shown in Figure 2.4b. (The numbered points in Figure 2.4b relate to the corresponding points in Figure 2.4a).

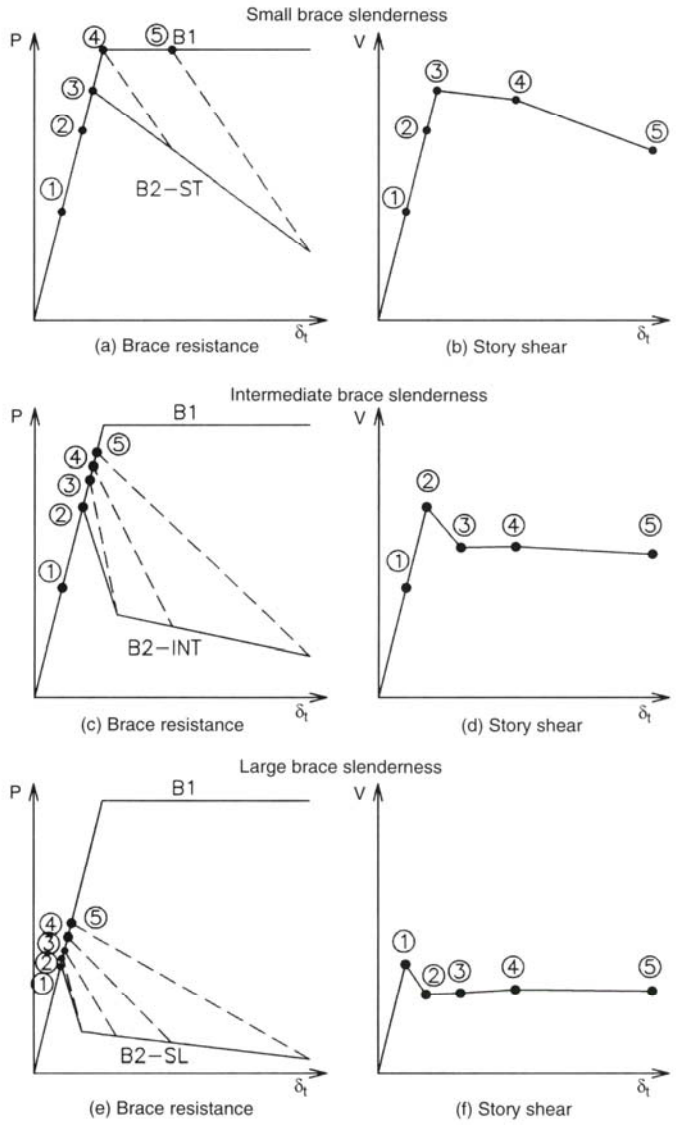

Figure 2.4 Force-displacement relations for an inverted-V-braced CBF with flexible beams (Adapted from Bruneau et al., *Ductile Design of Steel Structures*)

For intermediate braces, the tension yield force is significantly greater than the elastic buckling load (see Figure 2.4c), and a much larger unbalanced force could be applied to the beam. However, if the beam is flexible, the tension force in B1 remains essentially constant and cannot increase to P_y. Intermediate braces lose strength quickly with increasing deformation (see brace 2 in Figure 2.4c), so the story shear resistance reduces with increasing lateral displacement as shown in Figure 2.4d.

For slender braces, the tension yield force is much larger than the elastic buckling load. If the beam is flexible, the tension force in brace B1 remains essentially constant with increasing lateral displacement. However, given that the resistance of buckled slender braces decreases relatively slowly with increasing lateral displacement (see brace B2 in Figure 2.4e), the story shear resistance (see Figure 2.4f) remains relatively constant with increasing lateral displacement.

2.2.3.3 Stiff Beam Collapse Mechanism (Figure 2.5)

For the three types of braces, the assumption that the beam stiffness is large results in small beam displacements (δ_{bm}) per Equations 2.1 and 2.2. If δ_{bm} is small, the elongation of the tension brace B1 (δ_{brt}) will be approximately equal to the shortening of the compression brace B2 (δ_{brc}).

For stocky braces, the tension yield force is equal to or slightly larger than the elastic buckling load. Because the beam is stiff, the tension force in brace B1 continues to increase, producing an unbalanced force at the midspan of the beam equal to $(P_y - P_c)\sin\theta$. If the beam is strong, the deformation rates in braces B1 and B2 are identical. For larger lateral displacements (segment 4-5 in Figure 2.5b), the lateral resistance provided by the braces decreases slowly because the compression load in brace B2 drops with increasing lateral displacements.

For intermediate braces, the tension yield force is significantly greater than the elastic buckling load, and a much larger unbalanced force can be applied to the beam. Upon buckling of brace B2 (points 2 in Figures 2.5c and 2.5d), the tension force in brace B1 will increase at k_e kips per inch of brace elongation, and the compression force in brace B2 will decrease at $|k_{bb}|$ kips per inch of brace shortening. The resultant story shear force versus lateral displacement relation is shown in Figure 2.5d.

For slender braces, the tension yield force is much larger than the elastic buckling load. A large unbalanced force can be applied to the beam if the beam is strong. The tension force in brace B1 will increase at k_e kips per inch of brace elongation and the compression force in brace B2 will decrease at $|k_{bb}|$ kips per inch of brace shortening. The resultant story shear force versus lateral displacement relation is shown in Figure 2.5f. Upon buckling of brace B2 (point 2), the story shear force increases slowly because k_e is greater than k_{bb}. Following yielding of the tension brace at point 4, the story shear force decreases slowly with increasing displacements.

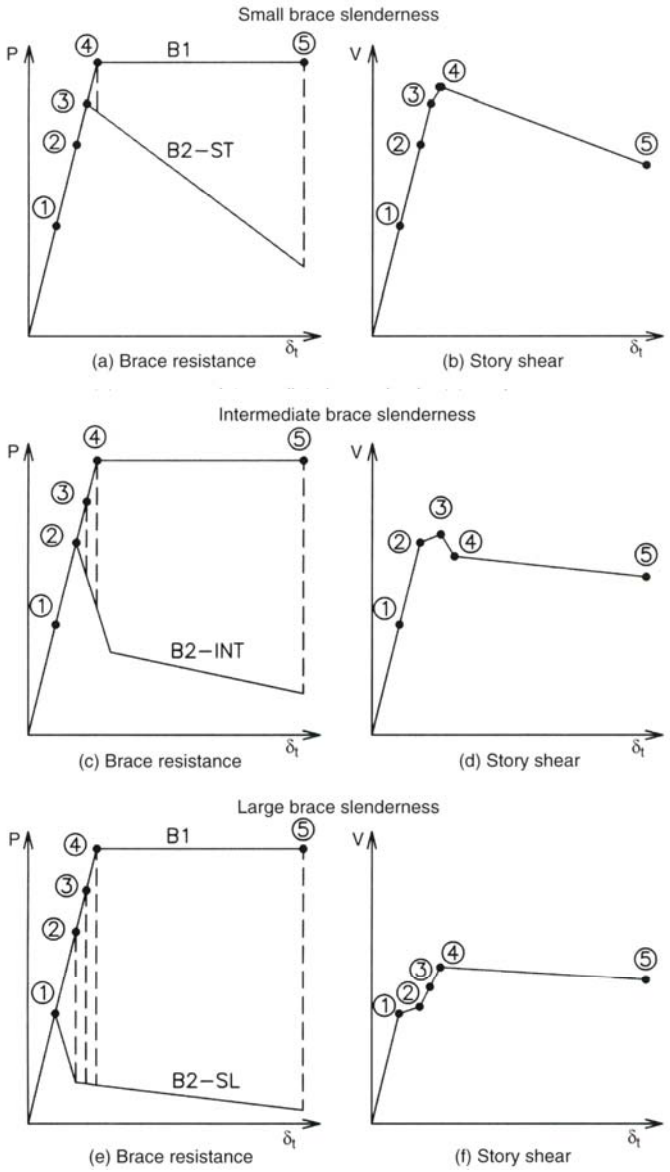

Figure 2.5 Force-displacement relations for an inverted-V-braced CBF with stiff beams (Adapted from Bruneau et al., *Ductile Design of Steel Structures*)

2.2.4 Factors Influencing the Inelastic Cyclic Response of a Special Concentrically Braced Frame

The inelastic cyclic response of a chevron-braced frame, which is a common configuration of the concentrically braced frame in the United States, is dependent upon many factors including the following:

1. The slenderness ratio and compactness of the bracing members
2. The relative axial strengths of the brace in compression and tension
3. The strength of the brace connections to the beams and columns
4. The degree of lateral restraint provided to the brace-to-beam connection
5. The stiffness, strength, and compactness of the beam into which the brace frames

In this work, it is assumed that the brace connections are sufficiently strong and that the brace-to-beam connection is adequately restrained against lateral-torsional buckling.

In the following sections some selected, relevant research projects are described. The intent of these sections is not to provide a complete summary of existing research. Rather, the intent is to highlight some behavioral modes that will need to be addressed in the design of zipper frames.

2.2.4.1 Bracing Members and Connections

Astaneh et al. (1986) investigated brace buckling in concentrically braced frames. Cyclic testing of specimens designed and detailed in accordance with typical provisions produced connection failures. For brace buckling in the plane of the gusset plates, the end connections should be designed for the full axial load and flexural strength of the brace. A realistic value of the rotational stiffness K should be used to represent the connection fixity. For brace buckling out of the plane of single plate gussets, weak-axis bending in the gusset is induced by member end rotations. This results in flexible end conditions with plastic hinges at midspan in addition to the hinges that form in the gusset plate. Satisfactory performance can be ensured by allowing the gusset plate to develop restrain-free plastic rotations. This requires that the free length between the end of the brace and

the assumed line of restraint for the gusset be sufficiently long to permit plastic rotations, yet short enough to preclude the occurrence of plate buckling prior to member buckling. A length of two times the plate thickness is recommended. The required strength of bracing connections should be adequate so that failure by out-of-plane gusset buckling or brittle fracture of the connections are not critical failure mechanisms. The minimum of the two criteria that (1) the nominal expected axial tension strength of the bracing member or (2) the maximum force that could be generated by the overall system determines the required strength of the bracing connection.

Tang and Goel (1987) conducted analytical studies on bracing systems designed in strict accordance with earlier code requirements for concentrically braced frames. The studies predicted brace failures without the development of significant energy dissipation. Failures occurred most often at plastic hinges (local buckling due to lack of compactness), or in the connections. Plastic hinges normally occur at the ends of a brace and at the brace midspan.

Tang and Goel (1989) showed that the post-buckling cyclic fracture life of bracing members generally decreased with an increase in slenderness ratio. However, an upper limit is provided to maintain a reasonable level of compressive strength. The slenderness limit for braces in Special CBFs is $1000/\sqrt{F_y}$, which is larger than the limit of $720/\sqrt{F_y}$ as specified for Ordinary CBFs in the AISC seismic provisions. In addition, in order to minimize the detrimental effects of local buckling and subsequent fracture during repeated inelastic cycles, width-thickness ratios of compression elements in bracing members have been reduced to be at or below the requirements for compact sections. This failure mode is especially prevalent in rectangular HSS with width-thickness ratios larger than the prescribed limits.

Xu and Goel (1990) proposed to use closer spacing of stitches and higher stitch strength than in Ordinary CBFs so as to restrict individual element bending between the

stitch points and consequent premature fracture of bracing members. Wider spacing is permitted under an exception when buckling does not cause shear in the stitches. Bolted stitches are not permitted within one-fourth of the clear brace length as the presence of bolt holes in that region may cause premature fractures due to the formation of plastic hinge in the post-buckling range.

Aslani and Goel (1991) focused on the case of double-angle and double-channel braces, where closer stitch spacing is required to achieve improved ductility and energy dissipation. This is especially critical for double-angle and double channel braces whose buckling results in large shear forces being imposed on the stitches. Studies also showed that placement of double angles in a toe-to-toe configuration reduces bending strains and local buckling.

Hassan and Goel (1991) established an analytical models of bracing systems that were designed to ensure stable ductile behavior when subjected to the same ground motion records as the earlier concentrically braced frame designs. The analytical results exhibited full and stable hysteresis without fracture.

2.2.4.2 Columns

Analytical studies of Hassan and Goel (1991) on SCBF have shown that columns can carry as much as 40 percent of the story shear. In the event of a major earthquake, columns in concentrically braced frames can undergo significant bending beyond the elastic range after buckling and yielding of the braces. Even though their bending strength is not utilized in the design process when elastic design methods are used, columns in SCBF are required to have adequate compactness and shear and flexural strength in order to maintain their lateral strength during large cyclic deformations of the frame. When columns are common to both SCBF and SMF in a dual system, their contribution to story shear may be as high as 50 percent. This feature of SCBF greatly

helps in making the overall frame hysteretic loops "full" when compared with those of individual bracing members which are generally "pinched".

2.2.4.3 Beams

V-braced and Inverted-V-Braced Frames exhibit a special problem in that an unbalanced vertical force is applied on the intersecting beam. In order to prevent undesirable deterioration of lateral strength of the frame, the SCBF provisions require that the beam possess adequate strength to resist this potentially significant post-buckling force redistribution in combination with appropriate gravity loads. Tests have shown that typical bracing members demonstrate a residual post-buckling compressive strength of about 30 percent of the initial compressive strength (Hassan and Goel, 1991) This is the maximum compression force that should be combined with the full yield force of the adjacent tension brace.

2.2.4.4 Local Buckling

Kanvinde et al. (2005) investigated the cyclic inelastic deformation of a bracing member under a phenomenon called Ultra-Low Cycle Fatigue (ULCF). Several tests have been performed to identify and quantify the underlying failure mechanisms of earthquake-induced ULCF. ULCF basically results from the large strains developed during local buckling at the center of bracing members, and Kanvinde et al. have established micromechanical models to simulate ULCF in steel structures. The preliminary testing results were in agreement with those obtained from detailed continuum-based ABAQUS and line-element-based OpenSEES analyses. In particular, the micromechanics-based models could capture the fundamental processes of void growth, collapse, and damage responsible for ULCF (Fell et al., 2006).

2.2.5 Concentrically Braced Frame with Zipper Columns

The adverse effect of the unbalanced vertical force in CBFs can be mitigated by using a zipper column with V- or Inverted-V bracing (Khatib et al., 1988). The intent of the zipper frame is to tie all brace-to-beam intersection points together, to force all compression braces in a braced bay to buckle simultaneously and then activate formation of the plastic hinges on the beams, and thereby to distribute the energy dissipation (damage) over the height of the building. Simultaneous brace buckling over the height of a building will produce a single-degree-of-freedom mechanism and result in a more uniform distribution of damage over the height of the building (Whittaker et al. 1990). However, during the period of the external excitation, the zipper columns in the frame can be in tension or compression, which makes the design for the zipper columns very complex.

Khatib et al. (1988) studied the behavior of a zipper frame using nonlinear response-history analysis. Comparing the response of the zipper frame with that of the other frame configurations, such as inverted-V-, V-, X-, split-X-, and strut-to-ground-braced frames, Khatib concluded the following:

1. The response of the zipper frame was less sensitive to ground motion characteristics.
2. The zipper frame achieved a more uniform distribution of damage over its height.
3. The zipper frame developed a trilinear story shear force-displacement relation.
4. The zipper frame concept could be successfully implemented with flexible beams and braces of intermediate slenderness.

2.3 Preliminary Design Procedure

As there is not currently an established design procedure for zipper frames, the first task in this dissertation was to develop a basic design procedure to proportion these

structures. This work was divided into two parts. First a series of comparison prototype structures was identified (Section 2.3.1). Then a preliminary design procedure was established, and a prototype frame designed (Section 2.3.2).

2.3.1 Prototype Design Frame

To provide clear comparisons to the performance of similar buildings with moment resisting frames (MRF), a "zipper" SIVBF subjected to the same loads as the 3-story SAC model building (FEMA-355C, 2000) was designed. The SAC model designed for the Los Angeles area was selected, and designed in one of the principal directions. The floor plan and elevation for this frame are shown in Figure 2.6. In later portions of the research (see Chapters 6 and 7), 9- and 20-story frames designed for the same project as moment frames will be redesigned as zipper ones, and their behavior assessed. A prototype consisting of one bay was selected for further analysis and testing from the zipper-braced SAC model building. The seismic weight assigned to this braced bay was 4824 kN (1084 kips), which was one-sixth of the entire building seismic weight. In the process of seismic design, the design seismic base shear was calculated to be 1206 kN (271kips) in accordance with the equivalent lateral force procedure in the International Building Code (IBC 2000). The design spectral response acceleration at short period was 1g, the response modification factor was 6, and the occupancy importance factor was 1.5. The members elected for the prototype zipper-braced frame are shown in Table 2.1. They were proportioned on the basis of a preliminary design procedure which is described in the next section.

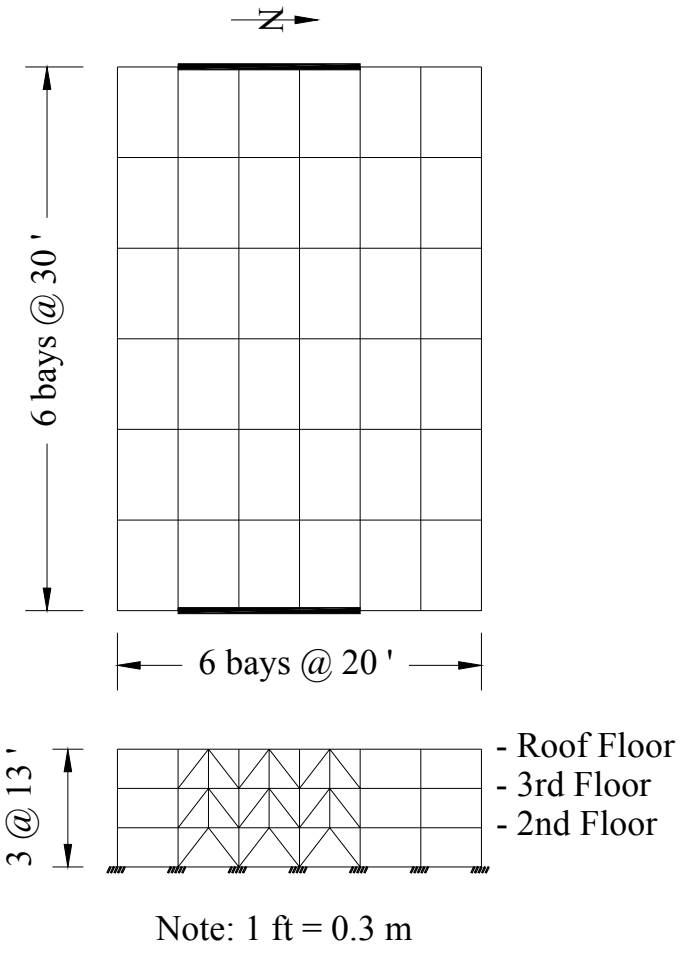

Figure 2.6 Floor plan and elevation for the 3-story SAC model building modified with zipper-braced system.

Table 2.1 Member sizes for the prototype zipper-braced frame.

Story	Braces	Columns	Beams	Zipper struts
3	HSS10x10x5/8	W10x77	W8x21	W8x48
2	HSS7x7x3/8	W10x77	W14x82	W8x24
1	HSS7x7x3/8	W10x77	W12x50	

2.3.2 Preliminary Design Methodology

2.3.2.1 Design Philosophy

As mentioned previously, the full-height zipper frame is potentially unstable once a full-height zipper mechanism forms. To overcome this weakness, a design procedure based on preventing buckling of the top-story braces is presented here. This procedure suppresses the formation of a complete collapse mechanism and delays the formation of plastic hinges at the midspan of the beams. As the lateral loads increase, the compression braces will buckle, the tension braces will yield, and finally the zipper strut will yield to form the mechanism shown in Figure 1.3. Because the performance of the top story is the key to the behavior of this structural system, this system has been labeled the "suspended zipper frame."

2.3.2.2 Design Procedure

The design of a suspended zipper frame can be accomplished by following a two-step design procedure. In Step I (strength design), the frame is sized to resist the actions which result from the gravity and lateral loads applied to a conventional inverted-V braced frame (i.e., the zipper columns are not present and the structure is similar to that shown in Figure 1.1). This phase fixes the size of the braces in all floors except the top story.

In Step II (capacity design), the zipper struts are added and other structural elements are redesigned except for the braces below the top-story level. In this preliminary design procedure, the zipper column is designed to resist the vertical unbalanced forces generated by the braces below the floor under consideration, assuming P_y (not $R_y P_y$ as will be done in the final design procedures) for the braces in tension and 0.3 times $\phi_c P_n$ for the braces in compression. The decision to use a tension brace force of P_y in the capacity calculations is intended to prevent excessive deformations in the

tension brace and to force yielding in the zipper strut soon after tension yielding in the brace. The almost simultaneous yielding of the tension brace and zipper column is intended to prevent the concentration of drift on a single story. The nominal value used for the compression capacity is in accordance with current codes, and reflects the capacity of a moderately slender brace after buckling. The shear capacity of the beams is ignored.

The top-story braces need to resist both the vertical unbalanced forces and the top-floor level equivalent lateral earthquake force. A factor of 1.7 times the top-floor level equivalent earthquake force is used because the top-story braces need to be elastic throughout the load history. This value of 1.7 needs to be verified further by considering the distribution of the system overstrength after the buckling of the all compression braces except for the top ones. In simple code language format, the design procedure can be summarized as follows:

1. Phase I (Strength Design)

The frame is designed to resist the effects of earthquake and vertical loadings from the load combinations stipulated by the Applicable Building Code without the aid of the zipper columns. This follows the conventional Special Inverted V-Braced Frame (SIVBF) design procedure.

2. Phase II (Capacity Design)

The frame designed in Phase I is modified as follows:

(1) Zipper struts

Zipper struts are added and designed to resist the vertical unbalanced forces generated by the braces located at the level below using P_y for the brace in tension and 0.3 times $\phi_c P_n$ for the brace in compression.

(2) Top-story braces

Top-story braces shall be designed to resist the vertical unbalanced forces collected by the zipper struts below the top story as well as the 1.7 times the top-floor equivalent earthquake force.

(3) Column Strength

The required axial compressive and tensile strength are determined using the maximum load transferred to the column considering the capacities of the adjacent braces in combination with the induced forces from the 1.7 times the top-floor equivalent earthquake force.

(4) Beams

Beams are checked as beam-column members as stipulated in Chapter H of the AISC LRFD Specification. The required strength is determined using the maximum load transferred to the beam considering the capacities of the adjacent braces.

The design of the prototype frame results in the following member sizes (Table 2.1).

2.4 Summary

This chapter first presented a brief overview of the existing research pertinent to this project. It then described a preliminary design procedure for zipper frames, and concluded with the design of a 3-story prototype frame. The latter will be used as the basis for the experimental studies to be used in this work.

CHAPTER 3

PUSHOVER TEST AND ANALYSIS OF THE 1/3-SCALE ZIPPER-BRACED FRAME

3.1 Introduction

This chapter first reports on the results of a pushover test on a zipper-braced frame model. The primary aims of the test were to validate the behavior envisioned in the preliminary design procedure developed in Chapter 2 and to verify the limit states to be used for a simplified design methodology based on pushover analysis. The chapter then describes simplified analytical models for predicting the pushover curve behavior of zipper frames and compares the results of simulation using this model with experimentally obtained results.

3.2 Test Program

3.2.1 Test Frame

The test frame, a 1/3-scale zipper frame model shown in Figure 3.1, was proportioned according to a set of similitude requirements (Table 3.1) that relate the model to the prototype structure. The scale of the specimen was controlled by the need to test a similar specimen on the shake table at the University at Buffalo. Table 3.1(a) summarizes the scale factors obtained from similitude considerations for the earthquake response of a structure. The member sizes for the reduced-scale model of the zipper-braced frame, as listed in Table 3.2, were determined on the basis of the products of these geometrical scale factors and the known member properties in the prototype. The final specimen had an actual scale factor close to 1/3.5.

The detailed design for the brace-beam-column connections in the model was carried out following the Uniform Force method described in the AISC LRFD manual. The details of the end brace connections in the second story are shown in Figure 3.2. In order to make all the braces, except the top ones, buckle out of plane as expected, the gusset plates at the ends of braces were designed with a free length of twice the gusset plate thickness, as recommended in the commentary to the 2005 AISC seismic provisions. The details of the end zipper strut connections are presented in Figure 3.3. Finally, columns were fully welded to base plates in order to obtain close to fixity conditions at the base of the structure. Details of the test frame are shown in Appendix A.

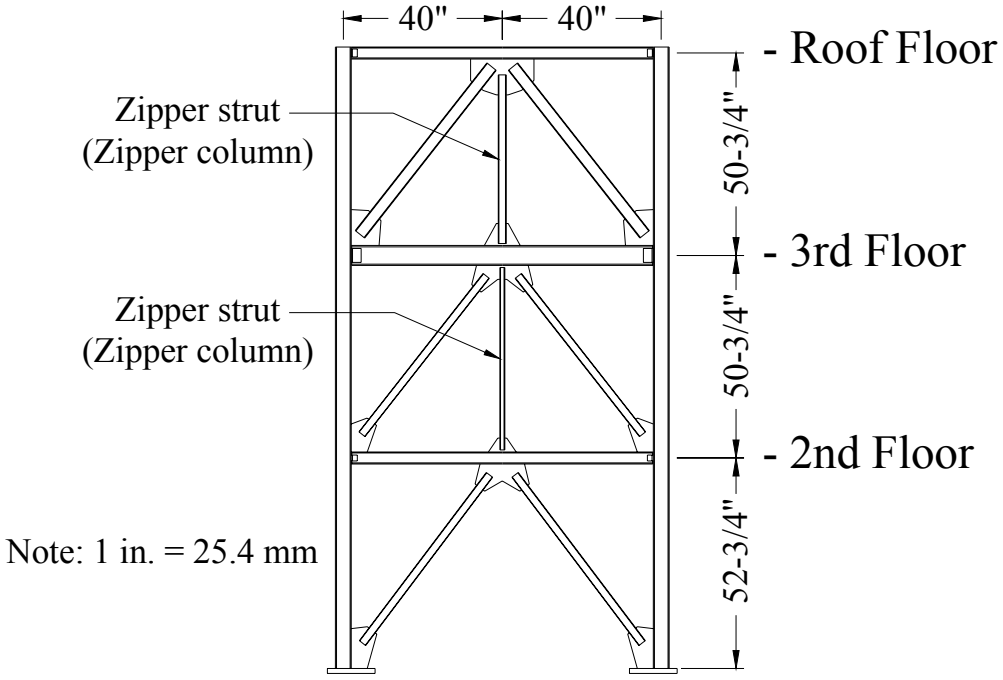

Figure 3.1 Elevation of the test frame.

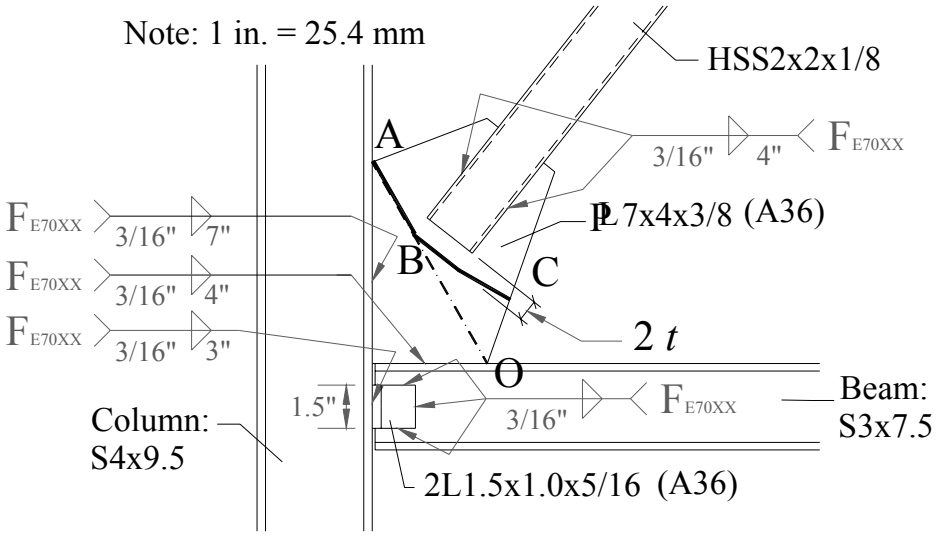

Figure 3.2 Seismic detailing for HSS brace-buckling out of plane.

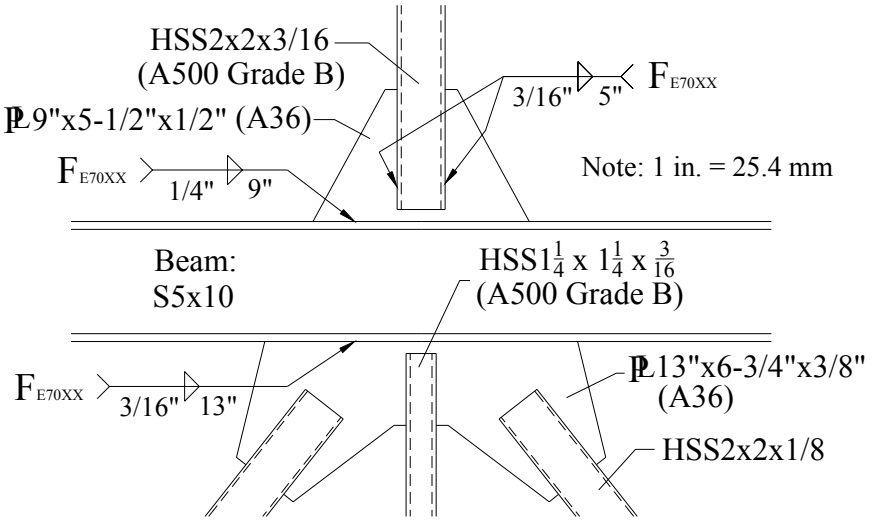

Figure 3.3 Zipper-brace-beam connections on the 3rd -floor level.

Table 3.1(a) Summary of scale factors for earthquake response of the 1/3-scale model.

Group	Quantity	Scale Factor
Geometry	Linear dimension	$S_L = 1/3$
	Area	$S_A = S_L^2 = 1/9$
	Moment of Inertia	$S_I = S_L^4 = 1/81$
Loading	Force	$S_Q = S_E S_L^2 = 1/9$
	Acceleration	$S_a = 1$
	Time	$S_t = [S_L S_a^{-1}]^{1/2} = 1/\sqrt{3}$
Material	Modulus	$S_E = 1$
	Mass	$S_m = S_Q S_a^{-1} = 1/9$

Table 3.1(b) Required and actually used properties of the members for the model.

Story		Braces		Columns		Beams		Zipper struts	
		A*	I**	A	I	A	I	A	I
	Required	0.73	0.43	1.84	3.03	1.19	2.61	-	-
1	Actual	0.84	0.49	2.79	6.76	2.20	2.91	-	-
	Scale used	***0.27***	***0.28***	***0.23***	***0.23***	***0.21***	***0.28***	-	-
	Required	0.73	0.43	1.84	3.03	1.96	5.87	0.58	0.55
2	Actual	0.84	0.49	2.79	6.76	2.93	12.30	0.67	0.12
	Scale used	***0.27***	***0.28***	***0.23***	***0.23***	***0.23***	***0.24***	***0.27***	***0.42***
	Required	1.71	2.03	1.84	3.03	0.50	0.50	1.15	1.23
3	Actual	1.89	2.46	2.79	6.76	1.66	2.50	1.19	0.64
	Scale used	***0.27***	***0.27***	***0.23***	***0.23***	***0.16***	***0.19***	***0.28***	***0.34***

*A is the cross-section area of a member.
**I is the moment of inertia of a member
Target scale is 1/3.5=0.29.

Table 3.2 Member sizes of the 1/3-scale zipper-braced frame model.

Story	Braces	Columns	Beams	Zipper struts
3	HSS3×3×3/16	S4×9.5	S3×5.7	HSS2×2×3/16
2	HSS2×2×1/8	S4×9.5	S5×10	HSS1.25×1.25×3/16
1	HSS2×2×1/8	S4×9.5	S3×7.5	

The braces as well as the zipper struts in the zipper-braced frame model were cold-formed welded and seamless hollow square section (HSS) made of ASTM A500 Grade B steel [nominal F_y=317 MPa (46ksi) and F_u=400 MPa (58ksi)]. The rest of the members were designed using A572 Grade 50 [nominal F_y=345 MPa (50ksi) and F_u=448 MPa (65ksi)]. The column base and gusset plates were made of ASTM A36 steel [nominal F_y=250 MPa (36ksi) and F_u=400 MPa (58ksi)]. The first- and second-story braces used a HSS2×2×1/8 with a cross section area, A_g, of 541.9 (mm^2) [0.84 (in^2)], a radius of gyration about the axis in the plane of the frame, r, of 19.3 (mm) [0.761 (in)], an expected yield factor, R_y , of 1.3, a yield stress, F_y , of 317 (MPa) [46 (ksi)], and a width-to-thickness ratio of both flange and web elements of the cross section, λ, of 14.2. Table 3.3 gives the lengths and slenderness ratios of the first- and second-story braces: the story, the member shape, the clear length of the braces as measured between the end gusset plates, L_n , the length between the plastic hinges forming in the gusset plates, L, and the length between the working points, L_w. In the AISC Seismic Provisions for SCBF, the width-to-thickness ratio of braces shall meet the seismic compact requirement, $\lambda_{ps} \leq 0.64\sqrt{E/F_y}$ (equal to 16.1 for F_y=317 MPa steel), and their slenderness ratio shall have $kL/r \leqq 4\sqrt{E/F_y}$, i.e., $kL/r \leqq 100$. As seen in Table 3.3, all braces met both these limits

and are within the intermediate range ($50 \leqq kL/r \leqq 110$) between stocky and slender elements.

Table 3.3 Lengths and slenderness ratios of the first- and second-story braces.

Story	Shape	L_n	L	L_w	kL/r ($k=1$)	kL_w/r ($k=1$)
2	HSS2×2×1/8	1080 (mm)	1322 (mm)	1641 (mm)	68.4	84.9
		42.53 (in)	52.03 (in)	64.62 (in)	68.4	84.9
1	HSS2×2×1/8	1140 (mm)	1382 (mm)	1681 (mm)	71.6	87.0
		44.90 (in)	54.40 (in)	66.20 (in)	71.6	87.0

3.2.2 Test Setup

The test was performed at the Structural Engineering Laboratory at Georgia Tech using the pushover testing method. As illustrated in Figure 3.4, the zipper frame was restrained by two supporting frames which prevented out-of-plane displacements. The test frame was mounted on a strong beam rigidly post-tensioned to the reaction floor, and the loads were applied through three single-ended actuators connected to a large reaction wall at each floor level.

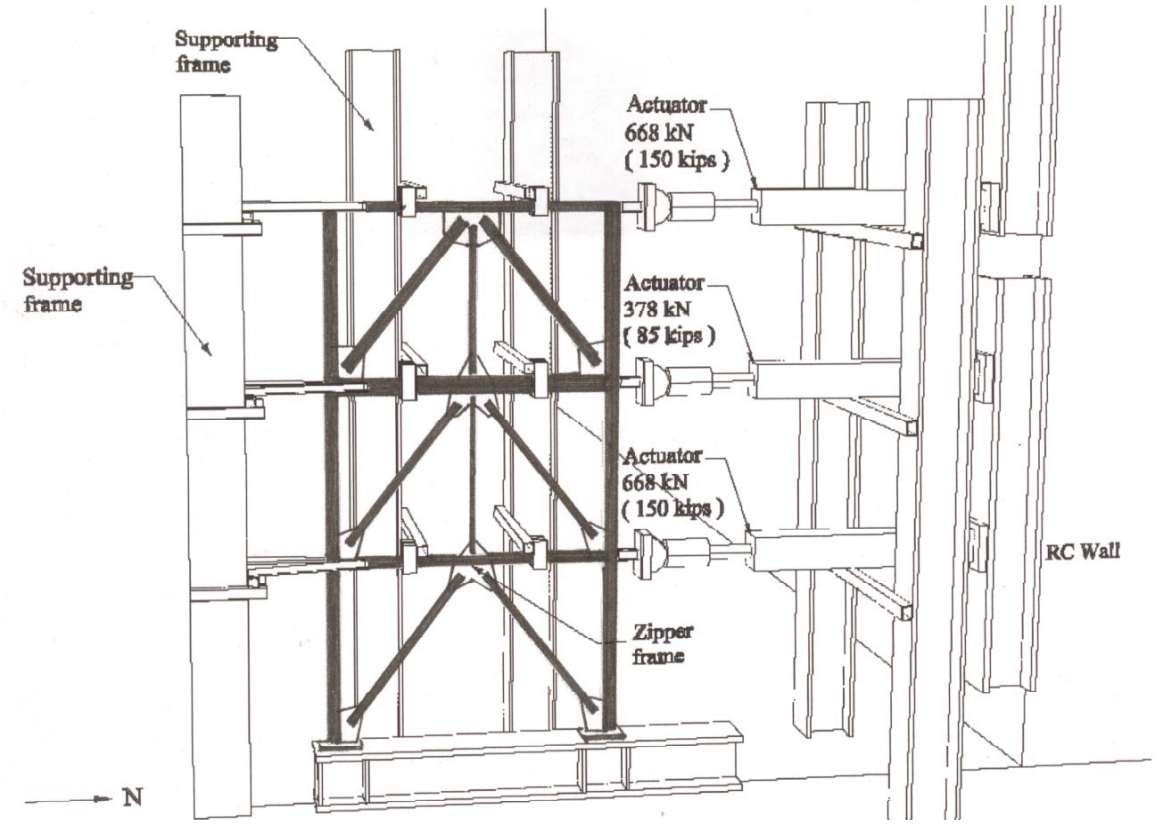

Figure 3.4 Experimental setup for the 1/3-scale zipper frame.

3.2.3 Instrumentation

In order to ascertain the actual system and element behavior, a large portion of the instrumentation was located close to but not on yielding regions. The instrumentation was intended to provide sufficient duplicative measures to ensure that all the forces in the members and joints could be verified by at least two independent methods. The overall instrumentation consisted of 112 channels, with a mixture of strain, displacement and load transducers. Figures 3.5 and 3.6 show the details of the instrumentation. A list of channels for instrumentation is shown in Appendix B. In addition, three video camcorders were used to record the first- and second-story deformations and the entire

front view of the experiment. Two digital cameras were used to take pictures of damage in each test stage. All this data has been input into the NEES data repository (https://central.nees.org/) and is available to other researchers with permission of the project P.I. The data will become public in 18 months.

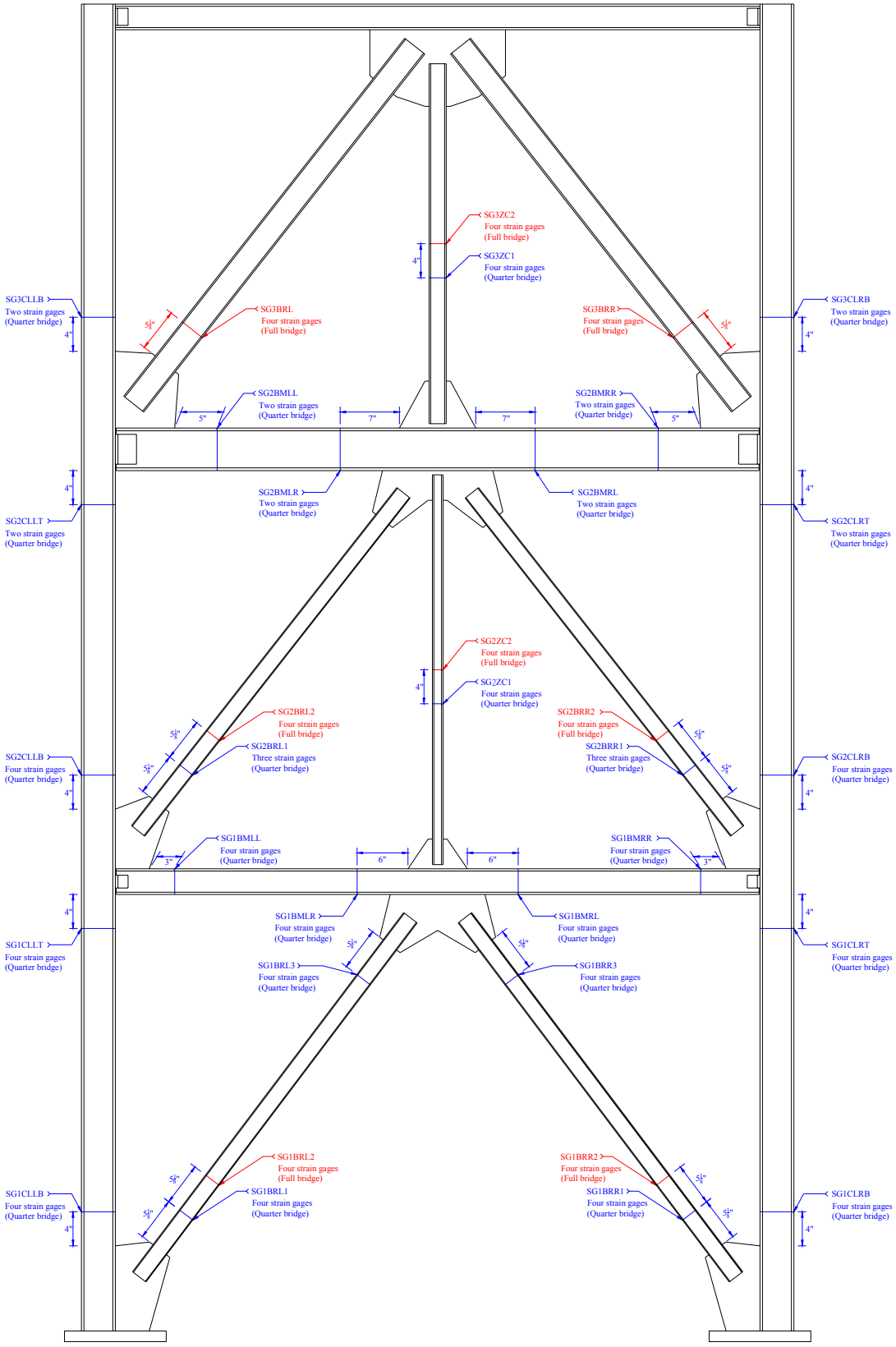

Figure 3.5 Locations and configurations of strain gages.

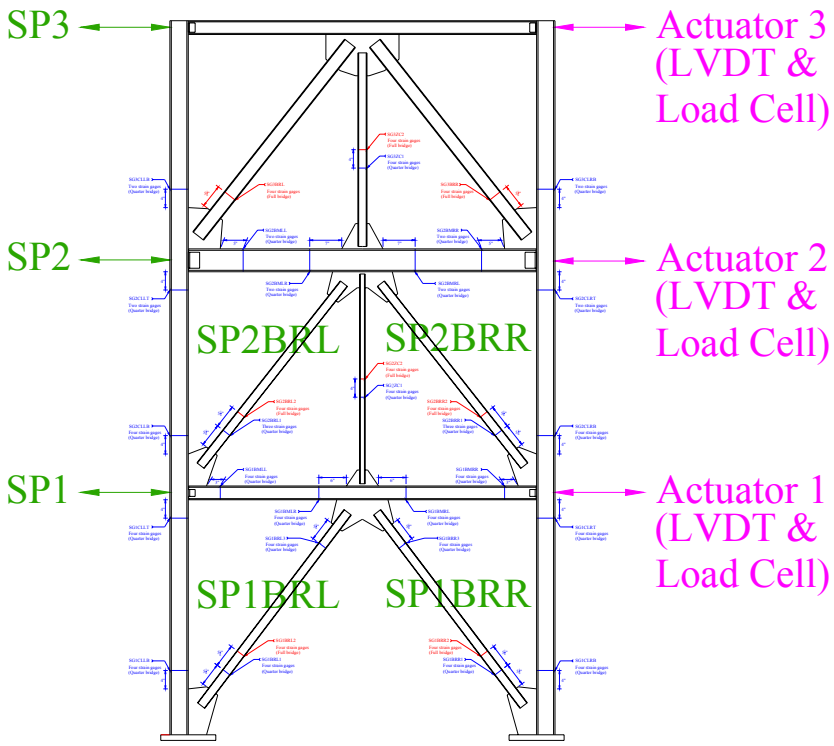

Figure 3.6 Arrangement of load and displacement transducers.

3.2.4 Applied Loading Histories

A set of three time histories of floor displacements (Figure 3.7) was input into three actuators at the floor levels of the test frame. These applied displacements were taken from the pre-experiment results of nonlinear static analyses of the reduced-scale model using OpenSEES. The OpenSEES model will be described in detail in Chapter 7. The analytical frame was subjected to a pushover loading consisting of an invariant lateral force distribution over the building height taken as $\mathbf{S}_1^* = \mathbf{m}\ \boldsymbol{\varphi}_1$, where $\mathbf{S}_1^*$ is the lateral force at each story shown in Figure 3.8, $\mathbf{m}$ is the mass matrix for which the second, third, and roof floor masses are 17.5 kN-s^2/m, 17.5 kN-s^2/m, and 19.3 kN-s^2/m,

respectively, and φ_1 is the first mode shape vector (Figure 3.8) (Chopra and Goel, 2002). The frame was pushed southwards (away from reaction wall, see Figure 3.4) to a roof displacement of +14.02 cm (+5.52 inches corresponding to roof drift ratio of +3.58%), then pulled northwards to -10.26 cm (-4.00 inches, -2.56%), and returned to -5.08 cm (-2.00 inches) where the base shear was close to zero.

The maximum positive value, 14.02 cm, of the roof displacement was designated as the target displacement. This value was the largest among the maximum roof displacements from the results of 20 nonlinear dynamic analyses performed on the model subjected to an ensemble of earthquakes, LA21 to LA40 (Somerville et al., 1997). In these analyses, four important assumptions were made. First, the damping ratios for the first and third modes were specified as 5% for constructing a Rayleigh damping spectrum. Second, the second-floor and third-floor beam-to-column connections were modeled as rigid instead of simple connections because of the considerable rigidity of the gusset plates connecting the brace, beam, and column in the model. Third, the ends of both the braces and suspended zipper struts were assumed as partially restrained connections with a rotational stiffness of 113 m-kN/rad (1000 in-kip/rad). This was meant to model a weak spring. Finally, the initial imperfection ratio of the braces was assumed to be $L_w/2000$. This initial imperfection was required to model the continuous out-of-plane displacements commonly observed in this member from the beginning of loading.

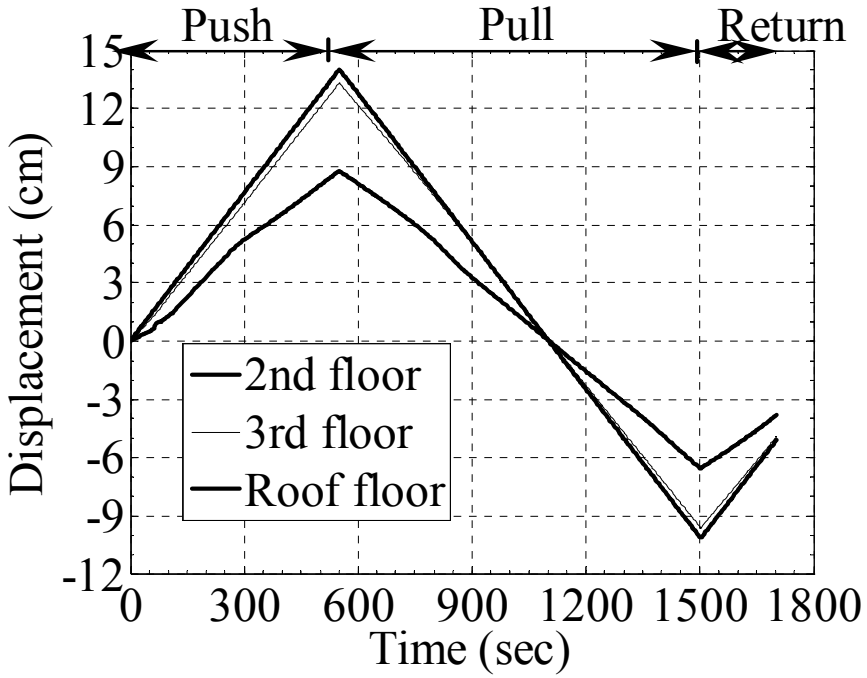

Figure 3.7 Applied displacement histories.

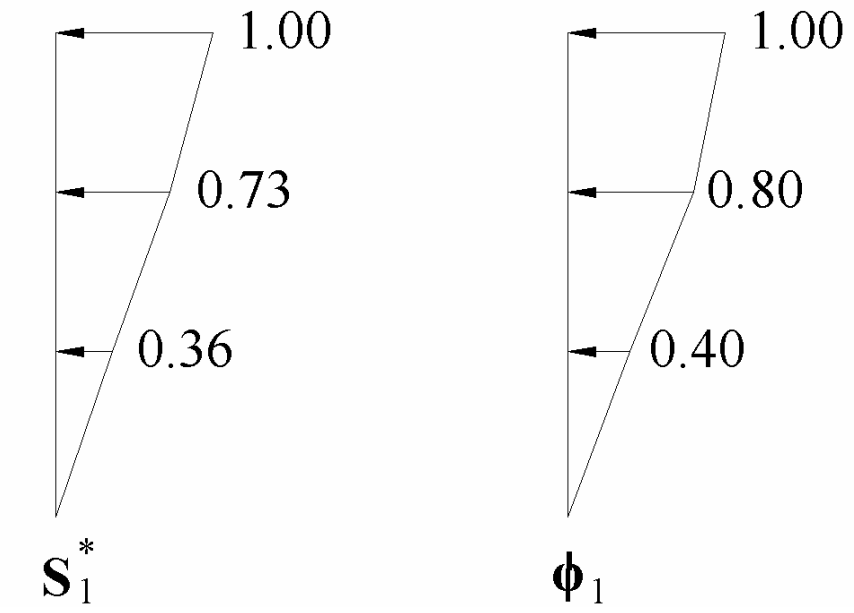

Figure 3.8 Force distribution $\mathbf{S}_1^*$, and first natural-vibration mode $\boldsymbol{\varphi}_1$

3.2.5 Estimation of the Axial Forces in the Braces

Although there were at least 8 strain gages configured as four quarter bridges and one full bridge in two sections of each brace, the data obtained from these strain gages is hard to interpret reliably once the braces had buckled. However, even though the brace had buckled, the adjacent members (beams and zipper struts) were still in the elastic range. By taking advantage of this feature and the concept of force equilibrium at the brace-beam-zipper strut intersection, as illustrated in Figure 3.9, the unknown in-plane axial forces in the braces can be computed throughout the load history by solving the following two simultaneous equilibrium equations:

$$(F_{brR} + F_{brL})_{,h} = H_{bmR} + H_{bmL} \quad (1)$$

$$(F_{brR} - F_{brL})_{,v} = V_{zc} + V_{bmR} + V_{bmL} \qquad (2)$$

in which F_{brR} and F_{brL} represent the axial forces in the right and left braces, respectively, H_{bmR} and H_{bmL} mean the axial forces in the right and left beams, respectively, V_{bmR} and V_{bmL} denote the shear forces in the right and left beams, respectively, and V_{zc} is the axial force of the zipper strut. The forces in the braces reported in this dissertation come from this type of analysis.

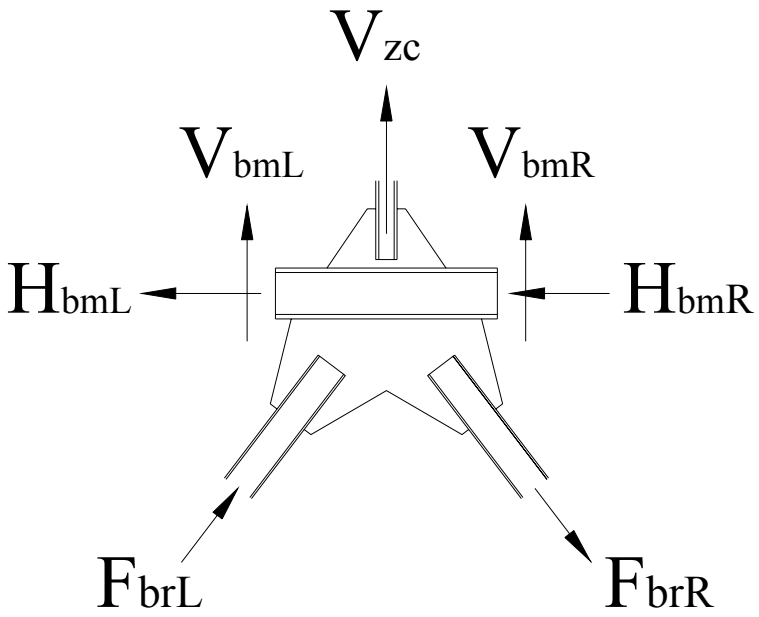

Figure 3.9 Force equilibrium at brace-beam-zipper strut intersections.

3.3 Test Results

3.3.1 Behavior of the Braces and Zipper Struts

During the pushing phase, inelastic out-of-plane buckling developed in the first-story south brace, with hinging occurring at the middle of the member and in the gusset plates. Figures 3.10 and 3.11 show the axial displacement vs. axial load for the first story braces; the forces were calculated as shown in the previous section, while the displacements came from the displacement transducers labeled SP1BRL and SP1BRR in Fig. 3.6.

From the experimental data shown in Figure 3.10, it appears that the first-story south brace buckled at an axial displacement of about -0.51 cm (-0.20") corresponding to

an axial load of -138 kN (-31 kips). As the lateral push was continued, the strength of this brace dropped gradually and approached its minimum post-buckling strength of about -36 kN (-8 kips), or 26 % of its first buckling strength. On the other side, the first-story north brace developed its tension ultimate strength of about 276 kN (62 kips), as shown in Figure 3.11. A summary of the measured maximum and minimum forces in the braces are listed in Table 3.4 and Table 3.5. The measured forces are further compared to the theoretical ones given by the expected yielding strength ($R_yF_yA_g$), expected strength ($R_tF_uA_g$), and expected buckling strengths with two different effective lengths of a brace.

The maximum difference in the vertical components of the axial forces sustained by the first-story braces can be estimated as 191 kN (43 kips) pulling down the second floor beam. This force exceeds the yielding strength, 178 kN (40 kips), of the second-story zipper strut, leading to yielding in the second-story zipper strut. This assessment of the unbalanced vertical force is in agreement with the measured axial force in the second-story zipper strut (Figure 3.12). For most of the test, the suspended zipper strut was subjected to tension forces, implying that the suspended zipper strut successfully transferred the unbalanced vertical forces into the second story.

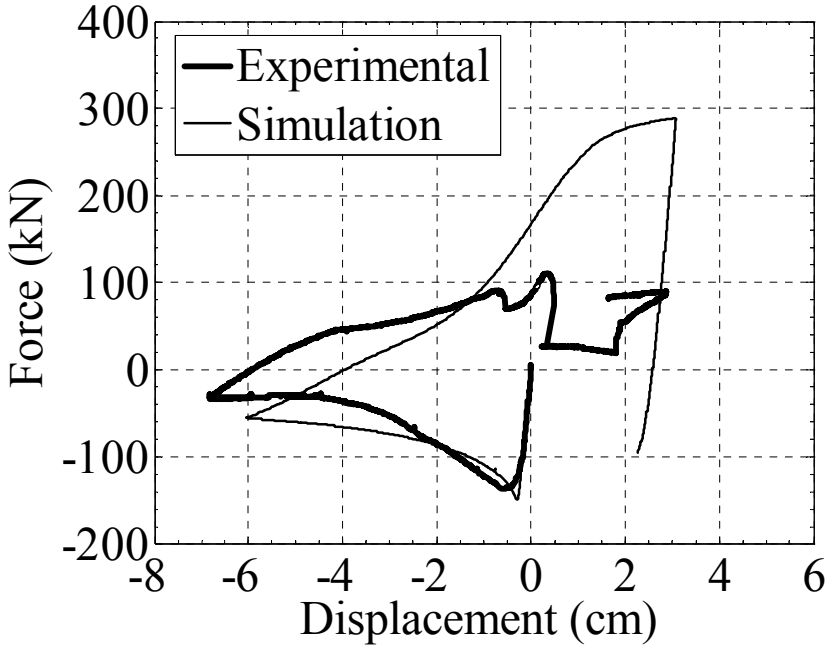

Figure 3.10 Hysteretic curve for the first-story south brace.

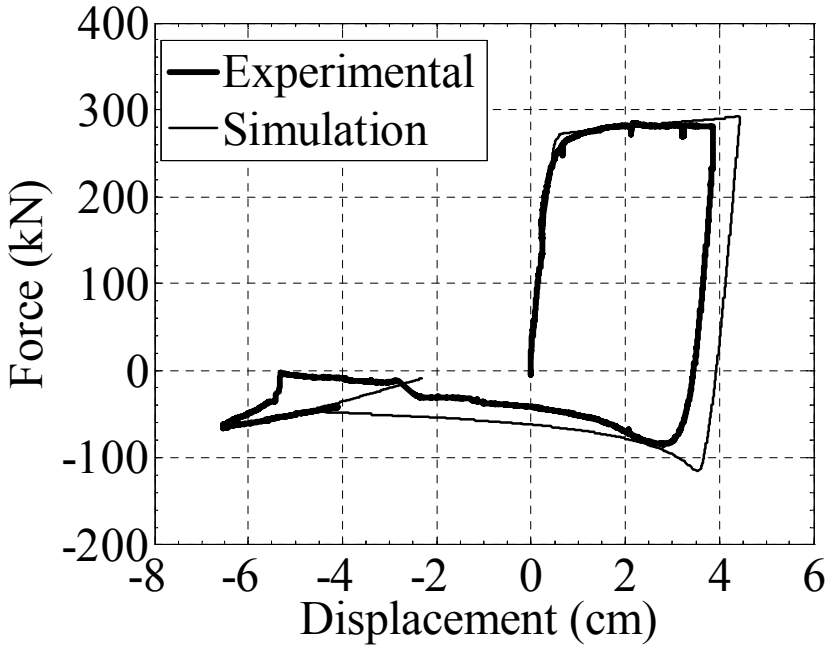

Figure 3.11 Hysteretic curve for the first-story north brace.

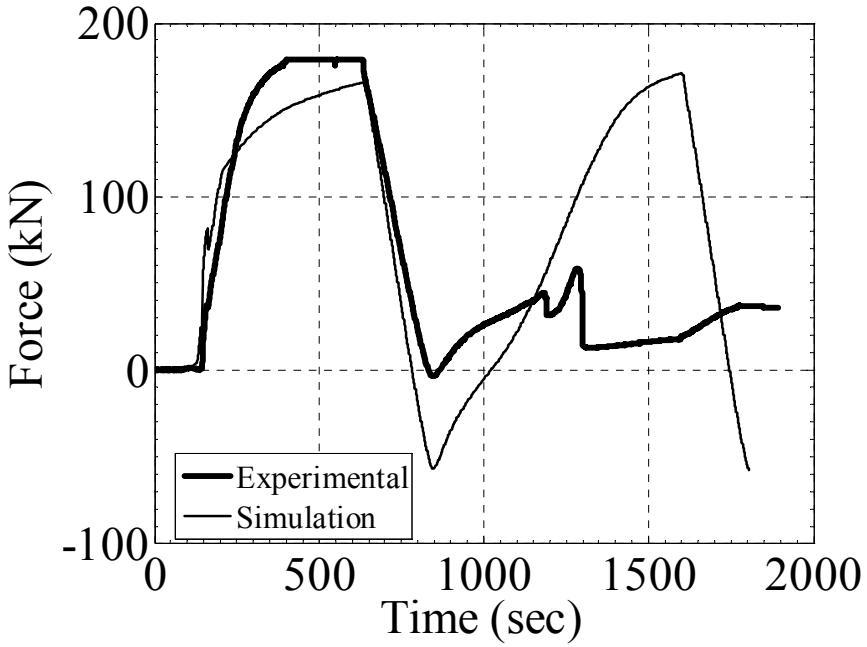

Figure 3.12 Force history for the second-story zipper strut.

Table 3.4 Comparisons between measured and theoretical tension forces.

Members		Measured maximum tension		Theoretical tension			
				Yielding		Strength	
				($R_yF_yA_g$)		($R_tF_uA_g$)	
Story	Braces	(kN)	(kips)	(kN)	(kips)	(kN)	(kips)
1	South	-	-	-	-	-	-
	North	276	62	224	50	282	63
2	South	-	-	-	-	-	-
	North	289	65	224	50	282	63

Table 3.5 Comparisons between measured and theoretical compression forces.

Members		Measured maximum compression		Theoretical buckling (R_yF_y & *kL/r, k=1*)		Theoretical buckling (R_yF_y & *kL/r, k=0.7*)	
Story	Braces	(kN)	(kips)	(kN)	(kips)	(kN)	(kips)
1	South	-138	-31	-143	-32	-168	-38
	North	-	-	-	-	-	-
2	South	-187	-42	-148	-33	-183	-41
	North	-	-	-	-	-	-

In the second story, buckling of the south brace occurred at an axial displacement of -0.51 cm (-0.20”), which corresponds to a force of about -187 kN (-42 kips), as shown in Figure 3.13. When the frame reached the target roof displacement, the compression force in the south brace decreased to -125 kN (-28 kips), while the force in the north brace showed extensive tension yielding at about 289 kN (65 kips) (Figure 3.14). The unbalanced vertical force generated by the second-story braces is estimated as about 129 kN (29 kips). Combining the yielding force of the second-story zipper strut and second-story unbalanced vertical force gives a total of about 307 kN (69 kips) pulling down the top-story hat truss system. Figure 3.15 shows that the third-story zipper strut was subjected to a maximum axial force of 289 kN (65 kip). This value is close to the estimated maximum transferred unbalanced vertical force of 307 kN (69 kips), indicating that most of unbalanced vertical forces had been transferred into the top story.

From the data discussed above, one can conclude that the expected loading path had been followed. Once the first- and second-story braces buckled, the induced unbalanced vertical forces were collected by the zipper struts and transferred to the top-story braces, forming a suspension frame system.

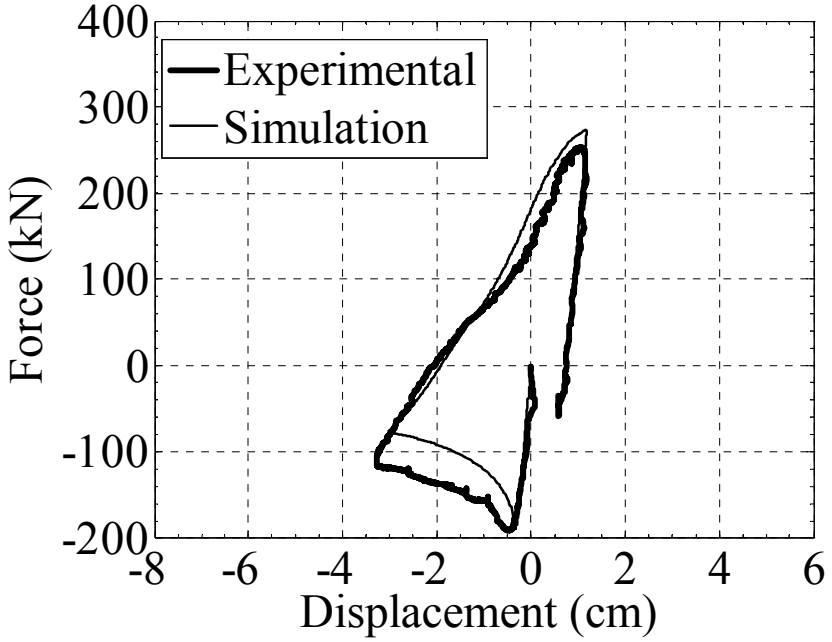

Figure 3.13 Hysteretic curve for the second-story south brace.

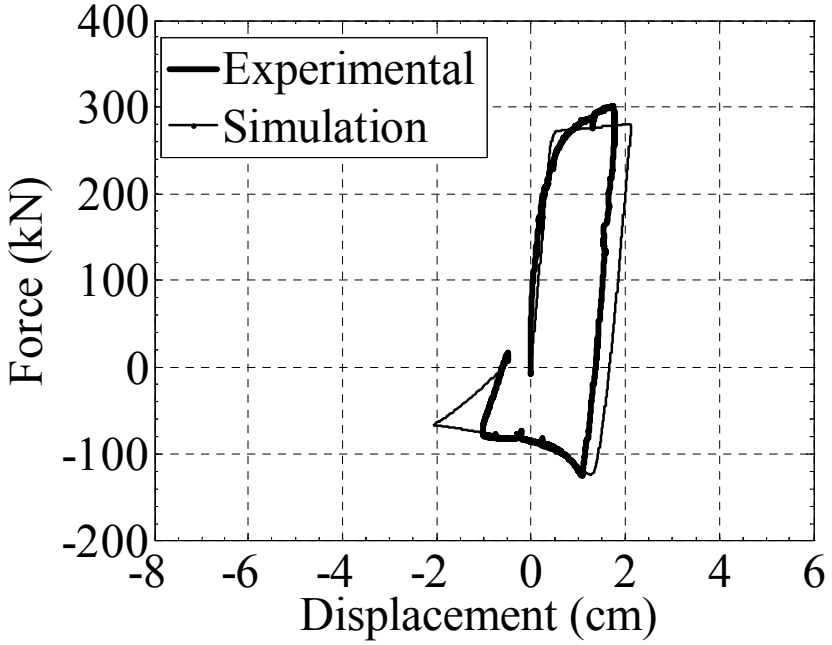

Figure 3.14 Hysteretic curve for the second-story north brace.

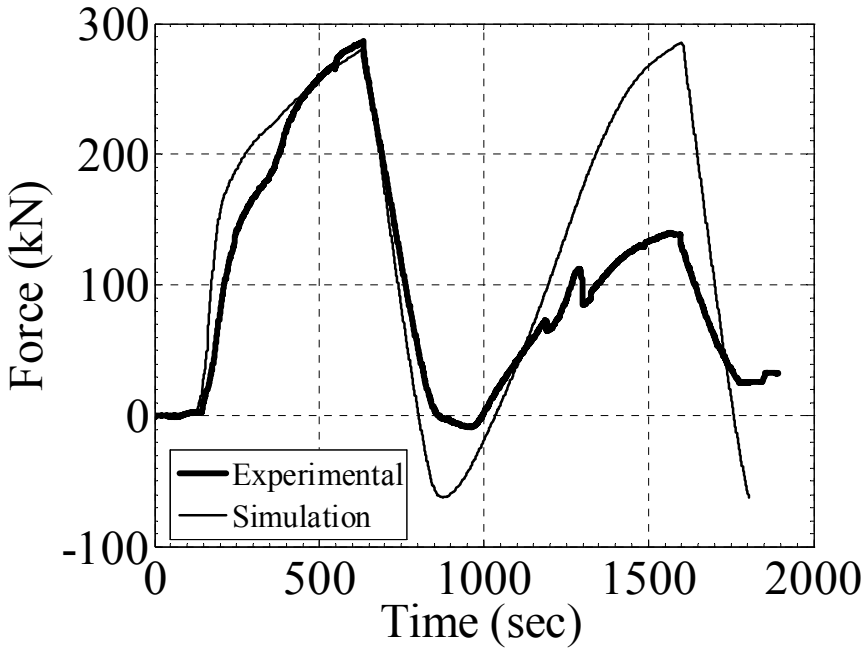

Figure 3.15 Force history for the third-story zipper strut.

3.3.2 Behavior of the Zipper-Braced Frame Model

As shown in Figure 3.16, the hysteretic behavior up to the target roof displacement can be represented approximately by a trilinear skeleton curve. The initial section corresponds to approximate linearly elastic behavior to Point A (Table 3.6). At Point A, the first-story south brace buckled, followed shortly by buckling of the second-story south brace at Point B (Table 3.6). As a result, the subsequent structural stiffness decreased. As the zipper frame was pushed to Point C, both the south column base and the first-story north brace started to yield (Table 3.6). The north column base yielded fully at a little beyond Point C, and the maximum lateral resistance of the zipper frame approached 280 kN (63 kips). At Point D (Table 3.6), the second-story zipper strut yielded. Upon further increases in roof displacement to Δ_r = 9.14 cm (3.60”), the second-

story north brace yielded. Finally, when pushed to the target roof displacement (Table 3.6), the zipper frame retained its maximum lateral-resistance capacity.

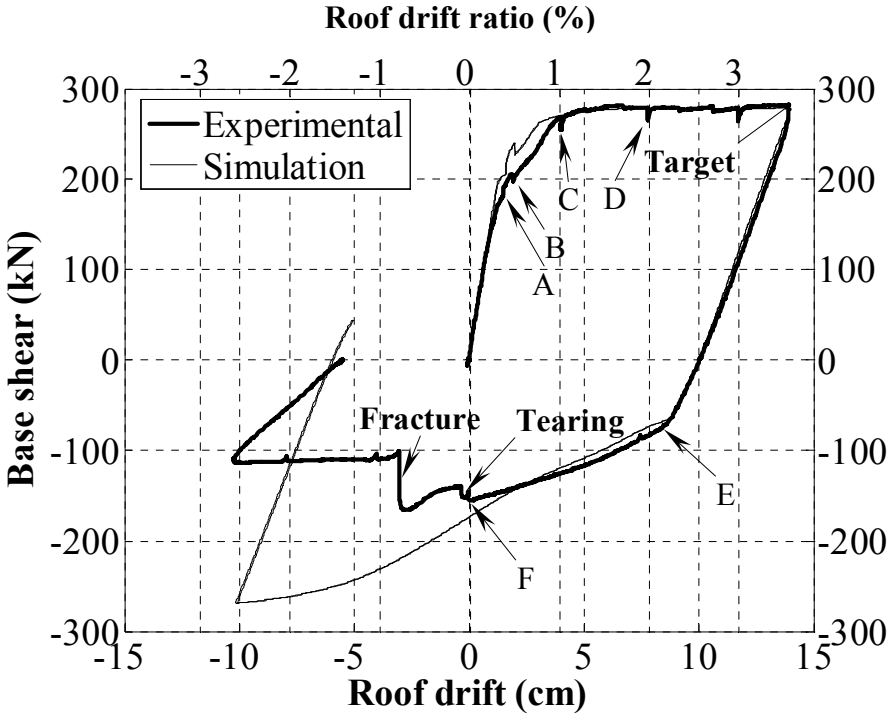

Figure 3.16 Hysteretic responses of the zipper-braced frame.

Table 3.6 Corresponding roof displacements and drift ratios as well as base shears.

Point	Roof displacement (Δ_r)		Drift ratio (α)	Base shear (V_{tot})	
	(cm)	(in)	(%)	(kN)	(kips)
A	1.52	0.6	0.39	187	72
B	2.29	0.9	0.58	205	46
C	3.81	1.5	0.97	271	61
D	7.62	3	1.94	276	62
Target	14.02	5.52	3.58	280	63
E	8.38	3.3	2.14	-76	-17
F	0.00	0.0	0.00	-156	-35
Fracture	-3.05	-1.2	-0.78	-102	-23

During the push test, in order to take some pictures of significant damage to the zipper frame and its individual members, the actuator displacements were paused at roof drift ratios of 1.00, 2.00, 3.00 %, and the target drift (Table 3.6). Figure 3.17 shows the deformation of the first story at a roof drift ratio 1.00%, in which the initial out-of-plane buckling of the south brace is evidenced by a large transverse displacement at midlength. A similar pattern but with a smaller displacement was also observed in the second-story south brace. At roof drift ratio 2.00%, it is evident that a kink had formed in the first-story south brace as a result of the localization of local buckling at the midlength of the brace (Figure 3.18). Figure 3.19 shows the deformation of the zipper frame at the target displacement. Both the first- and second-story south braces had significant plastic kinks at midlength and plastic hinges at the adjacent gusset plates. Extensive tension yielding of the first-story north brace and more limited yielding of the second-story north brace were also observed. At this stage plastic hinges had formed in the top and bottom sections of the first-story columns.

Figure 3.17 Deformation of the first story at roof drift ratio 1.00%.

Figure 3.18 Deformation of the first story at roof drift ratio 2.00%.

Figure 3.19 Deformation of the zipper frame at the target roof displacement.

Once the initial target displacement was reached (Figure 3.16), the zipper frame was unloaded and pulled back to the roof displacement -10.16 cm (-4.00”). When the zipper frame passed point E (Table 3.6), the first-story north brace initially buckled at a load of about -89 kN (-20 kips) (Figure 3.11), which was smaller than the first buckling

strength of -138 kN (-31 kips) of the first-story south brace (Figure 3.10). As the displacement was reversed, the north brace carried most of the lateral load as it had yielded extensively in tension during the initial push cycle. The heavily buckled south brace contributed little to the lateral resistance. Upon further pulling to a roof displacement of 5.08 cm (2.00”), the second-story north brace also buckled at a load of about -124 kN (-28 kips) (Figure 3.14). This was smaller than the buckling strength of -187 kN (-42 kips) of the second-story south brace (Figure 3.13). As the original position of the roof was reached (Point F), a portion of the middle of the first-story south brace, which had experienced local severe buckling during the pushing test, began to tear due to large tension force developed in the brace. At a roof displacement of -3.05 cm (1.20”), the torn section completely fractured, and the strength of the zipper frame decreased from -169 kN (-38 kips) to -102 kN (-23 kips). The deformation at a roof drift ratio of -1.00% is shown in Figure 3.20.

Figure 3.20 Deformation of the zipper frame at roof drift ratio of -1.00%.

3.3.3 Out-of-plane Buckling Trajectories of the First-story Braces

The brace design concept used in this zipper frame allowed the braces to buckle out-of-plane. This is currently the most widely used approach in design for braced systems. However, a potential drawback of such design is that the out-of-plane

deformation of the buckled braces will damage the adjacent nonstructural elements. Figure 3.21 shows the horizontal track of the middle point of the first-story south brace. In the pushing stage (OAB), the track could be interpreted as consisting of an approximate bilinear skeleton curve. In the first segment (OA), as the middle point of the brace moves to the south by about -1.27 cm (-0.50”), the out-of-plane deformation increases sharply from 0.00 cm (0.00”) to 8.89 cm (3.50”). In the subsequent segment (AB), the out-of-plane deformation increases gradually to 17.27 cm (6.80”), while the in-plane deformation increases to -5.59 cm (-2.20”). Unlike the first-story south brace, the first-story north brace was subjected to extensive tension yielding and elongation prior to going into compression. For this case, the out-of-plane deformation increased gradually up to 19.81 cm (7.80”), as shown in Figure 3.22. From comparing data in Figure 3.21 and in Figure 3.22, the out-of-plane deformation in the first-story north brace is clearly larger than that in the south brace.

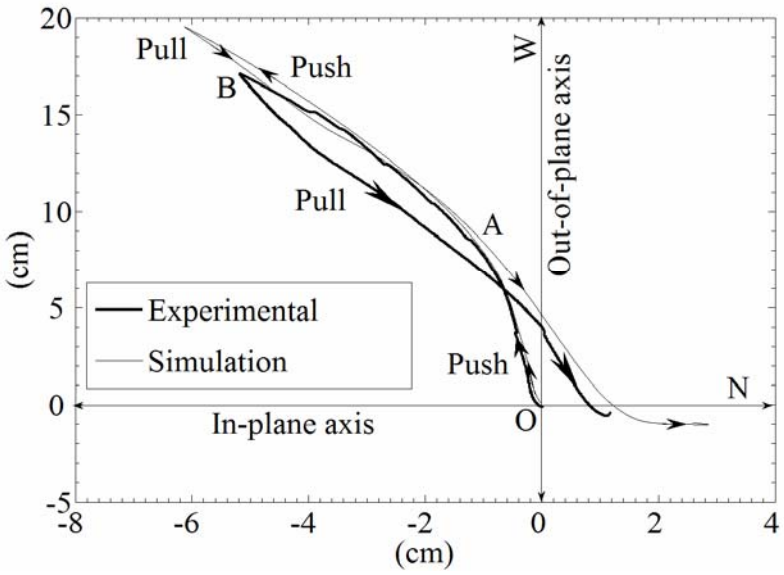

Figure 3.21 Horizontal track of the middle point of the first-story south brace for out-of-plane buckling during the pushing test.

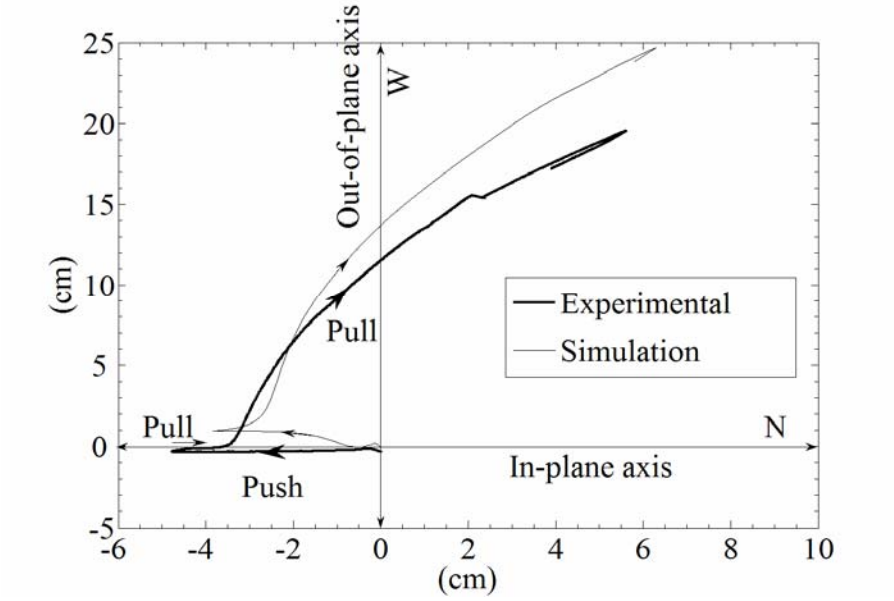

Figure 3.22 Horizontal track of the middle point of the first-story north brace for out-of-plane buckling during the pulling test.

3.4 Analytical Models

3.4.1 Two-dimensional Model

In order to get better match between the analytical and experimental results, the pre-experiment model having the bilinear behavior shown in Figure 3.23 was refined. Some adjustments in the parameters controlling the tensile strengths of the structural members and buckling strengths of the braces were made. In the refined model, the yielding strength of the beams and columns was increased to R_yF_y which is 379 MPa (55 ksi) instead of 345 MPa (50 ksi) (R_y is 1.1 for A572 Gr. 50 steel), while the yielding strength of the brace and zipper struts was increased to 427MPa (62 ksi) rather than 317 MPa (46 ksi) where R_y was set as 1.35 for A500 Gr. B steel, a little higher than the value 1.3 specified in the AISC Seismic Provisions. The initial imperfection ratios were increased from $L_w/2000$ to $L_w/200$ and $L_w/400$ for the first-story braces and second-story

braces, respectively. The end rotation spring stiffness for the first-story braces and second-story braces were decreased from 113 m-kN/rad (1000 in-kip/rad) to 45 m-kN/rad (400 in-kip/rad) and 68 m-kN/rad (600 in-kip/rad), for the first-story braces and second-story braces, respectively. The hysteretic responses of the refined model to the pushover loading are presented in Figure 3.16 and Figure 3.23.

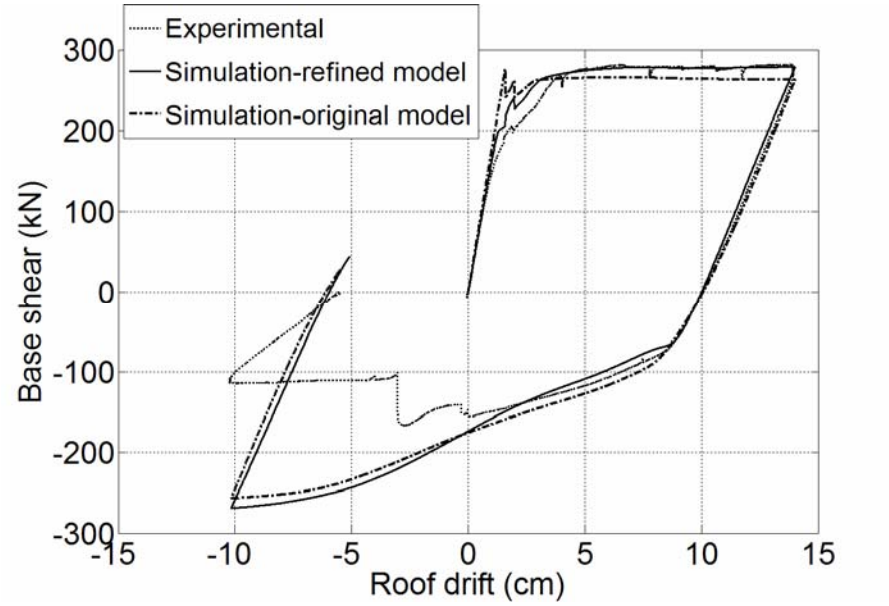

Figure 3.23 Comparisons of hysteretic responses between the test frame, refined, and original analytical models.

Comparisons of experimental results and results using the 2D refined model are presented in Figures 3.10 to 3.15. In general, the simulation can predict behavior satisfactorily until a portion of the middle section in the brace starts to tear. This is because the OpenSEES element used in these initial studies cannot simulate the reduction in the cross-section area after the brace begins to tear. Insofar as yielding and initial buckling strength, the analytical results are in good agreement with the experimental data. The analytical results confirmed the experimental observation that the initial buckling

strength of a brace subjected to tension first is smaller than that of a brace subjected to compression first.

3.4.2 Three-dimensional Model

A three-dimensional model was established for simulation of out-of-plane buckling of the braces. There are two major differences from the two-dimensional model. First, the initial imperfection ratio results from the out-of-plane direction. Secondly, for simplicity of simulation and predicting the maximum out-of-plane deformations of buckling, the connections of two ends of the braces are assumed to be pinned, that is, there is no end rotational spring specified in the brace ends. Figure 3.21 and Figure 3.22 illustrate that the 3D models can predict the trends of the real trajectories well but not generally the magnitude of the displacements. In Figure 3.21, the experimental and simulated lines in the segment of OA and the initial portion of segment of AB almost overlap. The maximum out-of-plane deformations obtained from simulation are larger than those from the experiment, which was expected because of the use of pinned end conditions.

3.4.3 Comparison between the Partial-height Zipper Mechanism with the Full-height Zipper Mechanism

In the typical zipper frame, in which there is no hat truss system in the top story, failure occurs when all the compression braces buckle and the generated unbalanced vertical forces pull all the beams down to form plastic hinges at their midspan. This failure mode is the so-called full-height zipper mechanism, which may lead a zipper SIVBF to become unstable if the beam-to-column connections and brace ends are pinned connections and the column bases form plastic hinges. This potentially unstable situation can be viewed as a geometrical nonlinear problem of a simple beam with a hinge at one end, a roller at the other, and one plastic hinge forming in the midspan due to a large

concentrated load applied at midspan. For this case, the load-deflection response depends primarily on the strain hardening ratio in the plastic hinge zone. In order to illustrate this issue, it was assumed that the brace-beam-column connections were not designed as FR connections and some re-analysis carried out for two other frames. In the first zipper frame model (Model 1), the original member sizes of the beams in the suspended zipper frame model were replaced by three W4x13 beams (W4x13 has 1.1 times M_p of S5x10), and the third-story braces were changed to the same size as the first- and second-story braces. As illustrated in Figure 3.24, this zipper frame showed significant degradation in strength immediately after the third peak, as a result of the buckling in the third-story compressive brace. This implies that these three beams are unable to sustain the unbalanced forces. In the second model (Model 2), the size of the beams was increased to W5×19 (has 2 times M_p of S5x10), and the response shows a strength decrease after buckling of the third story brace. If the beam size is increased, the unbalanced force generated in each story will be transferred completely through the beam to the column rather than through the zipper strut to the above braces which have not buckled yet. From the economical viewpoint, the strong beams are material-consuming and are not efficient, particularly in the case of a wide bay.

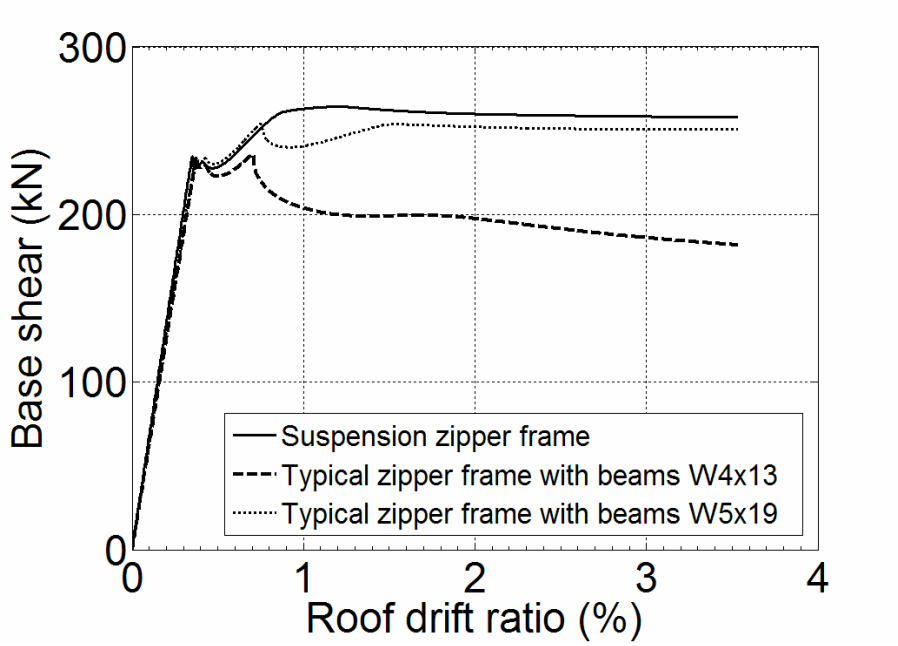

Figure 3.24 Comparison of pushover curves between the different zipper frames.

3.5 Conclusions and Recommendations

The performance of a special inverted-V-braced steel frame with zipper struts depends not only on the strength and ductility of the braces, but also on the sequence of yielding mechanisms. A coordinated experimental and analytical research program that focused on the pushover test of the 1/3 suspended zipper frame was conducted in an effort to better understand the performance of such frames, and to evaluate the adequacy of the preliminary design procedure. The following conclusions are drawn based on the results and observations presented herein.

1. The reduced-scale suspended zipper frame designed in compliance with the capacity design procedure exhibited great strength and ductility with a trilinear behavior. It remained stable when pushed to the target roof drift 14.02 cm (5.52”), or roof drift ratio 3.58%.

2. The residual strength of the frame, 37% of the ultimate strength, was considerable even after one first-story brace fractured and another one had severe compression buckling and tension yielding.
3. The theoretical load path was validated through this pushover test. Once buckling had occurred in the braces, the zipper strut functioned as a tension member, providing support at mid-span of the floor beams and transmitting the unbalanced vertical forces upwards to mobilize the unbuckled braces.
4. The second-story zipper strut exceeded its yielding strength slightly and the third-story zipper strut strength almost yielded when the zipper frame was pushed to the target roof drift. This is consistent with the theoretical expectations in the process of design of this zipper frame, and emphasizes the need in design to use expected values for material properties and a conservative estimate of the residual buckling strength.
5. Analytical results computed from relatively simple 2D and 3D models can predict the pushover curve of the zipper-braced frame and estimate the maximum deformation of out-of-plane buckling in the braces.
6. Suspended zipper-braced frames have better performance and are more stable and economic than typical zipper-braced frames.

CHAPTER 4

CYCLIC BEHAVIOR OF ZIPPER-BRACED FRAMES

4.1 Introduction

Following initial analytical and experimental pushover studies on the three-story zipper frame described in Chapter 3, a series of quasi-static cyclic tests were carried out on two reduced-scale models. One was subjected to a large near-fault ground motion (LA22 record) and one to a long, far field ground motion (1985 Chile record) in an attempt to bracket the behavior of this new structural system. The results of this experimental work are reported in this chapter.

4.2 Test Program 1: LA22 Record

4.2.1 Similitude Requirements

As noted previously, the scale of the specimen was controlled by the need to test a similar model on the shake table at the University at Buffalo. Table 4.1 summarizes the scale factors obtained from similitude considerations for the earthquake response of a structure. In this dissertation, a scale factor is defined as a ratio of a certain quantity of the model to the same quantity of the prototype. For instance, the sizes of the members for the reduced-scale model of the zipper frame, as listed in Table 3.2, were determined on the basis of the products of the geometrical scale factors and the known member properties in the prototype. As shown in the column of the modified scale factors in Table 4.1, the scale factor for acceleration was increased to 2, rather than usual 1, since the shake table could not handle the design mass for the prototype. This adjustment in the scale factor for acceleration resulted in a shorter time for the entire load history (time scale factor was reduced from $1/\sqrt{3}$ to $1/\sqrt{6}$) and in less mass in the model than in the

prototype (the mass scale factor decreased from 1/9 to 1/18). As the earthquake acceleration in the model should be twice the earthquake acceleration in the prototype, the reduced-scale frame was subjected to displacements corresponding to 200 % of the LA22 acceleration in these quasi-static tests. However, in the discussion of these quasi-static tests, the displacements corresponding to the 200 % acceleration will be labeled as the 100 % LA22 and 100 % 1985 Chile cases for consistency.

Table 4.1. Summary of scale factors for earthquake response of the one-third-scale model.

Group	Quantity	Scale Factors for the 1/3 model	Modified Scale Factors for the 1/3 model
Geometry	**Linear dimension**	$S_L = 1/3$	
	Area	$S_A = S_L^2 = 1/9$	
	Moment of Inertia	$S_I = S_L^4 = 1/81$	
Loading	**Force**	$S_Q = S_E S_L^2 = 1/9$	
	Acceleration	$S_a = \mathbf{1}$	$S_a = \mathbf{2}$
	Time	$S_t = [S_L S_a^{-1}]^{1/2} = \frac{1}{\sqrt{3}}$	$S_t = [S_L S_a^{-1}]^{1/2} = \frac{1}{\sqrt{3}} \times \frac{1}{\sqrt{2}} = \frac{1}{\sqrt{6}}$
Material properties	**Modulus**	$S_E = 1$	
	Mass	$S_m = S_Q S_a^{-1} = \mathbf{1/9}$	$S_m = S_Q S_a^{-1} = (1/9) \times \mathbf{(1/2)} = 1/18$

4.2.2 Applied Loading Histories

The displacement histories applied are shown in Figure 4.1. The applied floor displacement histories in Test 1, Test 2, and Test 3, corresponded to the responses of the model under 50%, 75%, and 100% of the LA22 earthquake, respectively. The LA22 ground motion with a peak ground acceleration of 0.92 g corresponds to the 1985 Takatori Kobe record in the fault-normal component. The applied displacements were taken from a nonlinear dynamical analysis of the reduced-scale model under the given

magnitude of the LA22 record. In these analyses, three assumptions were made: First, the damping ratios for the first and third modes were specified as 3% for constructing a Rayleigh damping spectrum. Secondly, the first-floor and second-floor beam-to-column connections were modeled as rigid instead of simple connections because of the considerable rigidity of the gusset plate connecting the brace, beam, and column. Thirdly, the ends of both the braces and suspended zipper struts were assumed as partially restrained connections with a rotational stiffness of 1000 kip-in/rad. The results of these analyses are shown as the analytical values in the figures in the following sections.

	Test 1	Test 2	Test 3
	(50% of LA22)	(75% of LA22)	(100% of LA22)
Time interval (one step):	1.0 sec	1.6 sec	0.4 sec
	Duration: 40.4 min	64.6 min	16.1 min

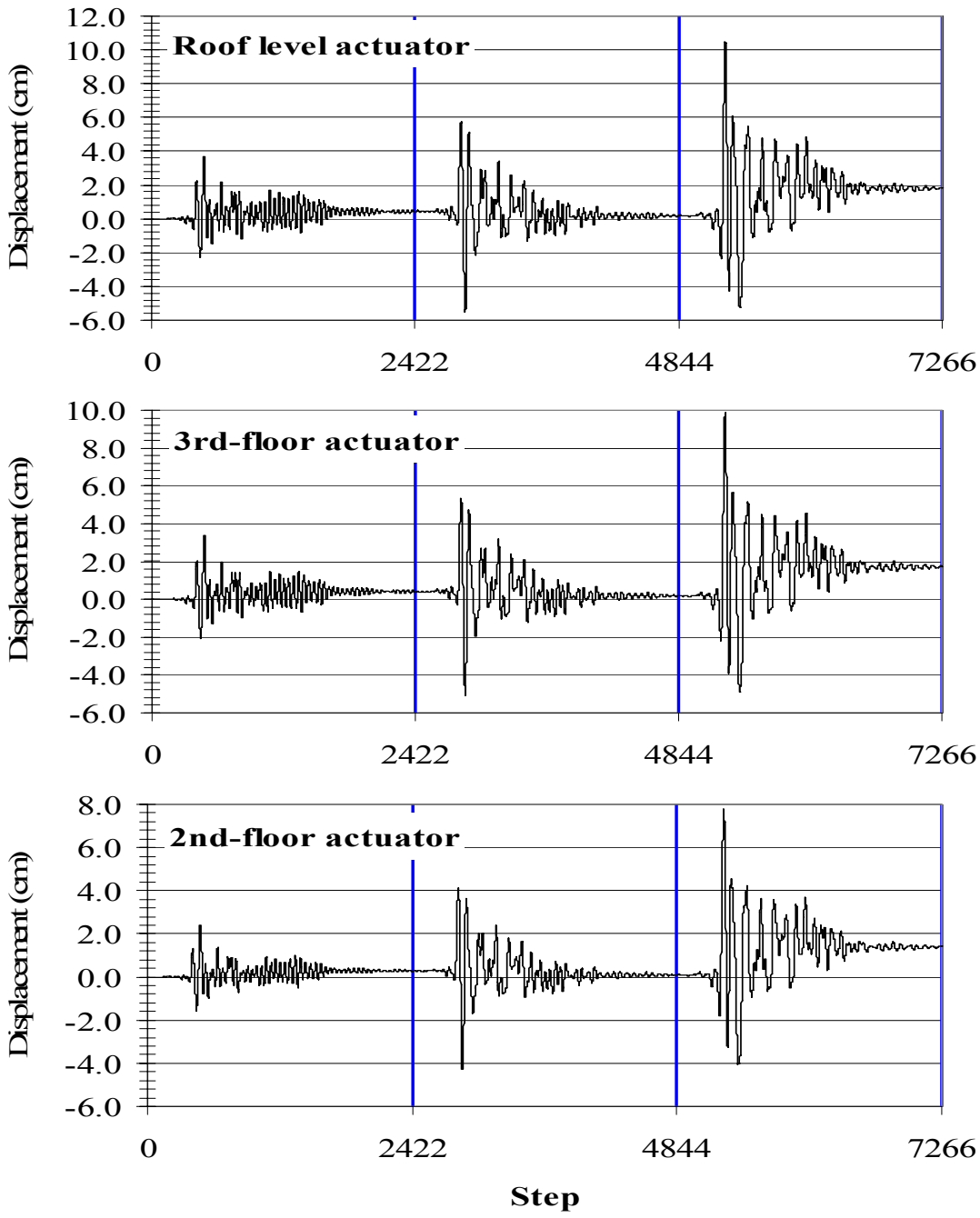

Figure 4.1 Applied displacement histories for 50, 75 and 100 % of the LA22 earthquakes.

4.2.3 Loading and Instrumentation

The loading and instrumentation schemes were identical to those used for the pushover test and described in Section 3.2.3. The performance of the instrumentation was verified through several load cycles of small deformation which subjected the frame to elastic base shear up to 16.7 % of its elastic capacity.

4.3 Response of the Test Frame to the LA22 Ground Motion

4.3.1 Test 1: 50% of LA22

In this initial test, inelastic out-of-plane buckling developed in the first-story south brace, with hinging occurring at the middle of the member and in the gusset plates. From the experimental data shown in Figure 4.2, it appears that the first-story south brace buckled at an axial load of about 151 kN (34 kips). Figure 4.3 shows that the first-story north brace yielded and carried about 267 kN (60 kips) in tension. As presented in Figure 4.4, the second-story zipper strut was subjected to tension forces for most of the test and its maximum tensile axial force was 98 kN (22 kips). This confirms that the zipper strut in the second story successfully transferred the unbalanced vertical forces generated by the braces below upon their buckling. As shown in Figure 4.5, the second-story south brace buckled slightly when the axial force reached about 178 kN (40 kips). However, the second-story north brace remained elastic and the reached maximum tension force was also near 178 kN (40 kips), as shown in Figure 4.6. These similar maximum tension and compression forces in the second-story braces caused little corresponding unbalanced vertical force throughout this load run. Due to this reason and the fact that the third-floor beam could provide some shear resistance, a smaller unbalanced vertical force acted in the third-story zipper strut as compared to the second-story, as shown in Figure 4.7.

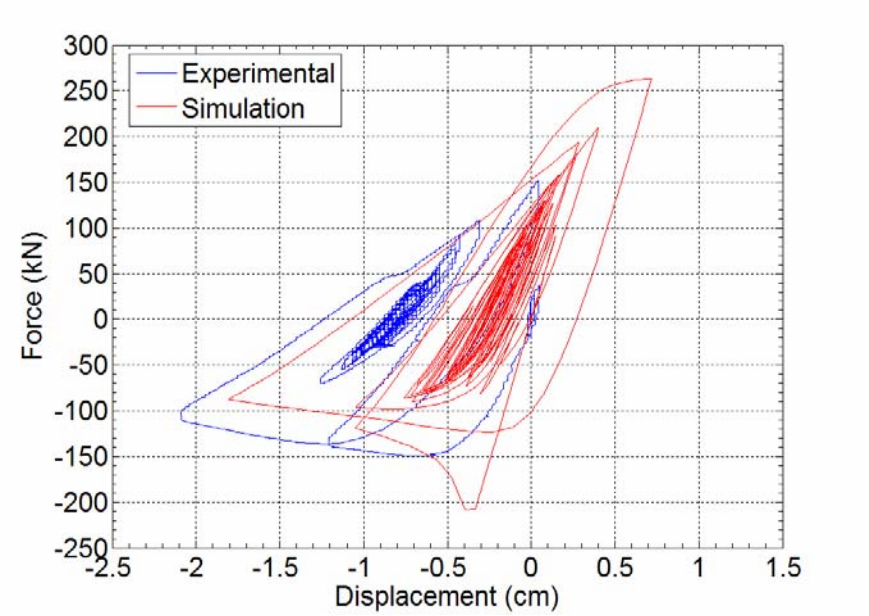

Figure 4.2 Hysteretic behavior of the 1st-story south brace (50% of LA22).

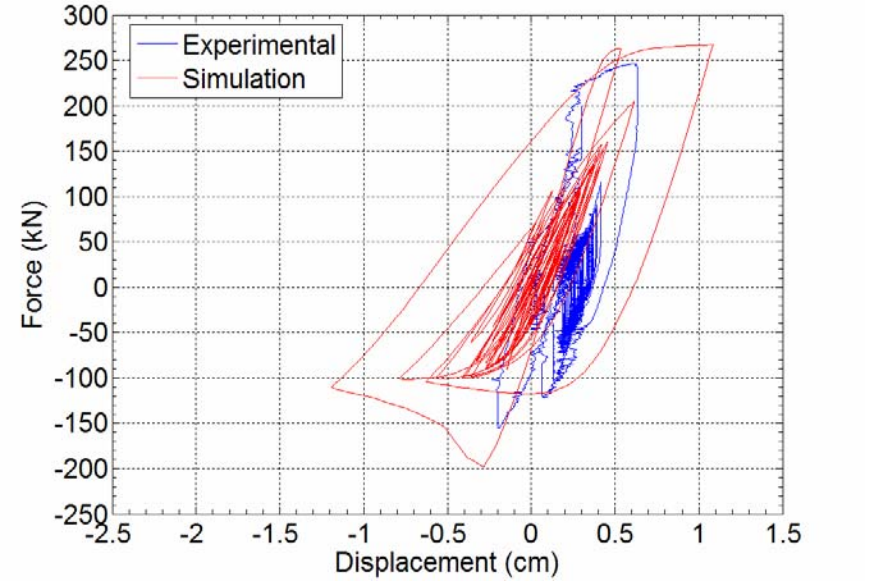

Figure 4.3 Hysteretic behavior of the 1st-story north brace (50% of LA22).

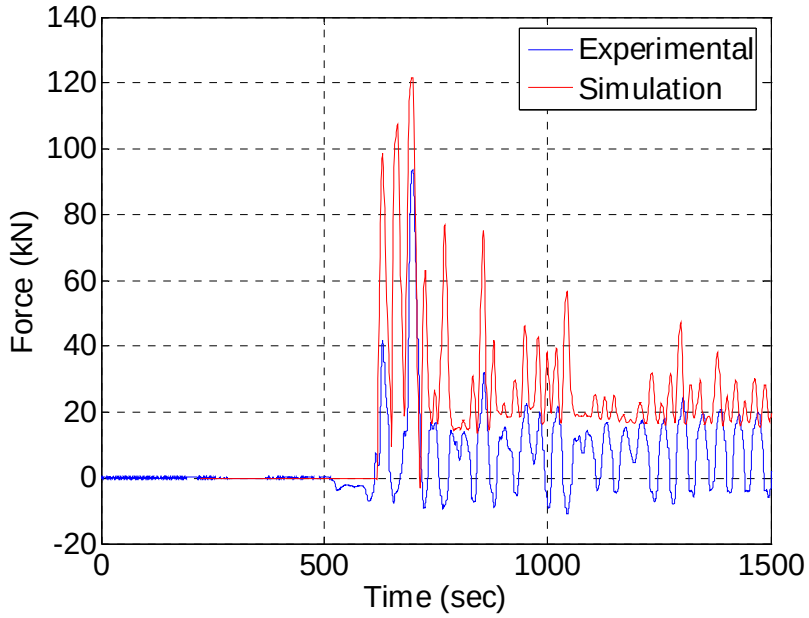

Figure 4.4 Force history of the 2nd-story zipper strut (50% of LA22).

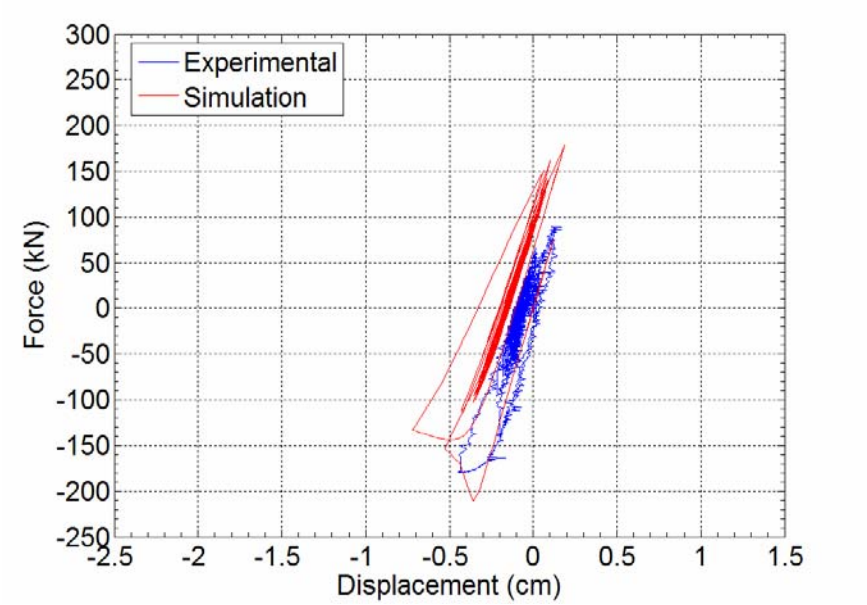

Figure 4.5 Hysteretic behavior of the 2nd-story south brace (50% of LA22).

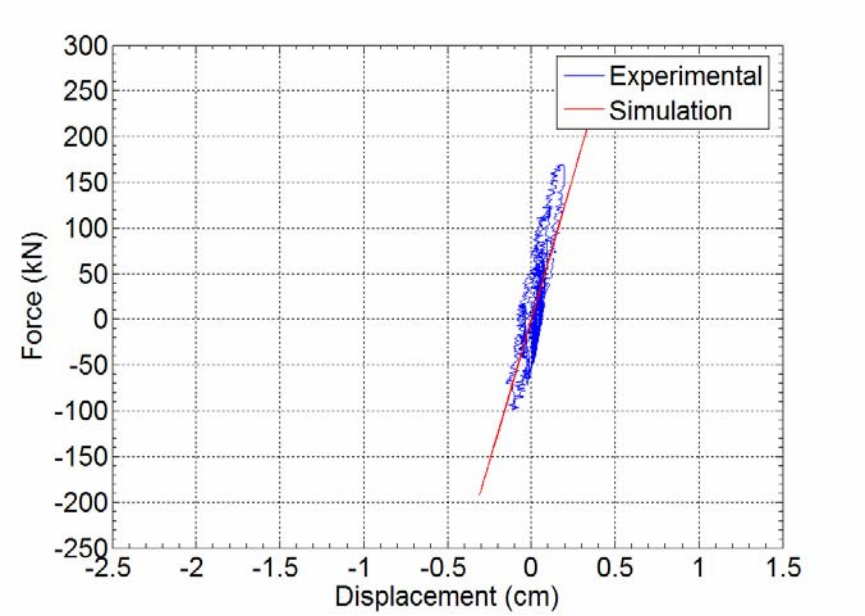

Figure 4.6 Hysteretic behavior of the 2nd-story north brace (50% of LA22).

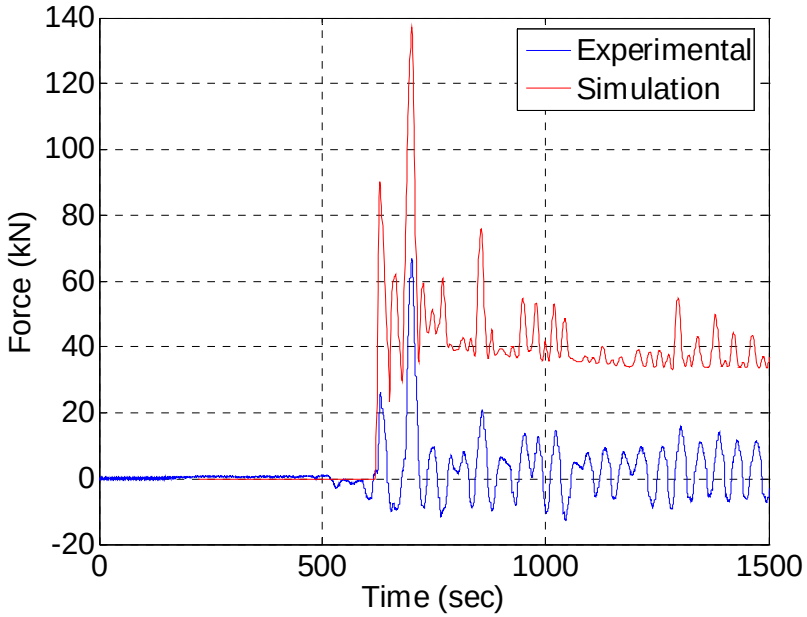

Figure 4.7 Force history of the 3rd-story zipper strut (50% of LA22).

Figure 4.8 presents the overall roof drift ratio vs. the base shear results. The bolted connections to the base beam and the actuators experienced some slip, leading to the pinching of the experimental curves observable in the figure. In the following tests, proper pretensioning at these locations limited such slip.

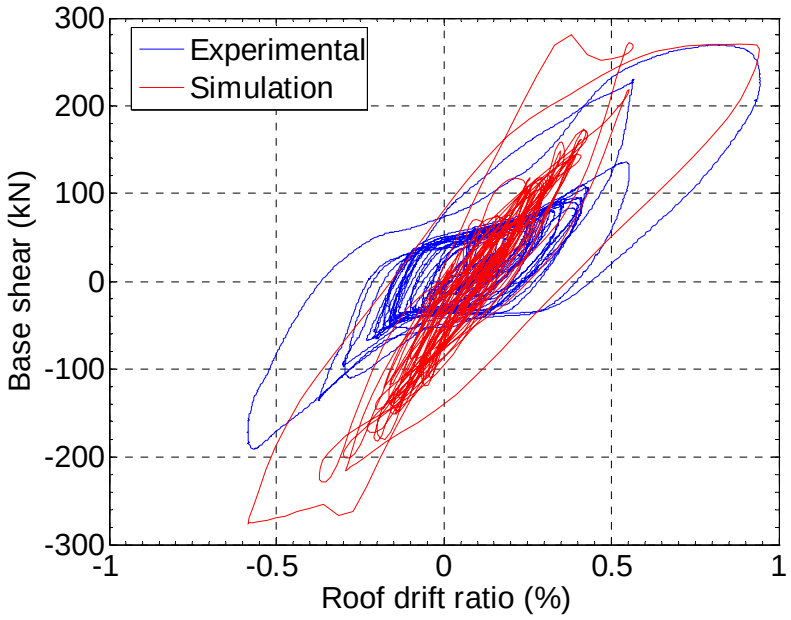

Figure 4.8 Hysteretic response of the zipper frame (50% of LA22).

4.3.2 Test 2: 75% of LA22

Following the 50% of LA22 tests, the same zipper frame was reused and loaded by the floor displacement histories corresponding to the response to 75% of LA22. To begin the test, the frame was displaced by the actuators to the residual displacements resulting from Test 1. These initial displacements were 0.257, 0.356, 0.366 cm (0.101, 0.140, and 0.144 in.) to the North with corresponding force of 0.294, 2.176, and -0.240 kN (0.066, 0.489, and -0.054 kips) in the first through third story, respectively. The shifting of the origin between analytical and experimental results shown in many of the

plots for the 75% and 100% cases is a result of a combination of (a) these initial displacements, (b) the smaller than anticipated unbalanced vertical force generated by the second-story braces, and (c) the redistribution of internal forces that resulted from small actuator movements in the days between the tests.

During the 75% test, both the first-story south and north braces evidenced significant buckling together with out-of-plane movement. From their hysteresis loops shown in Figure 4.9 and Figure 4.10, the post-buckling strengths decreased from -111 to -45 kN (-25 to -10 kips). In the second story, the braces buckled only slightly, with a residual strength decreasing to 11.79 kN (2.65 kips) for the left brace and -4.23 kN (-0.95 kips) for the right brace.

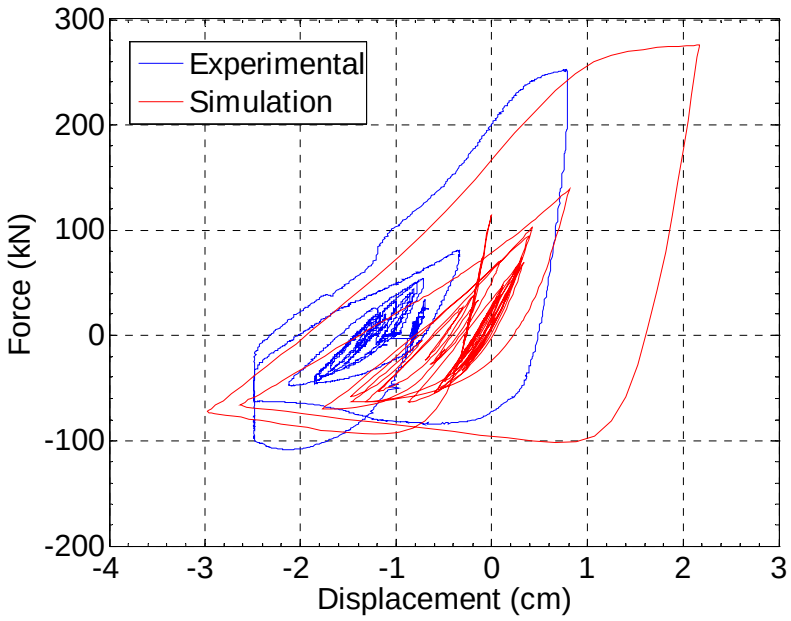

Figure 4.9 Hysteretic behavior of the 1st-story south brace (75% of LA22).

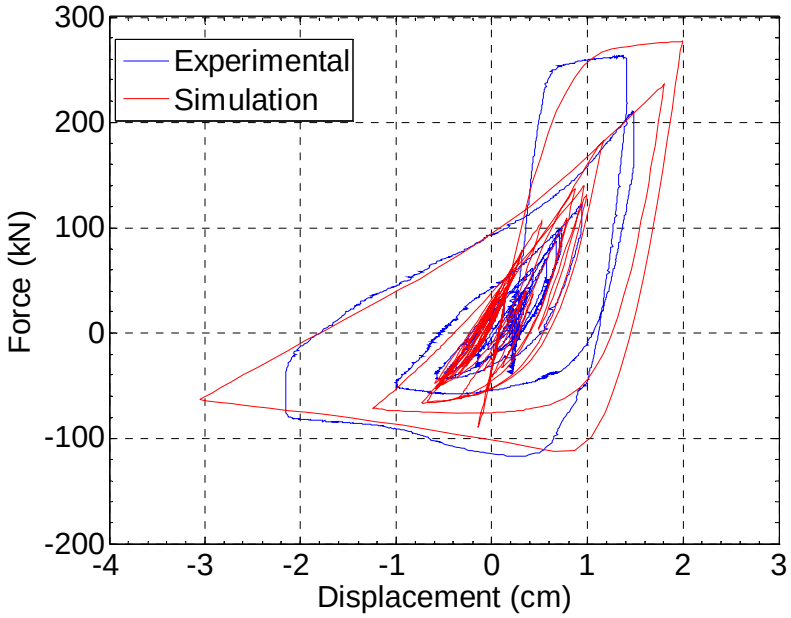

Figure 4.10 Hysteretic behavior of the 1st-story north brace (75% of LA22).

Figure 4.11 indicates that the second-story zipper strut was subjected to up to 129 kN (29 kips) of tension force and only a relatively modest -22 kN (-5 kips) of compression force. Most of the time, the strut carried only tensile forces. As shown in Figure 4.12, the third-story zipper strut behaved similarly to the second-story one. It sustained about the same maximum tension of 129 kN (29 kips), implying that it carried all the unbalanced vertical forces that were created in the first-story level as there was little contribution to the vertical loads from the second story. This is due to the fact that only slight buckling was noted in the second floor, and may also be attributable to the damage in the first story after the 50% run. Bending of the gusset plates in the first-story braces and yielding at the column bases were evident, as shown in Figure 4.13 and Figure 4.14. This is additional evidence that damage was localizing in the first story. However, the base shear vs. roof drift ratio curves (Figure 4.15) shows good energy-dissipating capability. Most of the pinching phenomena were eliminated. The only observable

pinching segments beginning after the largest push cycle were due to some slip between the ground and the base beam, irrelevant to the model itself behavior. The base shear at yield was about 267 kN (60 kips) with the maximum roof displacement approaching 5.8 cm (2.3 in), i.e., a roof drift ratio of 1.5%.

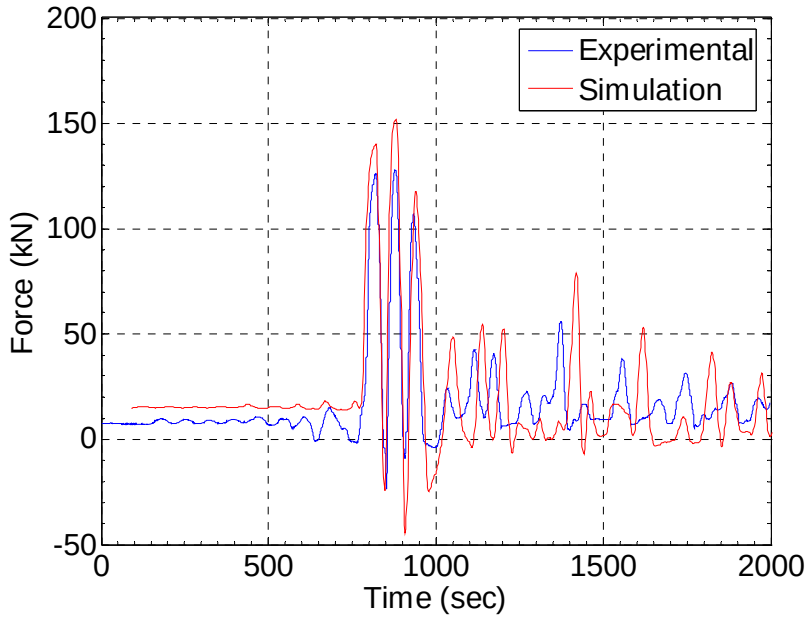

Figure 4.11 Axial load vs. time history of the 2nd-story zipper strut (75% of LA22).

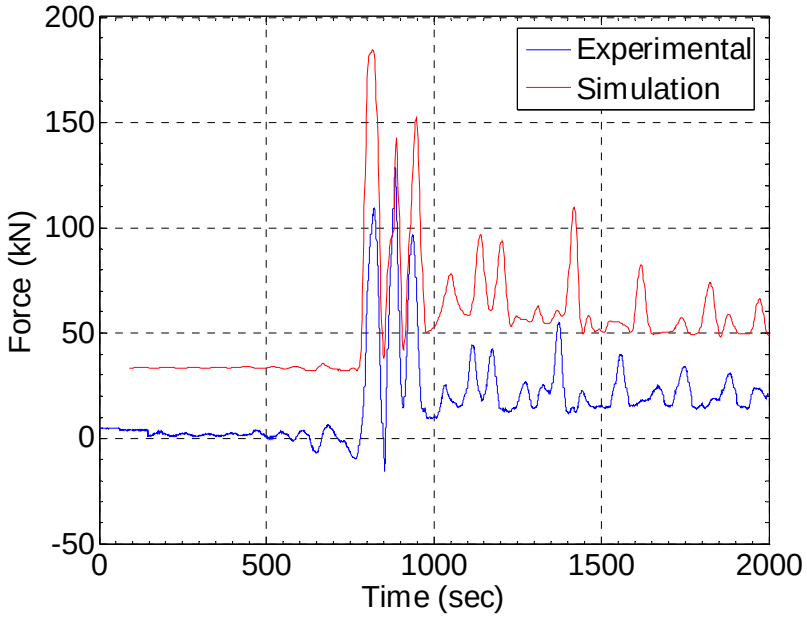

Figure 4.12 Axial load vs. time history of the 3rd-story zipper strut (75% of LA22).

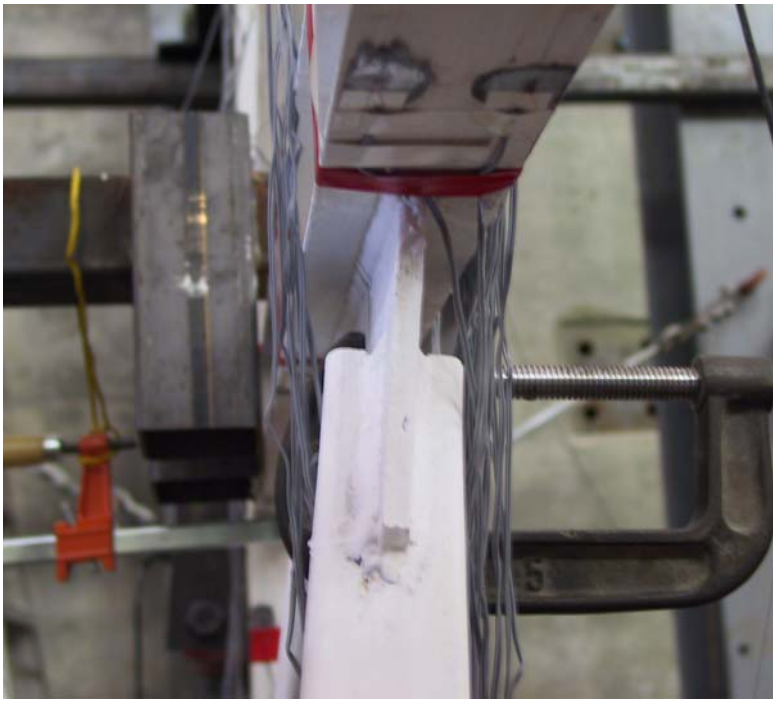

Figure 4.13 Gusset plate bent at the brace-to-beam intersection (75% of LA22).

Figure 4.14 Yielding at the column base (75% of LA22).

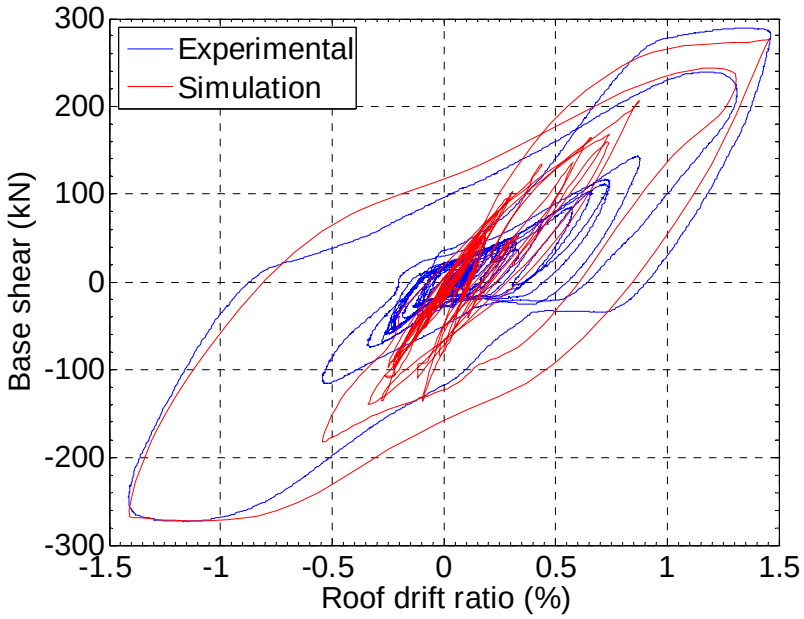

Figure 4.15 Hysteretic behavior of the zipper frame (75% of LA22).

4.3.3 Test 3: 100% of LA22

When subjected to 100% of LA22, the frame evidenced serious damage in the first story, as shown in Figure 4.16. The south brace fractured at the middle, while a very large residual buckling deformation was observed in the north brace. During the test, when the south brace was subjected to large tension, it had a partial fracture at mid-span, with a sudden drop in tensile strength. In the following cycle, a complete fracture occurred. On the other first story brace, a large tensile deformation [2.8 cm (1.1 in) or about 2% strain), as shown in Figure 4.17, was followed by a large post-buckling strength decrease from -45 kN (-10 kips) down to 9 kN (-2 kips).

In the second story, the braces had small residual displacements after the test (Figure 4.18). The second- and third-story zipper struts sustained 156 kN (35 kips) and 236 kN (53 kips), respectively when the frame was pushed to its largest deformation (Figure 4.19 and Figure 4.20). The difference in the axial forces between the second- and third-story zipper struts resulted from the second-story unbalanced vertical force due to buckling of the second-story south brace.

As presented in Figure 4.21, degradation in the base shear at Point A arises from fracture of the first-story south brace. After the largest cycle, when the zipper frame was pulled (negative base shear), the maximum base shear reached only -178 kN (-40 kips) rather than the previously maximum of 285 kN (64 kips).

Figure 4.16 First-story deformation (100% of LA22).

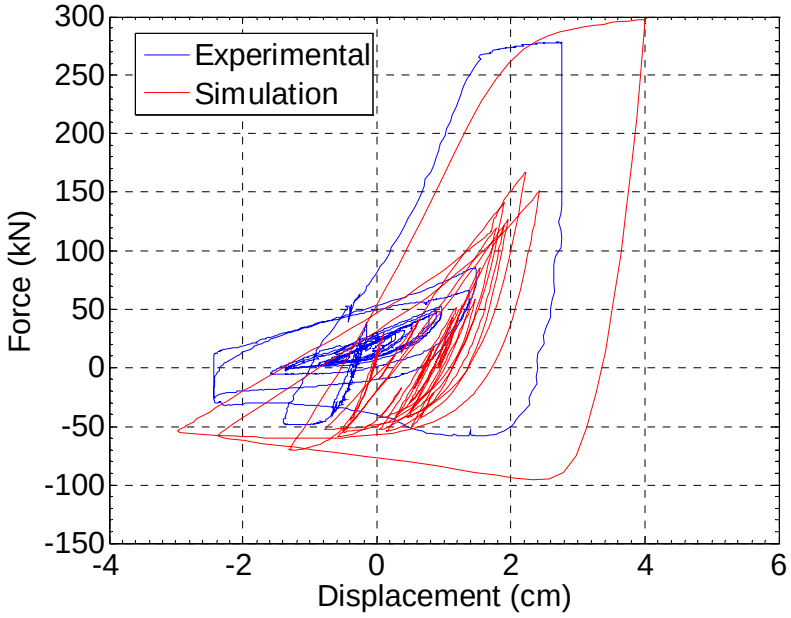

Figure 4.17 Hysteretic behavior of the 1st-story north brace (100% of LA22).

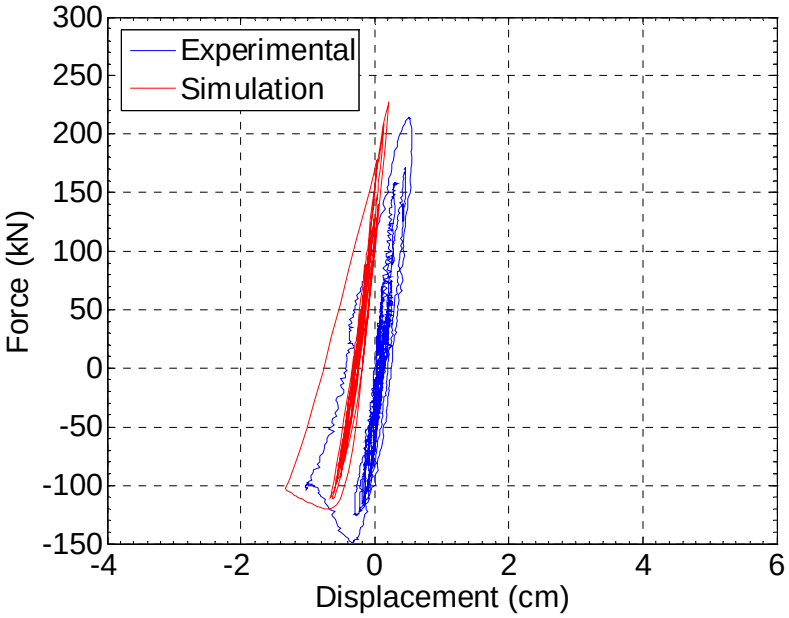

Figure 4.18 Hysteretic behavior of the 2nd-story south brace (100% of LA22).

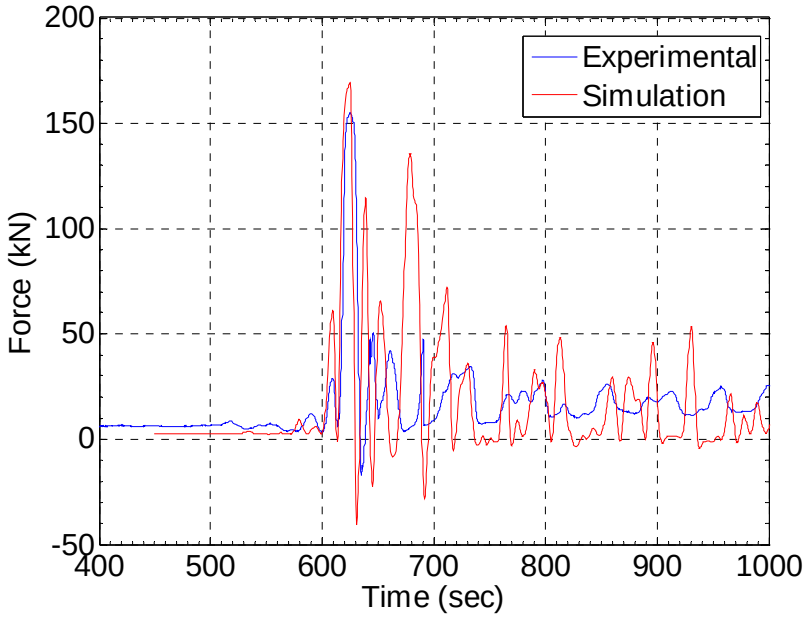

Figure 4.19 Force history of the 2nd-story zipper strut (100% of LA22).

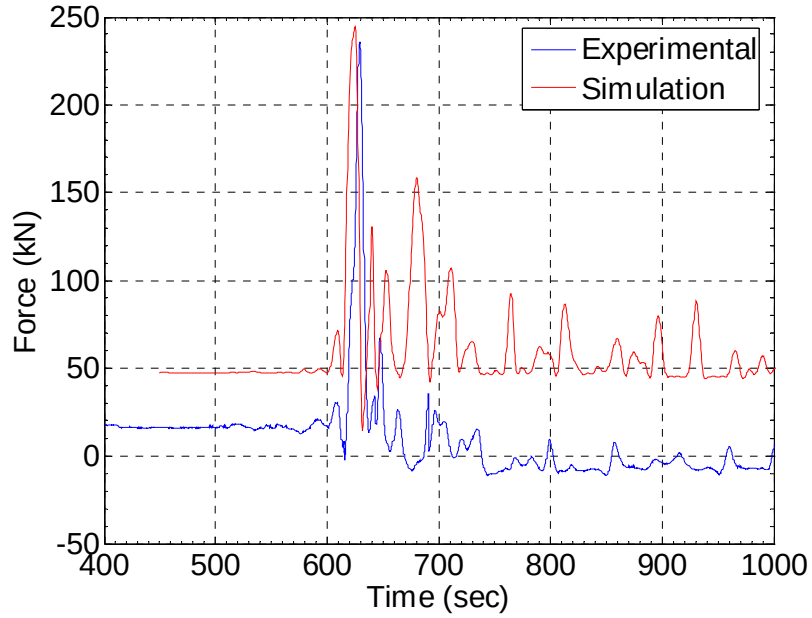

Figure 4.20 Force history of the 3rd-story suspended zipper strut (100% of LA22).

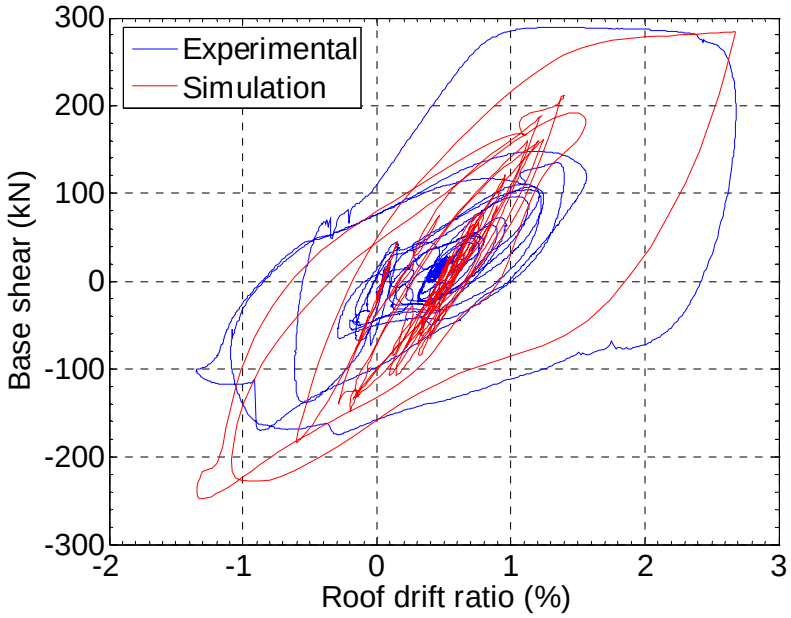

Figure 4.21 Hysteresis behavior of the suspended zipper frame (100% of LA22).

4.4 Test Program 2: 1985 Chile Record

4.4.1 Similitude Requirements

The similitude requirements were identical to those used for the LA22 test and described in Section 4.2.1.

4.4.2 Applied Loading Histories

The displacement histories applied are shown in Figure 4.22. The applied floor displacement histories in Test 1 and Test 2 corresponded to the responses of the model to 150% and 200% of the Chile earthquakes, respectively. This Chile ground motion, with a peak ground acceleration of 0.71 g, was recorded at the Llolleo station in 1985. The Llolleo station was located about 60 km from the epicenter and has an effective duration of 116 seconds. This source record was further magnified by 150 and 200 % (to a PGA of 1.07 and 1.42 g, respectively) to cause large compression buckling of the braces. The applied displacements were again taken from a nonlinear dynamical analysis of the reduced-scale model using the same assumptions as in Section 4.2.2.

	Test 1	Test 2
	(150% of Chile)	(200% of Chile)
Time interval (one step):	0.3 sec	0.3 sec
Duration:	67.21 min	67.21 min

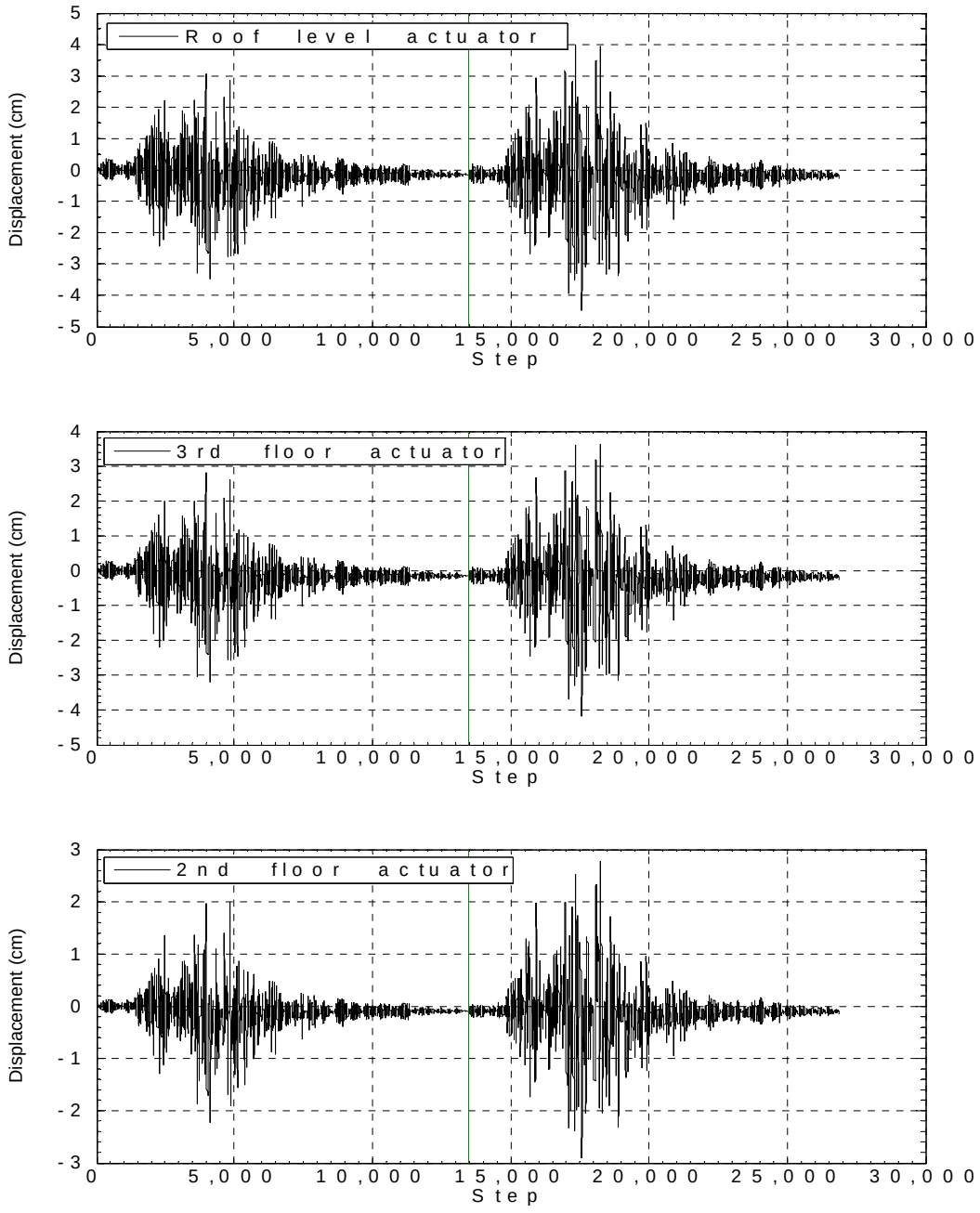

Figure 4.22 Applied displacement histories for 150 and 200 % of the Chile earthquakes.

4.4.3 Loading and Instrumentation

The loading and instrumentation schemes were identical to those used for the pushover test and described in Section 3.2.3.

4.5 Response of the Test Frame to the 1985 Chile Ground Motion

4.5.1 Test 1: 150% of Chile (PGA: 1.07 g)

In this initial test, the first-story braces first had slight inelastic out-of-plane buckling (Figure 4.23), followed by medium inelastic out-of-plane buckling with a kink occurring at midspan of the members and hinging developing in the adjacent gusset plates shown in Figure 4.24. From the experimental data shown in Figure 4.25, it appears that the first-story south brace buckled at an axial load of about -151 kN (-34 kips), and yielded slightly in tension at about 245 kN (55 kips). Figure 4.26 shows that the first-story north brace buckled first at about 178 kN (-40 kips), and afterwards yielded and carried about 245 kN (55 kips) in tension. Upon buckling of either of the first-story braces, the second-story zipper strut was subjected to tension forces for most of the test, as shown in Figure 4.27. Its maximum tensile axial force was 111 kN (25 kips). This illustrates that the zipper strut in the second story successfully transferred the unbalanced vertical forces generated from the braces below upon their buckling. As shown in Figure 4.28 and Figure 4.29, both the second-story braces buckled slightly when the axial force reached about 169 kN (-38 kips), resulting in the development of only a small unbalanced vertical force in the second-story throughout this load run. For this reason and the fact that the third-floor beam could provide some shear resistance, the third-story zipper strut sustained smaller unbalanced vertical forces than the second-story one, as shown in Figure 4.30.

Figure 4.23 Slight buckling with a lateral deflection at midspan of the brace.

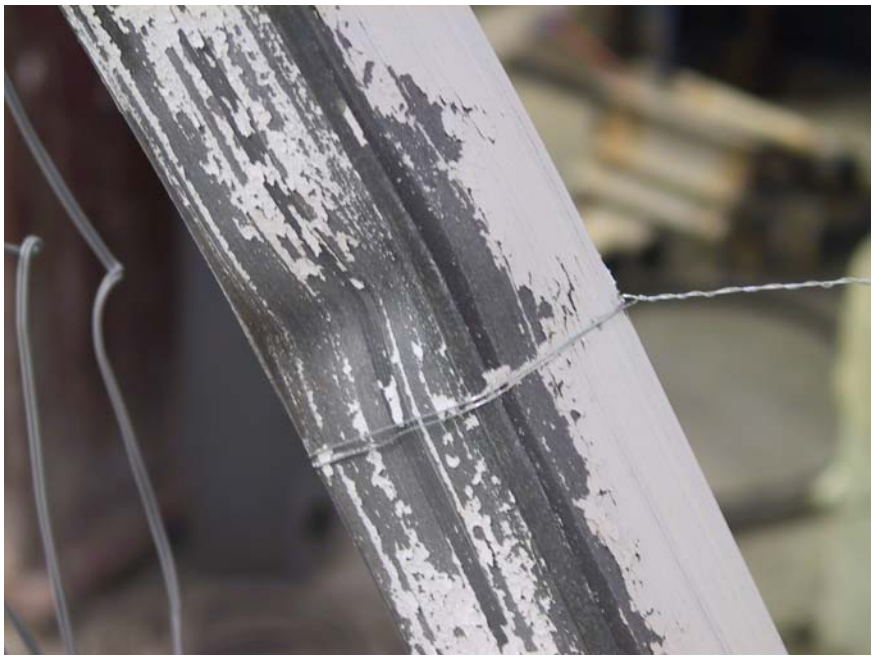

Figure 4.24 Medium buckling with a slight kinking at midspan of the brace.

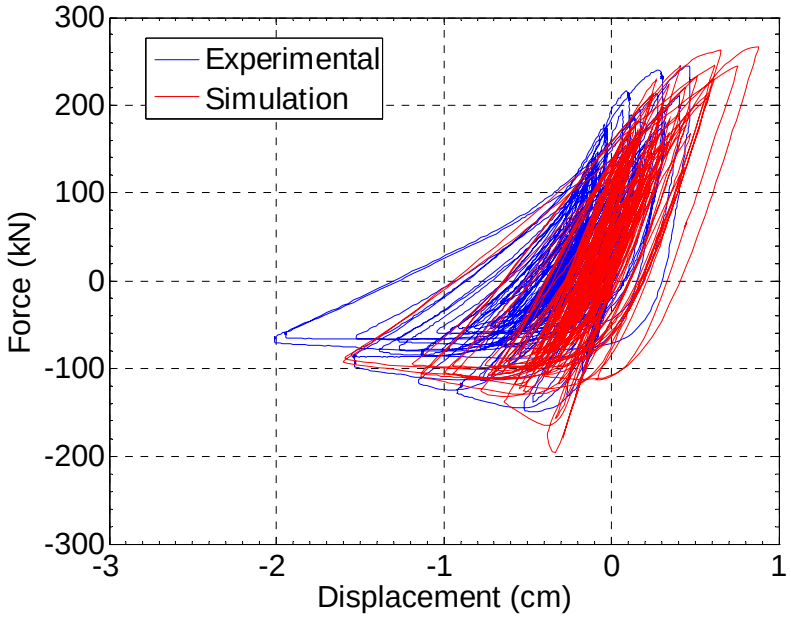

Figure 4.25 Hysteretic behavior of the 1st-story south brace (150% of Chile).

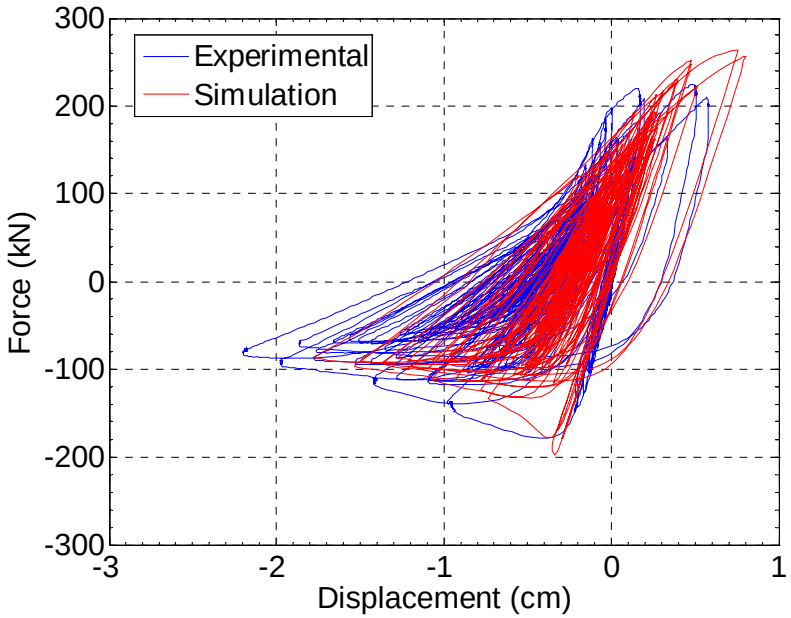

Figure 4.26 Hysteretic behavior of the 1st-story north brace (150% of Chile).

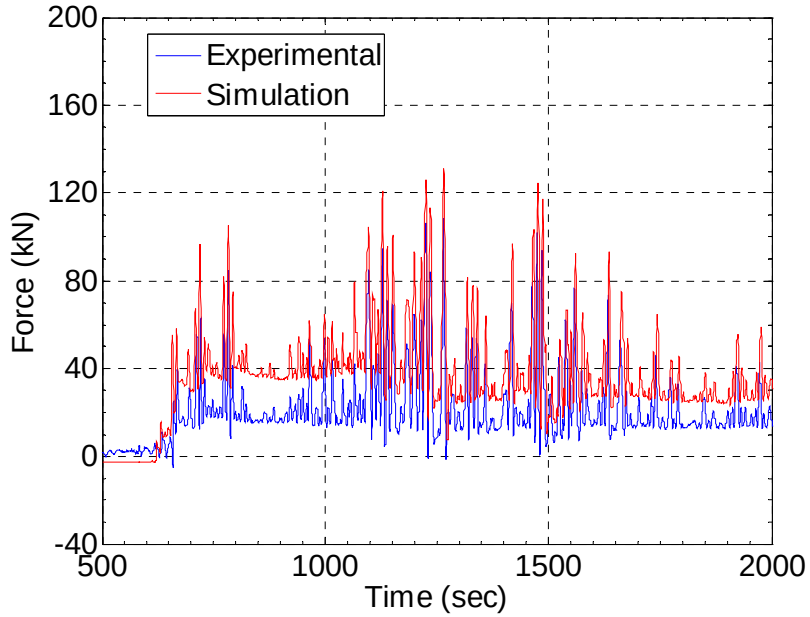

Figure 4.27 Force history of the 2nd-story zipper strut (150% of Chile).

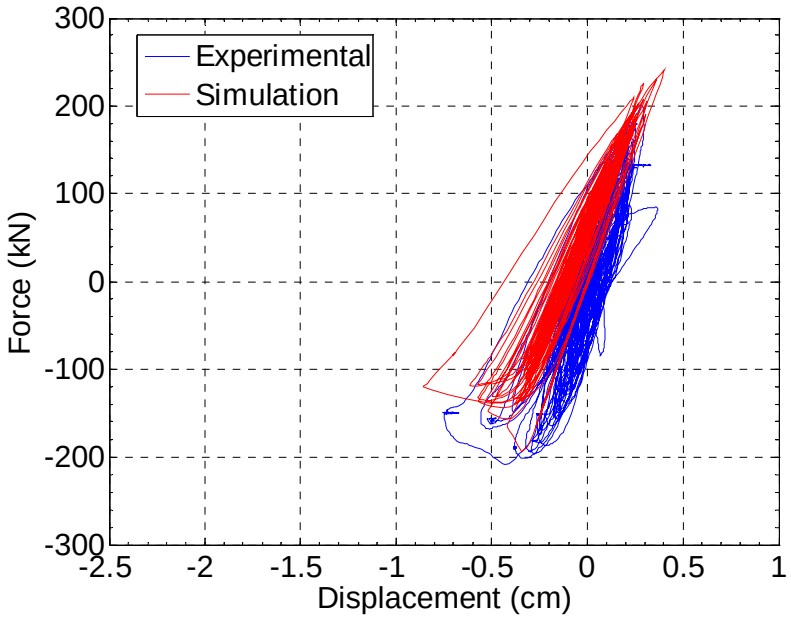

Figure 4.28 Hysteretic behavior of the 2nd-story south brace (150% of Chile).

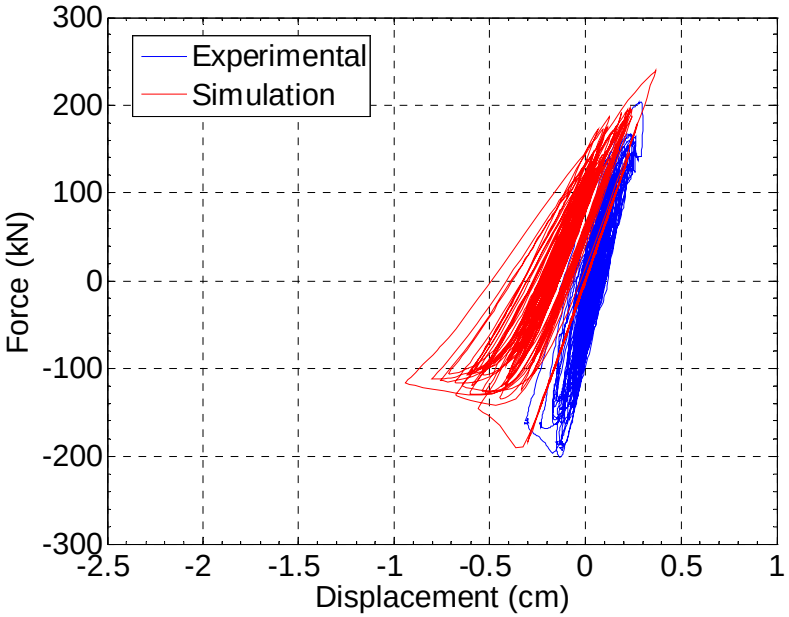

Figure 4.29 Hysteretic behavior of the 2nd-story north brace (150% of Chile).

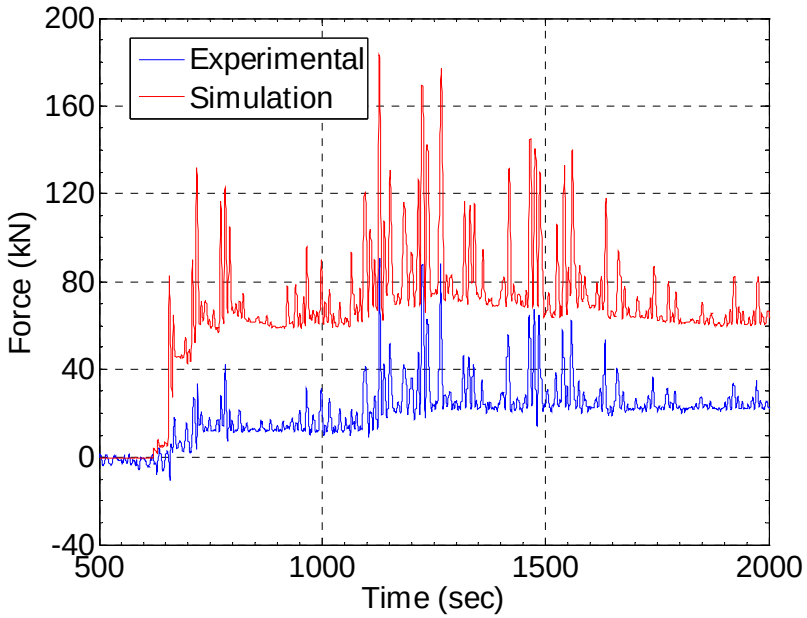

Figure 4.30 Force history of the 3rd-story zipper strut (150% of Chile).

Figure 4.31 presents the overall behavior of the zipper frame, i.e., its roof drift ratio vs. base shear. It indicates that the zipper frame developed its maximum strength of about 267 kN (60 kips) even though buckling had occurred in the compression braces. The simulation is in good agreement with the experimental results, particularly in the large cycles. From the standpoint of comparing the experimental hysteresis loop with the pushover curve (Figure 4.32), the zipper frame had entered the second of the trilinear behavioral stages.

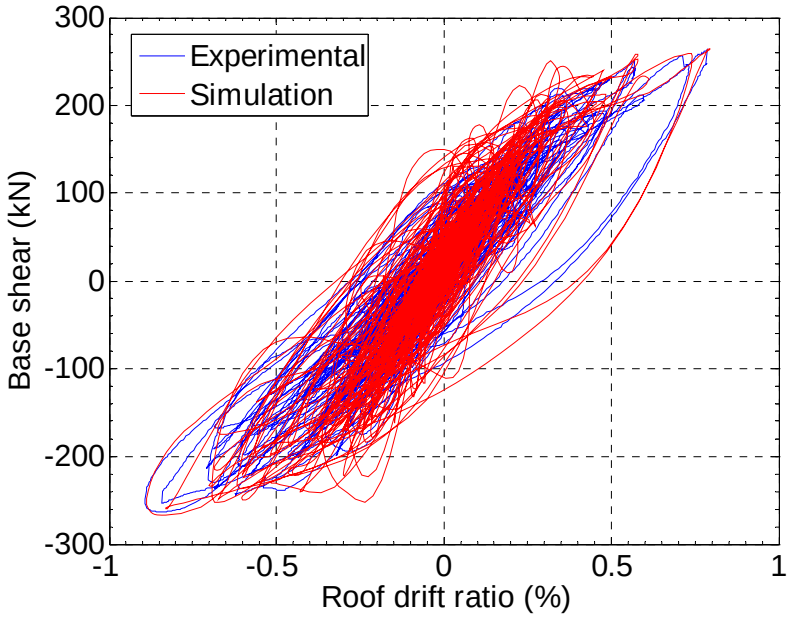

Figure 4.31 Hysteretic response of the zipper frame (150% of Chile).

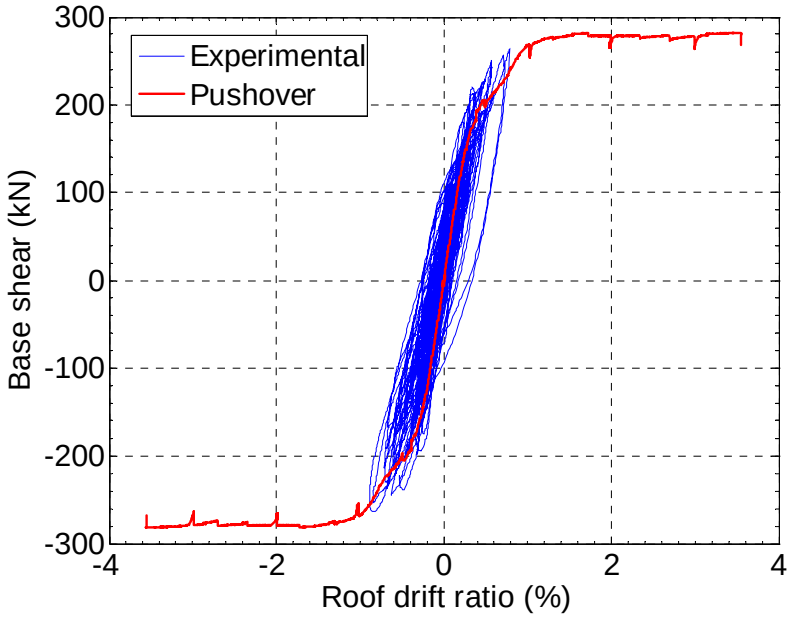

Figure 4.32 Comparison between the hysteretic loop and pushover curve (150% of Chile).

4.5.2 Test 2: 200% of Chile (PGA: 1.42 g)

When subjected to 200% of Chile, the frame evidenced serious low-cycle fatigue damage in the first story, as shown in Figure 4.33. Prior to complete fracture, the brace in compression suffered significant kinking, as shown in Figure 4.34, and then the brace in tension started to tear in the middle section, as illustrated in Figure 4.35. Following the remaining post-buckling strength of -67 kN (-15 kips) at the end of the 150 % test (Figure 4.25), the compression strength in the south brace continued decreasing to -22 kN (-5 kips) and then 0 kN (0 kips) when the complete fracture occurred at midspan, as shown in Figure 4.36. Prior to fracture, the sectional tearing reduced the cross-section area, resulting in a decrease in the tension capacity of the member, and impeded the reaching of the maximum previous loads. The first-story north brace experienced a similar fatigue damage process. Its hysteresis loop is presented in Figure 4.37. The induced unbalanced

vertical force was overcome by the second-story zipper strut. Figure 4.38 indicates that the maximum axial tension force sustained in the zipper strut was about 151 kN (34 kips) and the maximum axial compression force was -22 kN (-5 kips). In the second story, both the braces had slight buckling during this test, as shown in Figure 4.39 and Figure 4.40. Thus, the third-story zipper strut sustained a smaller magnitude of force than the second-story one (Figure 4.41). When comparing the experimental and simulation results, there is a shift between them (Figure 4.41) because the tension and compression forces acting in the second-story braces were almost the same [about 178 kN (40 kips), Figure 4.38 and Figure 4.39], as opposed to the simulated tension and compression forces which had distinct differences [267 kN (60 kips) for tension and -134 kN (-30 kips) for compression].

Figure 4.42 illustrates that the base shear decreased from -245 kN (-55 kips) to -89 kN (-20 kips) after both the first-story braces completely fractured. This post-failure strength of the zipper frame remained at about 89 kN (20 kips), which was one third of the ultimate strength. Figure 4.43 shows that, even though the zipper frame remained in the second stage, the structural strength would decrease due to fatigue damage to the braces.

Figure 4.33 Both the first-story braces completely fractured (200% of Chile).

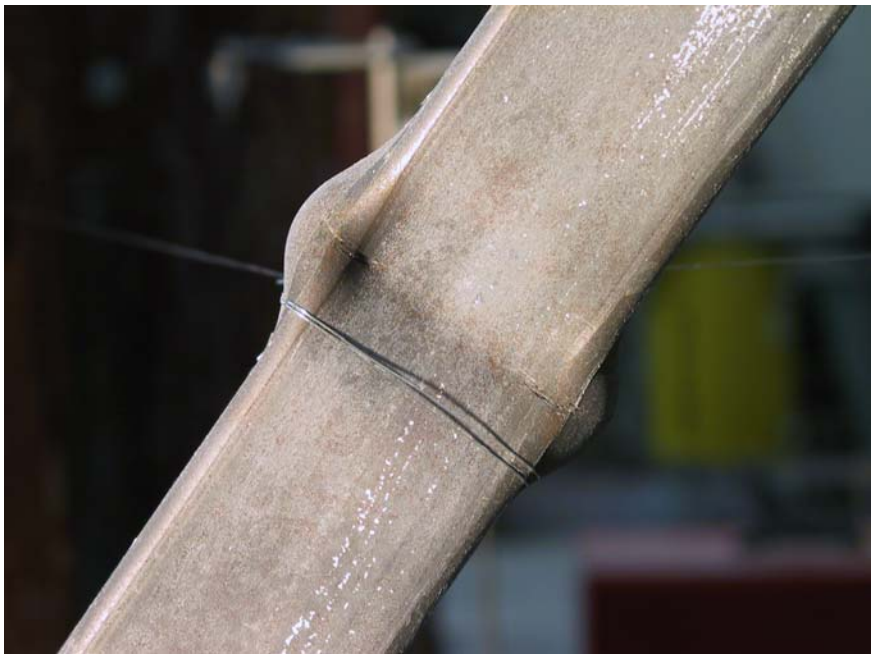

Figure 4.34 Significant kinking at midspan of the brace in compression.

Figure 4.35 Tearing in the partial section of the brace in tension after the heavy kinking.

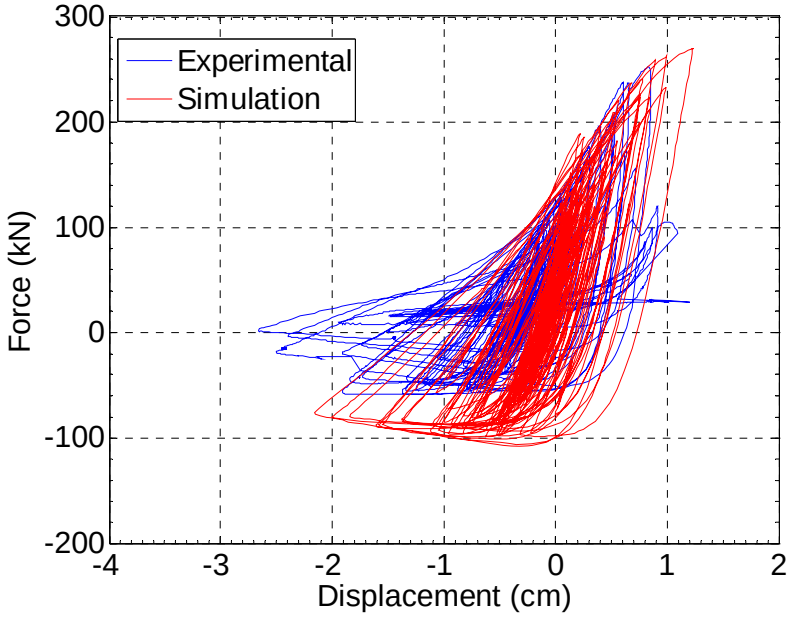

Figure 4.36 Hysteretic behavior of the 1st-story south brace (200% of Chile).

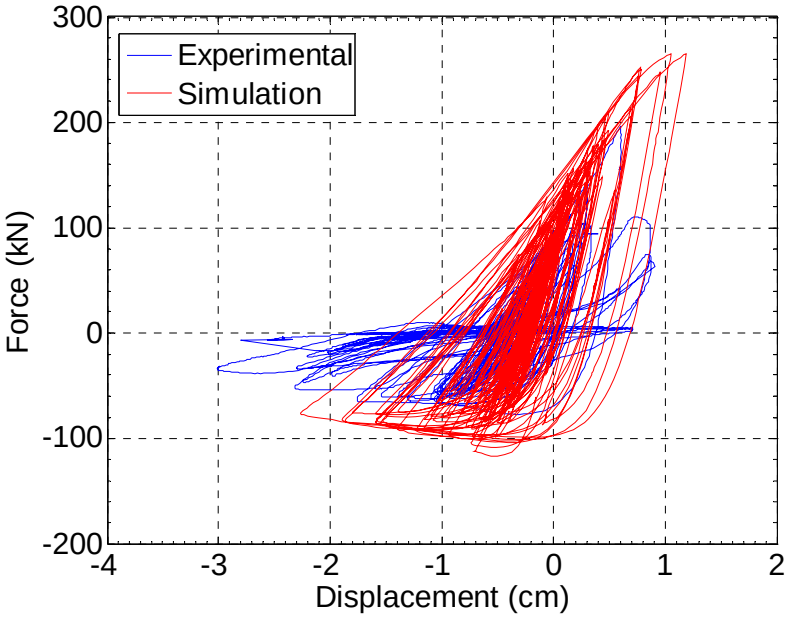

Figure 4.37 Hysteretic behavior of the 1st-story north brace (200% of Chile).

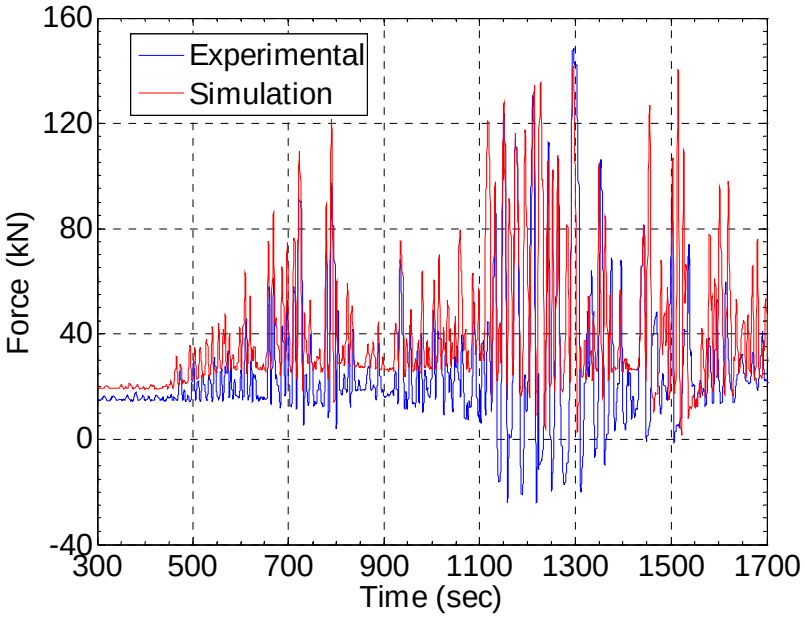

Figure 4.38 Force history of the 2nd-story zipper strut (200% of Chile).

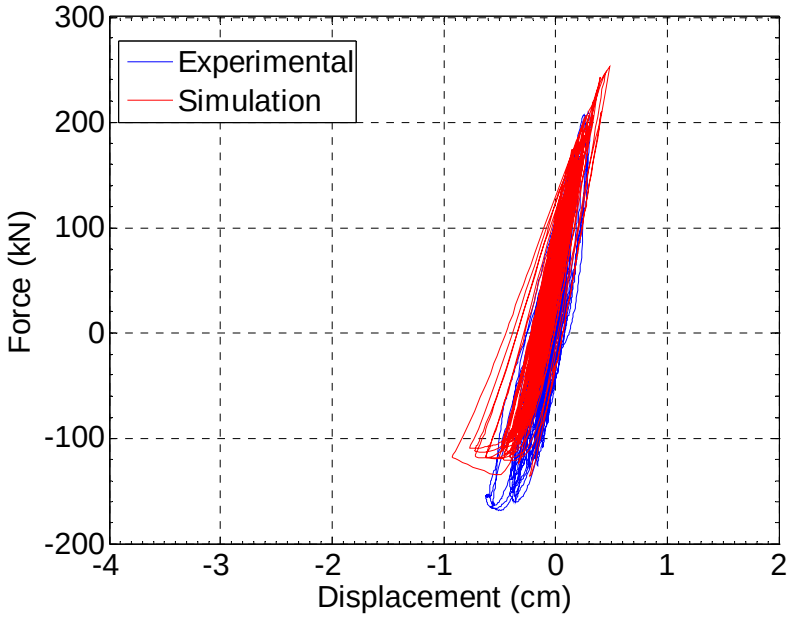

Figure 4.39 Hysteretic behavior of the 2nd-story south brace (200% of Chile).

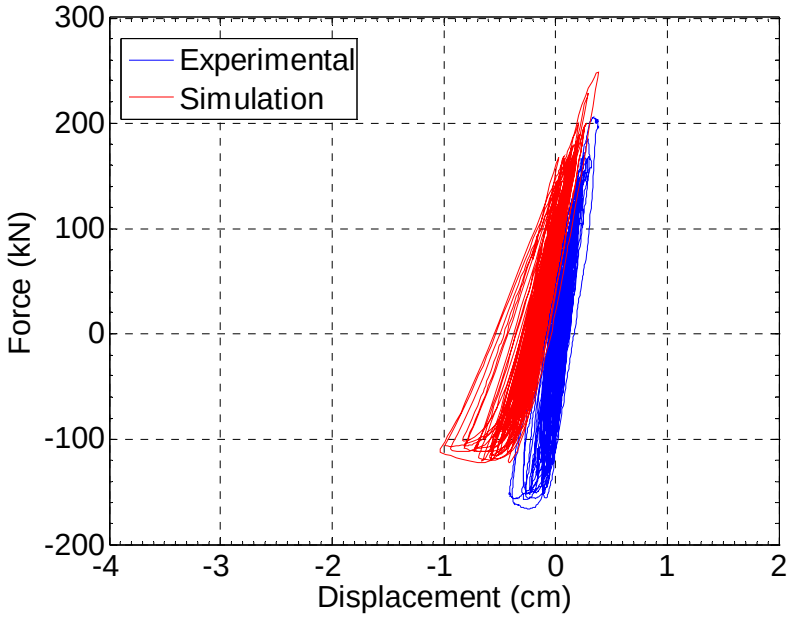

Figure 4.40 Hysteretic behavior of the 2nd-story north brace (200% of Chile).

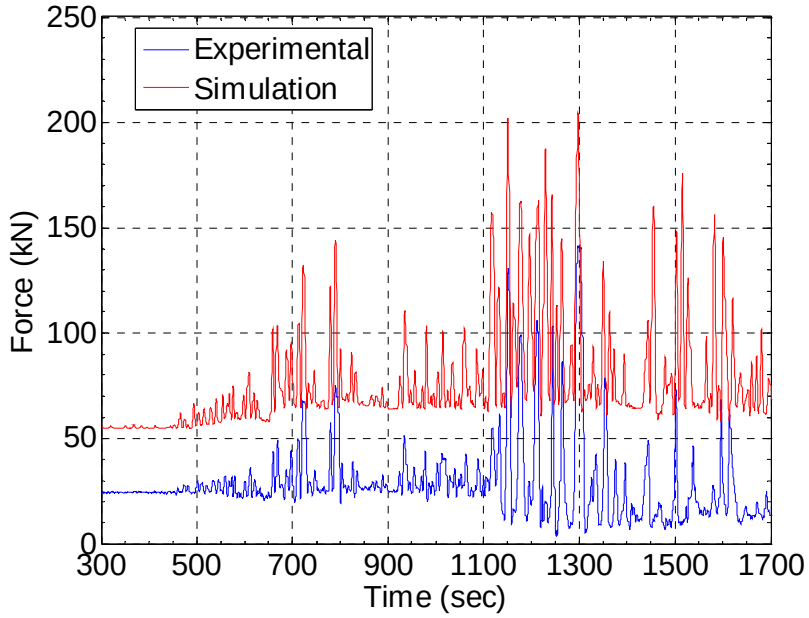

Figure 4.41 Force history of the 3rd-story zipper strut (200% of Chile).

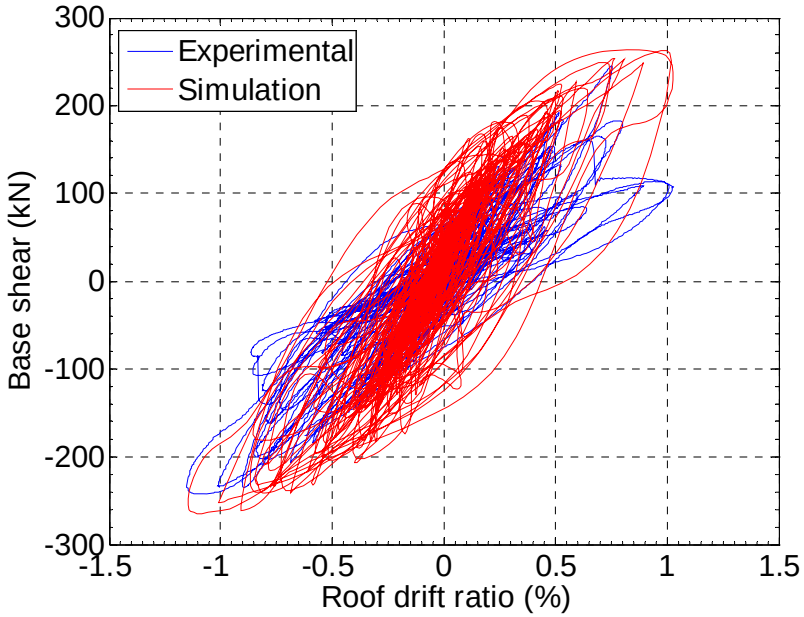

Figure 4.42 Hysteretic behavior of the zipper frame (200% of Chile).

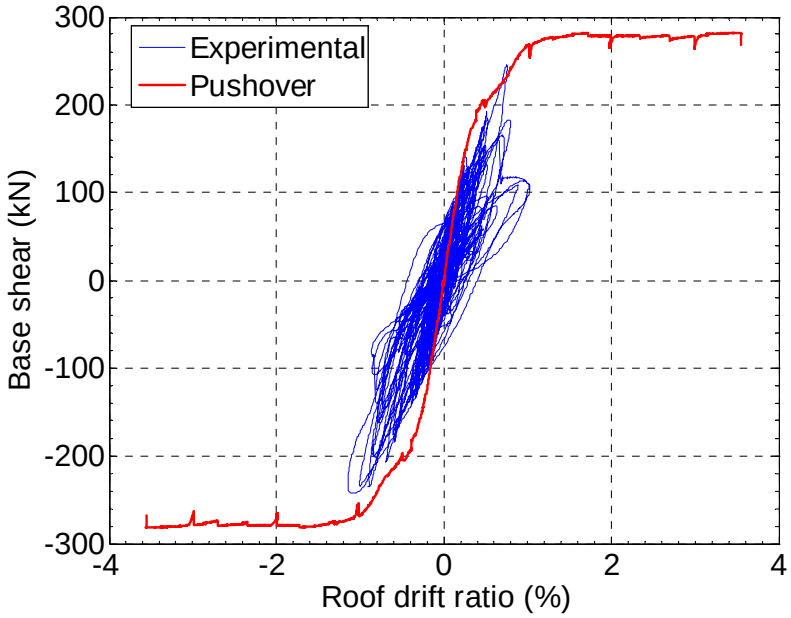

Figure 4.43 Comparison between the hysteresis loop and pushover curve (200% of Chile).

4.6 Summary and Conclusions

In the LA22 tests, the reduced-scale suspended zipper frame designed in compliance with the capacity design procedure (see Chapter 2):

1. Exhibited great strength and capacity to dissipate hysteretic energy and remained stable up to the roof drift ratio of approximately 2.6%.
2. Validated the assumed sequence of yielding. Once buckling had occurred in the braces, the zipper strut functioned as a tension member, providing support at mid-span of the beam and transmitting the unbalanced vertical forces upwards to mobilize the unbuckled braces.
3. Reached its yielding strengths in both the second- and third-story zipper struts, consistent with the theoretical expectations.

4. Evidenced a decrease in post-failure strength from 178 kN (40 kips) down to 111 kN (25 kips), after one first-story brace fractured and another one had severe compression buckling and tension yielding.

In the 1985 Chile tests, the reduced-scale suspended zipper frame designed in compliance with the capacity design procedure:

5. Exhibited great ductility and hysteretic energy dissipation and remained stable even when both first-story braces completely fractured in the test to 200% of the Chile record.
6. Showed that most of the unbalanced vertical forces arose from the first-story braces buckling under 150% of the Chile record.
7. Evidenced that although the source acceleration was multiplied by 1.5 (the PGA was increased up to 1.07 g), the braces did not even tear in the cross section during this test. For the 200% case, the first-story braces experienced larger deformation and a large number of cyclic vibrations, leading to the fatigue damage to the sections at midspan of the braces.
8. Showed that the post strength of such a frame, after the two first-story braces completely fractured, was observed to decrease from 178 kN (40 kips) down to 111 kN (25 kips), and further to 89 kN (20 kips), one third of the ultimate strength.

CHAPTER 5

DESIGN METHODOLOGY

5.1 Design Philosophy

The basic design objective for a zipper-braced frame is to mitigate the typical soft-story mechanism associated with braced frames by distributing more uniformly both story drift and energy dissipation over the height of the building. There are three main components of this innovative system. The first component is the zipper struts which forces simultaneous buckling of all stories except the top one and then leads to tension yielding of all braces [Figure 5.1(a)]. The second component is the hat truss, which prevents the formation of a full plastic mechanism and thus provides large deformation capacity. The third component is the columns, which transmit the forces back to the foundation.

From the standpoint of base shear versus the roof drift response, the zipper-braced frame exhibits tri-linear response with large ductility, as shown in Figure 5.1(b). As presented in Figure 5.1(a), simultaneous buckling in the compression braces and the nature of negative post-buckling stiffness change the initial structural stiffness slope. However, the strength of the whole frame continues to increase, first reaching its yielding strength and then entering a hardening range due to the yielding in the tension braces.

Based on (1) the observations on the pushover and cyclic tests mentioned in Chapters 3 and 4, and (2) the concepts given in the latest AISC Seismic Provisions for Structural Steel Buildings, a design procedure updating the preliminary one given in Chapter 2, is presented in Section 5.2. This section is written in code-type language, with the provisions given first, along with commentary. This follows the format used for

prequalified connections in FEMA 358, but with the provisions intended to cover the entire system rather than just the connections.

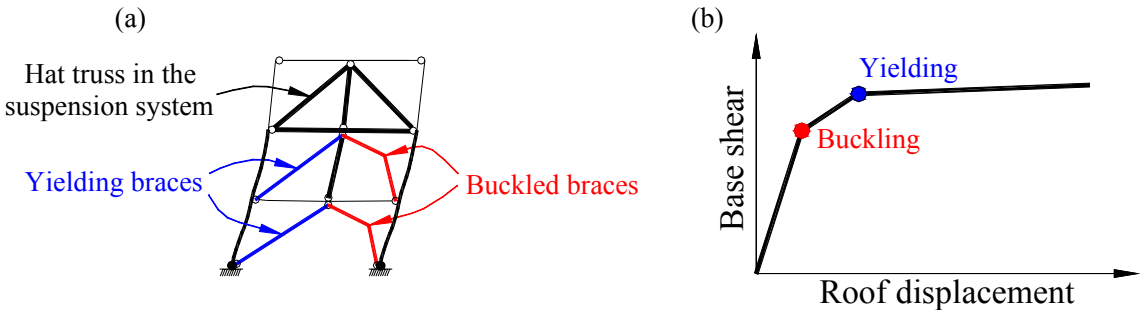

Figure 5.1(a) Zipper mechanism and (b) Tri-linear behavior.

5.2 Updated Design Procedure

The design of zipper frames shall consist of a two-step procedure. The first is a strength design phase for the braces (Section 5.2.1), in which the presence of the zipper elements is ignored. The second is a capacity design phase (Section 5.2.2), in which the zipper struts are added and other structural elements are redesigned except for the braces below the top-story level.

5.2.1 Phase I (Strength Design)

The braces shall be designed to resist the effects of earthquake and vertical loadings from the load combinations stipulated by the Applicable Building Code without the aid of the zipper struts.

Commentary: This phase follows the conventional Special Inverted V-Braced Frame (SIVBF) design procedure. The braces are assumed to resist all the lateral loads, with the critical compression braces designed to carry a force equal to $\phi_c A_g F_{cr}$. *This phase fixes*

the sizes of the braces in all stories except the top story. Preliminary design for the other elements should be carried out, but the design of the beams shall ignore the shear force at the centerline resulting from the unbalanced forces induced by the braces.

5.2.2 Phase II (Capacity Design)

In this phase, the zipper struts are added and other structural elements are redesigned except for the braces below the top-story level. The frame designed in Phase I is further modified according to the following sequence, which follows the redistribution of the unbalanced vertical forces.

5.2.2.1 Zipper struts

Zipper struts shall be designed to resist the vertical unbalanced forces generated by the braces and zipper element located on the level below. The brace forces shall be taken as $R_y F_y A_g$ for the brace in tension and 0.3 times P_n for the brace in compression.

Commentary: The zipper strut is designed to resist all the vertical forces from the members framing from below. In order to channel most of the unbalanced vertical force from the braces into the story above, the beam needs to be flexible. As a result, the contribution of the shear capacity of the beams to overcoming the unbalanced vertical forces is ignored in this design step.

5.2.2.2 Top-story braces

The top-story braces from Phase I shall be redesigned to resist the forces corresponding to (1) the smaller of all the vertical unbalanced forces collected in the top story zipper element or its yield strength, and (2) the overstrength equivalent lateral earthquake force ($\Omega_0 Q_E$) at the roof level, with Ω_0 equal to 2.0.

Commentary: The top story is intended to remain elastic and thus needs to be designed for the maximum vertical forces that can be delivered by the zipper elements from below

and a conservative estimate of the horizontal inertial forces from the roof. The overstrength factor, Ω_o, is taken as 2 for the zipper frame system (same as the code-stipulated overstrength factor for special CBFs) because the system overstrength after the buckling of the all compression braces and the yielding of the all tension braces except for the top ones is estimated as double of the design base shear.

5.2.2.3 Columns

The required axial compressive and tensile strengths are determined using the maximum load transferred to the column considering the capacities of the adjacent braces (use the required strengths instead of capacities for the top story braces) and the effect of the unfactored vertical loading.

Commentary: In the process of design, each story column of zipper-braced frames is assumed to be pinned connections, ignoring the flexural capacity provided in real continuous columns. This process will result in fairly uniform column sizes over the height of the structure. The resulting sizes of the first-story columns are similar to those of conventional special inverted-V-braced frames.

5.2.2.4 Beams

Beams shall comply with beam-column provisions as stipulated in Chapter H of the AISC LRFD Specification. The required strength shall be determined using the maximum load transferred to the beam considering the capacities of the adjacent braces and the effect of the unfactored vertical loading.

Commentary: (use the required strengths instead of capacities for the top story braces)

5.2.2.5 Bracing connections

The design for the brace-beam-column connections follows the Uniform Force method described in the AISC LRFD manual.

Commentary: In order to make all the braces, except the top ones, buckle out of plane, the gusset plates at the ends of braces should be designed with a free length of twice the gusset plate thickness, as recommended in the AISC seismic provisions. However, the yield line does not need to be perpendicular to the axial line of the bracing member. A tapered gusset plate is recommended for the brace-to-beam connection to provide both flexibility for out-of-plane brace buckling and larger ductility for in-plane brace yielding.

CHAPTER 6

DESIGN EXAMPLES OF ZIPPER-BRACED FRAMES

6.1 Introduction

Three office buildings with zipper-braced systems were designed to carry the same loads as the 3-, 9-, and 20-story SAC moment resisting frames (FEMA 355C) designed for downtown Los Angeles. In the Los Angeles area for the 2 % probability of exceedance in 50 years, the mapped spectral accelerations for the short period and the 1 sec period are 2.16g and 0.72g, respectively, with a PGA of 0.90 g. The design code used was the 2005 ASCE-7 (henceforth ASCE 7-05) for loads and the 2005 AISC LRFD and Seismic Provisions with the zipper frame design procedure for member and frame design. The lateral load design of all LA structures was controlled by the seismic load provisions from Chapter 12 of ASCE 7-05. The buildings were designed as if located on stiff soil (site class D as per ASCE 7-05 definitions). An importance factor of 1.5 was assigned to the buildings in accordance of Occupancy Category IV. This is a significant departure from the SAC building, and was intended to determine if zipper frames could be applicable even to critical structures. The response modification coefficient, R, of this type of seismic force-resisting system was taken as 6, consistent with other ductile braced systems (special steel concentrically braced frames).

The floor plans and elevations for the buildings were predetermined, as shown in Figure 6.1. The location of the zipper-braced frames is shown by the bold lines in Figure 6.1, and take up the same number of bays as for the special moment frames in the original SAC designs. All the columns in the perimeter zipper-braced frames are bent about the strong axis. The strong axis of the gravity columns is oriented in the NS direction.

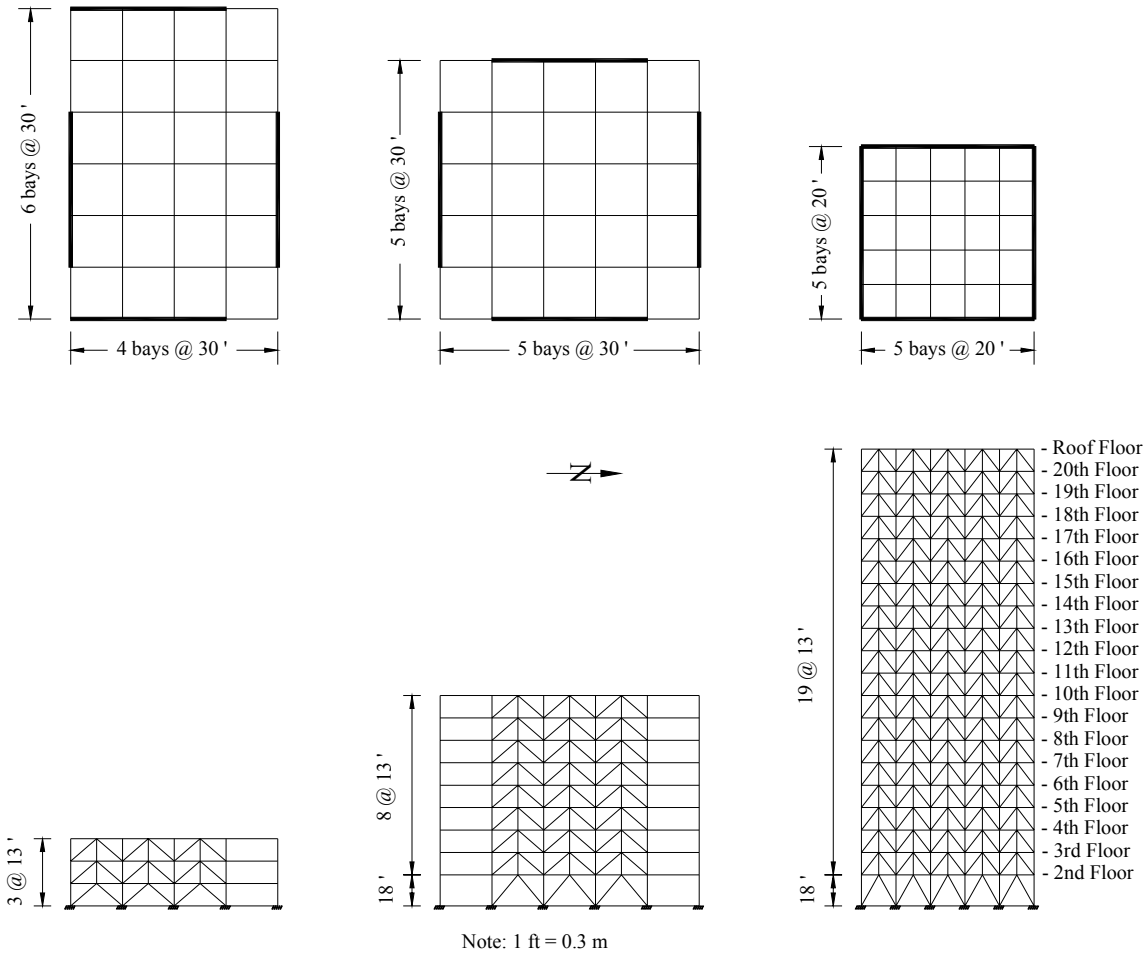

Figure 6.1 Floor plans and elevations for model buildings.

The loading used for the analysis of the frames result in the following floor load distribution (steel weight is assumed as 13 psf for all designs):

Floor dead load for weight calculation: 96 psf

Roof dead load: 83 psf

Reduced live load (floor and roof): 20 psf

The seismic mass for each of the entire structures is given in Table 6.1. The mass per frame is this tabulated value divided by the number of braced bays present.

Table 6.1 Seismic mass (kips-sec^2/ft) for the 3-, 9-, and 20-story structures.

	3-story structure	9-story structure	20-story structure
Roof	70.90	73.10	40.06
Floor 3	65.53	-	-
Floor 3-9	-	67.86	-
Floor3-22	-	-	37.76
Floor 2	65.53	69.04	38.63
TOTAL	201.96	617.16	758.37

6.2 Design of the 3-Story Zipper-Braced Model Building

In the NS direction, the 3-story building consists of two zipper-braced frames, each containing three braced bays in the perimeter of the building. An elevation of one of the braced bays is shown in Figure 6.2. For design, the beam-to-column connections as well as brace-to-beam and zipper-to-beam intersections are assumed to be pinned. Gravity unfactored uniformly distributed roof dead loads of 1.25 kips/ft, floor dead loads of 1.44 kips/ft, and live loads of 0.3 kips/ft were applied along the beams. The seismic lateral loads were calculated in accordance with the equivalent lateral force procedure described in Section 12.8 of ASCE 7-05. In subsection 12.8.1.3, ASCE 7-05 specifies that for regular structures five stories or less in height and having a period, T, of 0.5 s or less, C_s is 'permitted' to be calculated using a value of 1.5 for S_s. However, in this design, C_s was computed still using values of 2.16g for S_s and 0.72g for S_1. This results in a stronger frame than that used in the previously mentioned SAC designs. Those frames were designed on the basis of the requirement in IBC 2000 that for regular structures five stories or fewer in height having a period T, of 0.5 s or less, the design spectral response accelerations, S_{DS} and S_{D1}, need not exceed the values calculated using values of S_S and S_1 of 1.5g and 0.6g, respectively. Using ASCE 7-05, assuming an importance factor of 1.5, and without the permissible reductions in the design spectral response accelerations, the

seismic base shear was calculated to be 390 kips per braced bay, with the floor loads being 203 kips, 125 kips, and 62 kips from the roof to second floor levels, respectively.

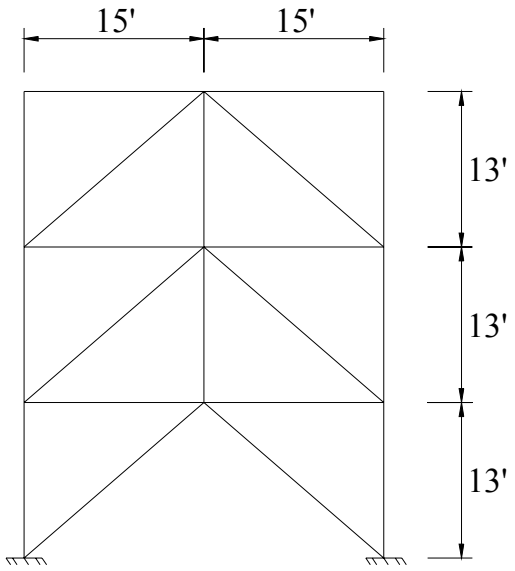

Figure 6.2 Elevation of one zipper-braced bay to be designed.

In this design example, member forces induced by the lateral seismic loads and by vertical loads were initially calculated separately as established in Section 5.2.1. Based on the applicable loading combination, the braces were sized first to resist the actions resulting from the application of these two forces in the strength design phase. In the next design step as established in Section 5.2.2, the rest of the structural members such as the zipper struts, columns, and beams were evaluated and redesigned in the capacity design phase. Finally, the building was checked against the allowable story drift limit 0.015h, where h is the story height. A flow chart of the design procedure is shown in Figure 6.3.

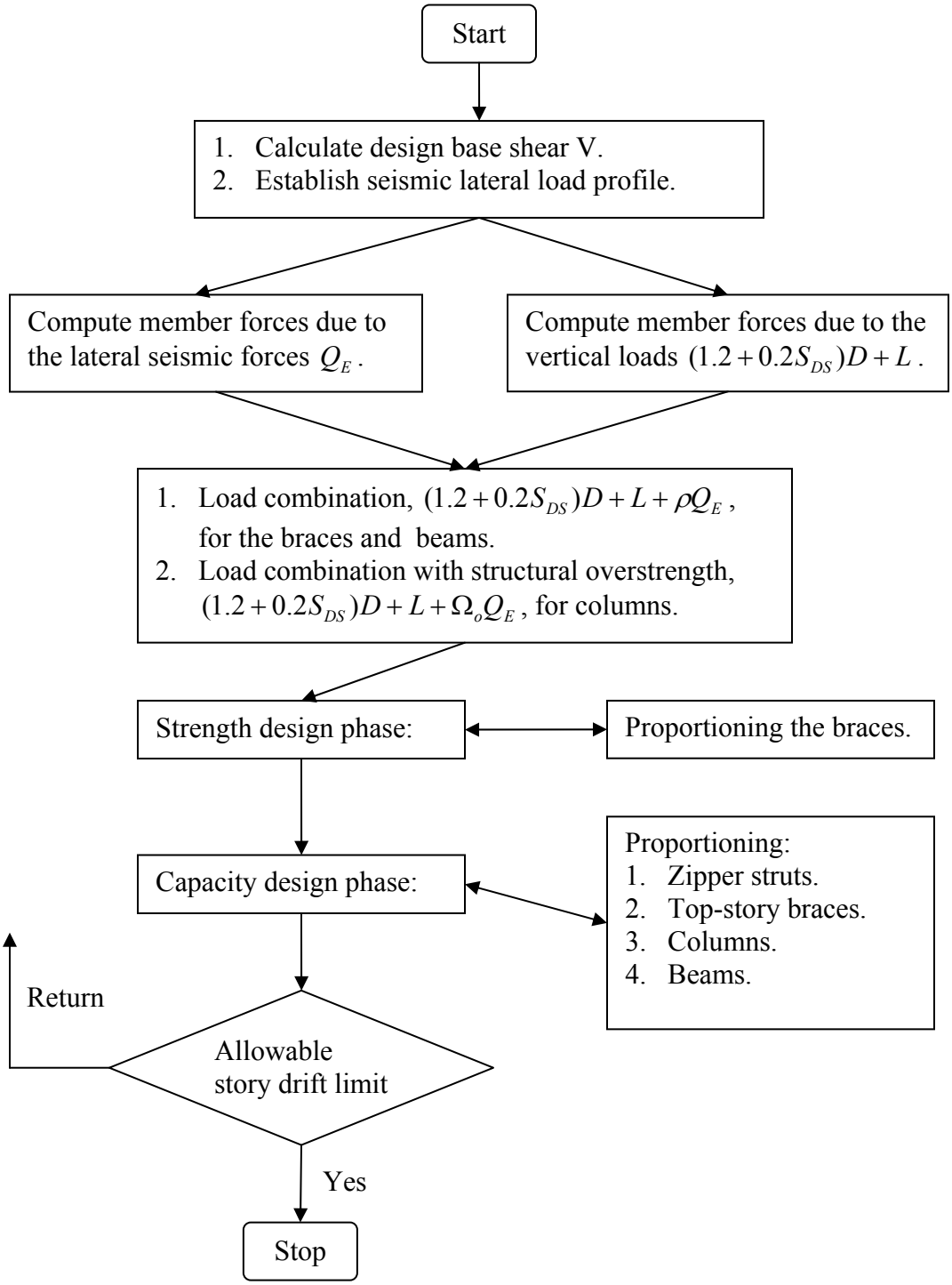

Figure 6.3 Flowchart of a design procedure for the zipper-braced frame.

6.2.1 Forces due to Earthquake Loading

Because the zipper struts are designed to sustain the unbalanced vertical forces arising from buckling in the braces in the capacity design phase and do not contribute to the lateral resistance in the strength design phase, consideration of the zipper struts can be omitted in the strength portion of the design. The unfactored lateral seismic forces are distributed over the height of the braced bay, as shown in Figure 6.4.

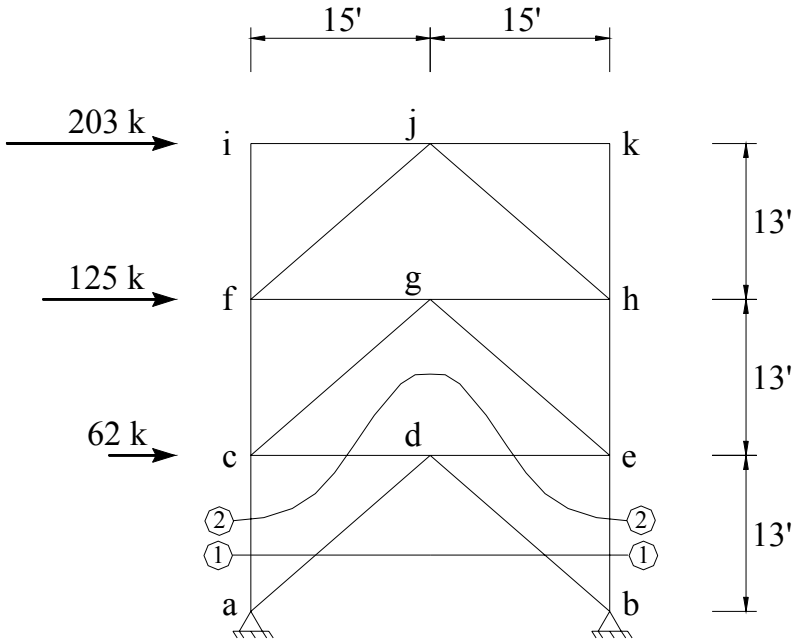

Figure 6.4 Braced bay subjected to the unfactored lateral seismic loading.

6.2.1.1 Determination of the forces in the braces

The forces in the left and right first-story braces are designated F_{da} and F_{db}, respectively, where the subscripts refer to the two end nodes of the member as shown in Figure 6.4. A positive value of the force is defined as tension, and a negative value as compression. At

section 1-1, summation of the horizontal forces applying to the top free-body diagram is zero, which gives the following equation, if the column shears are ignored.

$$\sum F_x = 0 = (203 + 125 + 62) - \left(\frac{15}{19.85}\right)F_{da} + \left(\frac{15}{19.85}\right)F_{db}$$

At joint *d*, the force equilibrium in the vertical direction can be expressed as

$$\sum F_y = 0 = -\left(\frac{13}{19.85}\right)F_{da} - \left(\frac{13}{19.85}\right)F_{db}$$

Solving the above two equations gives the first-story brace forces.

$$F_{da} = 258 \text{ kips}$$

$$F_{db} = -258 \text{ kips}$$

Similarly, the forces in the second- and third-story braces are

$$F_{gc} = 217 \text{ kips}, \; F_{ge} = -217 \text{ kips}$$

$$F_{jf} = 134 \text{ kips}, \; F_{jh} = -134 \text{ kips}$$

6.2.1.2 Determination of the forces in the columns

At section 2-2, taking moments about point *e* results in the axial force (F_{ca}) in column *ca*.

$$\sum M_e = 0 = 125 \times 13 + 203 \times 26 - 30 \times F_{ca}$$

$$F_{ca} = 230 \text{ kips}$$

From vertical force equilibrium in the free-body diagram above section 2-2, the axial force (F_{eb}) in column *eb* is

$$F_{eb} = -230 \text{ kips}$$

Similarly, the forces in the second- and third-story columns are

$$F_{fc} = 88 \text{ kips}, \; F_{he} = -88 \text{ kips}$$

$$F_{if} = F_{kh} = 0 \text{ kips}$$

6.2.1.3 Determination of the forces in the beams

At section 2-2,

$$\sum F_x = 0 = 203 + 125 + 62 + F_{cd} - F_{ed}$$

Because the horizontal forces equilibrate at joint *e*,

$$\sum F_x = 0 = -F_{ed} - \left(\frac{15}{19.85}\right) F_{eg}$$

Given the force of the second-story right brace F_{eg}, which has been computed in 6.2.1.1, solving these two equations above leads to the beam axial forces in two segments, *ed* and *ce*.

$$F_{ed} = 164 \text{ kips}$$

$$F_{cd} = -226 \text{ kips}$$

Similarly,

$$F_{hg} = 101 \text{ kips}, \; F_{fg} = -226 \text{ kips}$$

$$F_{kj} = 0 \text{ kips}, \; F_{ij} = -203 \text{ kips}$$

A summary of the axial member forces due to the unfactored lateral seismic loads is presented in Table 6.2.

Table 6.2 Axial member forces due to the unfactored lateral seismic loads.

	Braces (kips)		Columns (kips)		Beams (kips)	
Story	Left	Right	Left	Right	Left	Right
3	134	-134	0	0	-203	0
2	217	-217	88	-88	-226	101
1	258	-258	230	-230	-226	164

6.2.2 Forces due to Factored Vertical Loading $(1.2+0.2S_{DS})D+L$

The zipper struts can carry some parts of the forces in the beams or in the bracing members after the capacity design introduced later is completed. However, for the sake of conservatism in the design of the bracing members and beams, the zipper struts will also be ignored in this stage. The vertical loads are factored based on $(1.2+0.2S_{DS})D+L$ with $S=0$ which is the vertical portion of the basic load combination rule 5 for strength design, $(1.2+0.2S_{DS})D+L+\rho Q_E+0.2S$, in AISC 7-05. A schematic diagram of the braced bay subjected to factored vertical loading is shown in Figure 6.5.

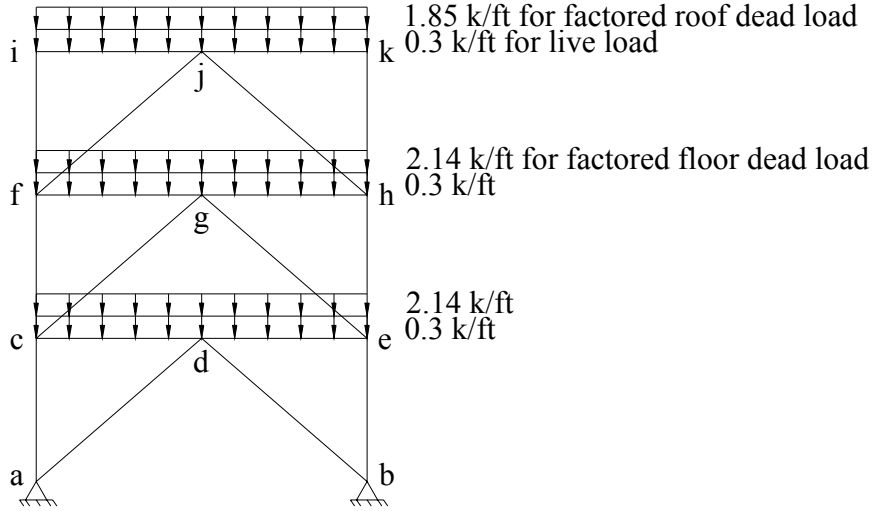

Figure 6.5 Braced bay subjected to vertical loading.

6.2.2.1 Determination of the forces in the braces

The beams can be treated as two-span continuous beams of 30 feet total length and supported at the ends and middle with pinned connections. The reaction provided by the braces below at midspan for such as a continuous beam is $5w_uL/8$, in which w_u is the factored uniformly distributed loading and L is the beam length. When the forces in the

first-story braces are considered, the vertical force equilibrium at joint *d* results in the following equation.

$$\sum F_y = 0 = -F_{da}\frac{13}{19.85} - F_{db}\frac{13}{19.85} - \frac{5}{8}\times(2.14+0.3)\times 30$$

Also because of $F_{da} = F_{db}$, $F_{da} = F_{db} = -35$ kips.

Similarly, the second- and third-story brace forces due to the factored vertical loading are

$$F_{gc} = F_{ge} = -35 \text{ kips}$$

$$F_{jf} = F_{jh} = -31 \text{ kips.}$$

6.2.2.2 Determination of the forces in the columns

The determination of the column forces starts at the top story level and progresses downward to the first story level. When the third-story columns are considered, they support the roof-floor beam at joints *i* and *h*. For instance, the left column force is computed as follows.

$$F_{if} = -\frac{3}{8}\times(0.3+1.85)\times 15 = -12 \text{ kips}$$

The top right column is also subjected to the same load; thus $F_{kh} = -12$ kips. The second-story columns sustain not only the forces transferred from the beams, but also the forces resulting from the adjacent members such the columns and braces above. By considering the vertical force equilibrium at joints *f* and *h*, the second-story column forces can be computed. For example, at joint *f*,

$$\sum F_y = 0 = -F_{fc} + F_{fi} + F_{fj}\frac{13}{19.85} - \frac{3}{8}\times(0.3+2.14)\times 15$$

$$F_{fc} = -46 \text{ kips}$$

The second-story right column has the same load; thus $F_{he} = -46$ kips. Similarly, the first-story column forces can be determined as $F_{ca} = F_{eb} = -83$ kips.

6.2.2.3 Determination of the forces in the beams

Uniformly distributed loading along the beam will cause a maximum negative moment at midspan that is $-w_u L^2/32$. Also, the forces transferred from the braces above lead to tension in the beam. For example, considering the horizontal force equilibrium at joint *c*, the axial force in the second-floor beam is

$$\sum F_x = 0 = F_{cd} + F_{cg}\frac{15}{19.85}$$

$$F_{cd} = 26 \text{ kips}$$

$$M_d = -\frac{1}{32}\times(0.3+2.14)\times 30^2 = -69 \text{ ft-kips}$$

A summary of the member forces due to the factored vertical loading is shown in Table 6.3. Table 6.4 lists the member forces due to unfactored vertical loading (*D*+*L*). These are required for use in the capacity design phase.

Table 6.3 Member forces due to the factored vertical loads.

	Braces		Columns		Left beams		Right beams	
Story	Left (kips)	Right (kips)	Left (kips)	Right (kips)	Axial force (kips)	Bending (ft-kips)	Axial force (kips)	Bending (ft-kips)
3	-31	-31	-12	-12	0	61	0	61
2	-35	-35	-46	-46	23	69	23	69
1	-35	-35	-83	-83	26	69	26	69

Table 6.4 Member forces due to the unfactored vertical loads.

	Braces		Columns		Left beams		Right beams	
Story	Left (kips)	Right (kips)	Left (kips)	Right (kips)	Axial force (kips)	Bending (ft-kips)	Axial force (kips)	Bending (ft-kips)
3	-22	-22	-9	-9	0	43	0	43
2	-25	-25	-33	-33	17	49	17	49
1	-25	-25	-59	-59	19	49	19	49

6.2.3 Strength Design

The seismic load combination 5 (Eq. 4.1) specified in Section 12.4.2.3 of ASCE 7-05 was adopted as the critical basic load combination for strength design.

$$(1.2D + 0.2S_{DS}) + L + \rho Q_E = F_v + F_E \qquad (4.1)$$

in which F_v represents the member forces induced by the factored vertical loads of $(1.2 + 0.2S_{DS})D + L$, as previously computed and listed in Table 6.3, Q_E stands for effects of horizontal seismic forces (Table 6.2), and F_E is the amplified earthquake effects corresponding to ρQ_E, i.e., Q_E is multiplied by a redundancy factor ρ (for simplicity, the maximum value of 1.3 is used for ρ). When the design of columns is performed, the seismic load effects must be modified to account for system overstrength. The basic combination for strength design with overstrength factor shall be determined in accordance with Eq. 4.2 (Section 12.4.3.2 in ASCE 7-05) as follows:

$$(1.2D + 0.2S_{DS}) + L + \Omega_0 Q_E = F_v + F_E \qquad (4.2)$$

where the system overstrength factor, Ω_0, for concentrically braced frames is specified as 2. A summary of demands of the members in the strength design phase is shown in Table 6.5.

Only the proportioning of the bracing members is carried out in this phase. This is because the lateral resistance of the entire structure is provided primarily by the braces. The rest of sizes of the structural members are redesigned and updated due to the larger member force demands during the capacity design phase.

Table 6.5 Demands of the structural members in the strength design phase.

Story	Braces		Columns		Left beams		Right beams	
	Left (kips)	Right (kips)	Left (kips)	Right (kips)	Axial force (kips)	Bending (ft-kips)	Axial force (kips)	Bending (ft-kips)
3	144	-205	-12	-12	-264	61	0	61
2	247	-317	130	-222	-271	69	155	69
1	301	-371	377	-542	-268	69	239	69

6.2.3.1 Design of the bracing members

The design of the first-story brace is illustrated next. The critical combination is controlled by the compression force. The first-story right brace *db* is subjected to a compression force as shown below and the resulting force is the same as that shown in Table 6.5.

$$F_T = F_V + F_E = -35 - 1.3 \times 258$$
$$= -371 \text{ kips}$$

Select a HSS $8 \times 8 \times \frac{5}{8}$ ($\phi_c P_n = 439$ kips, $F_y = 46$ ksi, cited from Table 4-4 in AISC Manual). This brace also meets the requirements of the slenderness ratio and seismic compact section stipulated in Section 13.2 and Table I-8-1, respectively, in AISC Seismic Provisions for steel structures. Note that a HSS $8 \times 8 \times \frac{1}{2}$ provides $\phi_c P_n = 367$ kips, which is less than the required strength.

6.2.4 Capacity Design

After the sizes of the braces were determined in the strength design phase, the design for zipper struts and redesign for the other structural members is performed using the brace capacities. The sequence is identical to the load path of the partial-height zipper mechanism as follows: zipper struts, top-story braces, columns, and finally beams.

6.2.4.1 Design of the zipper strut *dg*

The second-story zipper strut functions as a tension member to overcome the unbalanced vertical forces corresponding to the difference between the tension and compression capacities at ultimate, $R_y F_y A_g$ and $0.3P_n$, respectively, as shown in Figure 6.6.

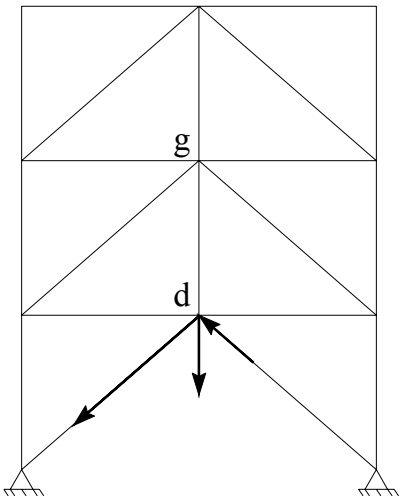

Figure 6.6 First-story unbalanced vertical force sustained by the second-story zipper strut.

Initially, the first-story braces provide the second-floor beam with support at midspan. However, when the first-story brace buckles, the braces can no longer provide support and the second-story zipper strut starts to take over. As a result, the required strength for the second-zipper strut is the combination of the unbalanced vertical force and the reaction at midspan of the second-floor beam induced by unfactored vertical loads.

$$(T_{zip})_u = \frac{5}{8} \times (0.3 + 1.44) \times 30 + (R_y F_y A_g - 0.3P_n) \times \frac{13}{19.85}$$
$$= 579 \text{ kips}$$

Use W 12×45 ($\phi_t P_n = 590$ kips, $F_y = 50$ ksi) meeting the seismically compact criteria.

6.2.4.2 Design of the third-story zipper strut *gj*

The third-story zipper strut sustains not only the second-story unbalanced vertical force and the reaction at midspan of the third-floor beam, but also the required force in the second-story zipper strut, as shown in Figure 6.7. The required force for the third-story zipper strut is computed as follows:

$$(T_{zip})_u = \frac{5}{8} \times (0.3 + 1.44) \times 30 + (R_y F_y A_g - 0.3 P_n) \times \frac{13}{19.85} + 646$$
$$= 1060 \text{ kips}$$

Use W 12×96 ($\phi_t P_n = 1270$ kips, $F_y = 50$ ksi) because W 12×87 does not meet the seismically compact criteria.

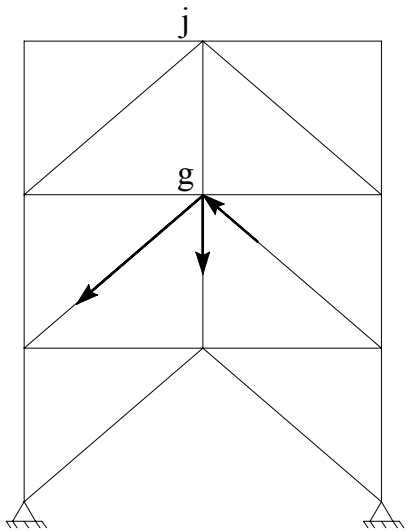

Figure 6.7 Second-story unbalanced vertical force sustained by the 3nd-story zipper strut.

6.2.4.3 Redesign of the top-story bracing members *jf* and *jh*

The top-story braces are redesigned and updated at this stage because, when the structure develops its ultimate strength, they have to remain elastic so as to overcome the unbalanced vertical forces generated by the braces below. Accordingly, the required strength for the third-story braces should consider both the required force in the third-story zipper strut and the forces induced by the horizontal seismic loads including structural overstrength. The third-story right brace, for example, is subjected to the force of 1060 kips from the third-story zipper in combination with twice the member force of -268 kips [i.e., $2\times(-134)$ kips], induced by twice the horizontal seismic loads (See Table 6.2) as well as the reaction at midspan of the roof-floor beam (Figure 6.8). The process of computation is presented as follows:

$$F_{jh} = -\frac{1}{2}\left(\frac{5}{8}\times(0.3+1.25)\times 30+1060\right)\frac{19.85}{13}-268$$
$$= -1100\,\text{kips}$$

Use W14×132 ($\phi_c P_n = -1300$ kips, $F_y = 50$ ksi, Table 4-1 in AISC Manual) because W14×120 does not meet the seismically compact criteria.

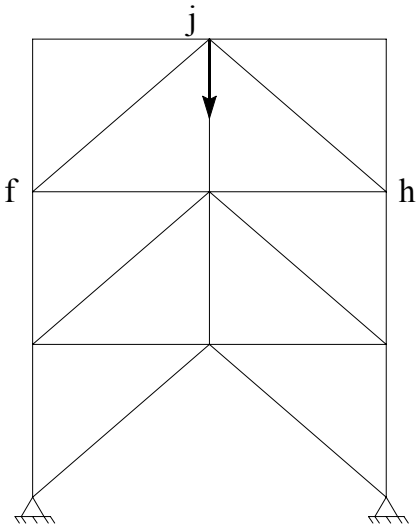

Figure 6.8 Required forces for the top-story braces.

6.2.4.4 Design of the first-story column *eb*

For the first-story column *eb*, the required force (Figure 6.9) is calculated by superimposing the required force from the third-story right brace, the minimum post-buckling strength from the second-story right brace, and the axial member force induced by the unfactored vertical loads (Table 6.4). The required strength for column *he* is calculated as follows:

$$(P_u)_{eb} = [(P_u)_{\text{top–story brace}} + 0.3(P_n)_{\text{second-story brace}}] \times \frac{13}{19.85} + (F_{eb})_v$$

$$= (-1100 - 0.3 \times 408) \times \frac{13}{19.85} - 59$$

$$= -860 \; kips$$

This required strength is larger than the demand obtained in the strength design phase. Use W12×96 ($\phi_c P_n = 1050$ kips, $F_y = 50$ ksi), which satisfies the seismic provisions for the seismic compact sections.

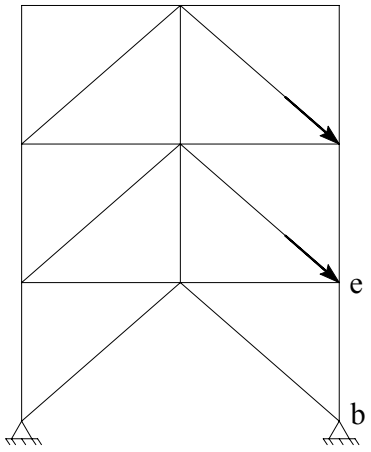

Figure 6.9 Required force for the first-story column.

6.2.4.5 Design of the third-floor beam *gh*

Both the top-story braces are subjected compression, leading to tension in the third-floor beam. From the horizontal force equilibrium at joint *h*, the required axial force can be determined as follows:

$$T_u = -(P_u)_{\text{top-floor brace}} \times \frac{15}{19.85} + (F_{gh})_v$$
$$= -(-1100) \times \frac{15}{19.85} + 17$$
$$= 848 \text{ kips}$$

Also, the bending moment at midspan of the third-floor beam from the demand in the strength design phase, which is 69 ft-kips from Table 6.5, needs to be reanalyzed and checked. Use $W10 \times 88$ [$T_u/\phi_t T_n + 8/9 * (M_u/\phi_b M_n) = 0.86 \le 1.0$, when F_y = 50 ksi is used], which meets the seismically compact criteria.

6.2.4.6 Member sizes for the zipper-braced bay

Table 6.6 shows a summary of the member sizes for the zipper-braced bay proportioned on the basis of the previous design.

Table 6.6 Summary of the member sizes for the 3-story zipper-braced bay.

Story	Braces	Columns	Beams	Zipper struts
3	W14x132	W12x96	W8x58	W12x96
2	HSS8x8x1/2	W12x96	W10x88	W12x45
1	HSS8x8x5/8	W12x96	W10x88	

6.2.5 Allowable Story Drift Limit

With the occupancy category IV and belonging to structures 4 stories or less with interior walls, partitions, ceilings and exterior wall systems that have been designed to accommodate the story drifts (Table 12.12-1 in ASCE 7-05), the allowable story drift for the 3-story zipper frame is $0.015h_{sx}$, where h_{sx} is the story height below Level x. Figure 6.10 displays the design story drifts along the height of the 3-story zipper frame under the strength level seismic forces, which are less than the allowable story drifts. In the story drift determination, the design story drift were computed as the difference of the elastic displacements at the Levels considered and below multiplied by a factor of C_d/I_E, in which C_d is the amplification factor and 5 for this type of seismic force-resisting system.

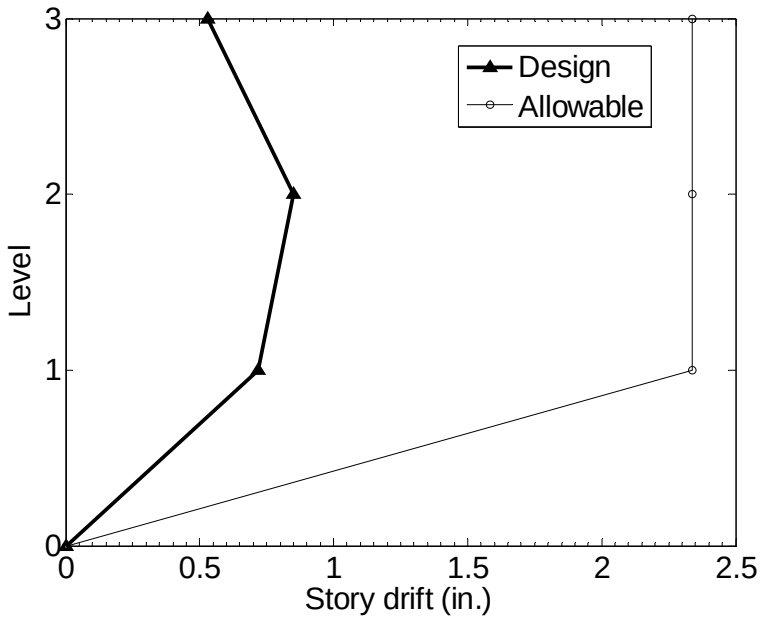

Figure 6.10 Examination of the design story drift.

6.3 Design of the 9-Story Zipper-Braced Model Building

Following the same design procedure, the 9-story zipper-braced bay was proportioned, the member sizes of which are listed in Table 6.7.

Table 6.7 Summary of the member sizes for the 9-story zipper-braced bay.

Story	Braces	Columns	Beams	Zipper struts
9	W14x398	W14x257	W10x68	W14x398
8	HSS7x7x1/2	W14x257	W14x257	W14x370
7	HSS8x8x1/2	W14x257	W10x88	W14x342
6	HSS8x8x5/8	W14x283	W10x88	W14x283
5	HSS9x9x5/8	W14x283	W12x96	W14x233
4	HSS9x9x5/8	W14x311	W12x96	W14x193
3	HSS10x10x5/8	W14x311	W12x96	W14x132
2	HSS10x10x5/8	W14x342	W12x96	W14x82
1	HSS12x12x5/8	W14x342	W12x96	

6.4 Design of the 20-Story Zipper-Braced Model Building

Following the same design procedure, the member sizes of the 20-story zipper-braced bay were selected as listed in Table 6.8.

Table 6.8 Summary of the member sizes for the 20-story zipper-braced bay.

Story	Braces	Columns	Beams	Zipper
20	W14x550	W14x68	W10x30	W36x800
19	HSS5x5x5/16	W14x426	W24x279	W14x730
18	HSS5.5x5.5x5/16	W14x426	W10x30	W14x730
17	HSS6x6x3/8	W14x426	W10x30	W14x665
16	HSS6x6x1/2	W14x426	W10x39	W14x665
15	HSS6x6x1/2	W14x426	W10x39	W14x605
14	HSS6x6x5/8	W14x455	W10x45	W14x550
13	HSS6x6x5/8	W14x455	W10x45	W14x550
12	HSS7x7x1/2	W14x455	W10x45	W14x500
11	HSS7x7x1/2	W14x455	W10x45	W14x455
10	HSS7x7x1/2	W14x455	W10x45	W14x398
9	HSS7x7x1/2	W14x455	W10x45	W14x370
8	HSS8x8x1/2	W14x500	W12x50	W14x342
7	HSS8x8x1/2	W14x500	W12x45	W14x283
6	HSS8x8x1/2	W14x500	W12x45	W14x233
5	HSS8x8x1/2	W14x550	W12x45	W14x193
4	HSS8x8x1/2	W14x550	W12x45	W14x159
3	HSS8x8x1/2	W14x550	W12x45	W14x109
2	HSS8x8x1/2	W14x605	W12x45	W14x68
1	HSS9x9x5/8	W14x605	W12x50	

CHAPTER 7

ANALYTICAL STUDY OF ZIPPER-BRACED FRAMES

7.1 Introduction

Based on the design examples in Chapter 6, the seismic performance of three analytical models for the 3-, 9-, and 20-story zipper frames are discussed in this chapter. These models are used to investigate the behavior of the zipper frames by both nonlinear static analyses (pushover analyses) and nonlinear dynamic analyses using the OpenSEES program.

For the zipper frames under a set of pushover loads, the pushover curve can be approximated by a tri-linear curve that provides three base shear levels in addition to the design seismic base shear: a buckling base shear, a yielding base shear, and an ultimate base shear. These values are used to distinguish the structural strengths at which whether the braces begin to buckle, yield, and approach the ultimate strength.

The nonlinear dynamic analyses consisted of a suite of 20 ground motions (LA21 to LA40, Somerville et al., 1997) representative of a 2%-in-50-year probability of exceedence for the Los Angeles area. The demand forces for the zipper struts and top-story braces are compared to the required forces computed in the course of design in order to verify the appropriateness of the design in such members. Similarly, the interstory drift demand ratios are also examined and further evaluated statistically. Finally, the PGAs for the ground motion ensemble are further scaled so as to match the design spectrum at the structural fundamental period of each structure and nonlinear analyses are repeated. The statistical values of the mean plus one standard deviation of the peak interstory drift ratios for the modified ground motion ensemble are then compared to the allowable insterstory drift ratio limit specified in ASCE 7-05.

7.2 Three-Story Zipper-Braced Model Building

7.2.1 Pushover Analysis

A 2D pushover analysis/nonlinear static analysis was performed using OpenSEES (PEER) to estimate the maximum strength and deformation capacities of the zipper frames designed in the previous chapter. For the simulation of the behavior of the bracing members (Appendix C), nonlinear beam-column elements with the fiber section function were used. An additional joint was added at the middle length of a bracing member with an initial imperfection of L/150 in the direction perpendicular to the element. Two rotational springs with stiffness of 79 m-kN/rad (700 in-kips/rad) were added at the ends of a brace to increase the post-buckling strength. The beams and columns were modeled also using nonlinear beam-column elements with the fiber section function, which can track the yielding status of the prescribed fibers in the flanges. P-δ effects were considered using the Corotational Transformation command available in OpenSEES.

The resulting pushover curve, plotted as the roof drift ratio Δ vs. the base shear coefficient *C* (defined as the base shear divided by the seismic weight per one braced bay) is shown in Figure 7.1 at two different scales of the drift value. Figure 7.1(a) indicates a very ductile structure and can be well approximated by a tri-linear curve with three stages [(0% ~ Δ_b=0.20%), (Δ_b ~ Δ_y=0.68%), (Δ_y ~ Δ_o=11.05%)]. In stage 1, the structure behaves as linearly elastic until the first buckling occurs in a compression brace [Figure 7.1(b)]. The maximum base shear in this stage is called the buckling base shear, corresponding to C_b=0.55 and 2643 kN (594 kips). This is larger than the design seismic base shear of 1736 kN (390 kips, C_s=0.36) by a buckling overstrength factor, Ω_b, of 1.52. The buckling overstrength factor, Ω_b, is defined as the buckling base shear divided by the design seismic base shear. Note that the design seismic base shear was the summation of the equivalent lateral force used in the course of design. In stage 2, the compression braces buckle and their capacities tend towards the minimum post-buckling strength, while the

tension braces continue to attract load until their tension yield capacities are reached. The yielding base shear is 3916 kN (880 kips, C_y=0.81) and the corresponding overstrength Ω_y is 2.26. After yielding in the tension braces, the base shear enters a hardening range and approaches the ultimate base shear of 4223 kN (949 kips, C_o=0.88) at the roof drift ratio Δ_o=11.05 %. The structural ultimate overstrength Ω_o is 2.43.

According to Table 12.2-1 in ASCE 7-05, the response modification factor *R* is 6. The elastic base shear is the multiplication of the design base shear by a factor of *R*/*I*, leading to 6942 kN (1560 kips, C_{eu}=1.44). The corresponding elastic roof drift ratio is Δ_e=0.53 %. The triangular area under the red line shown in Figure 7.1(b) corresponds to the total elastic input energy, or energy demand (E_d) of 218 m-kN (1929 in-kips). In order to provide a conservative structure, the energy capacity (E_c), which can be viewed as the area under the pushover curve (roof drift vs. base shear), should be greater than the energy demand. This requires that the structure should remain stable until the roof drift ratio reaches 0.68 % [E_c=219 m-kN (1940 in-kips)], which is almost the same as the yielding roof drift ratio (Δ_y=0.68 %) and far away from the ultimate roof drift ratio Δ_o. If the area under the pushover curve up to the ultimate drift ratio is considered, E_c is 4456 kN (39423 in-kips) or about 20.4 times that from an equivalent elastic system. This demonstrates the considerable overstrength and deformation capacity of the zipper system. While not a fair comparison, it is interesting to note that the same frame but with no zipper elements would behave as shown in Figure 7.1(c) with small lateral strength and low ductility. For the sake of comparison, pushover curves of SAC LA 3-story structures with a moment-resisting system are shown in Figure 7.1(d). The design base shear for the moment resisting frame in Fig. 71(d) was XX kips (V/W of 0.08).

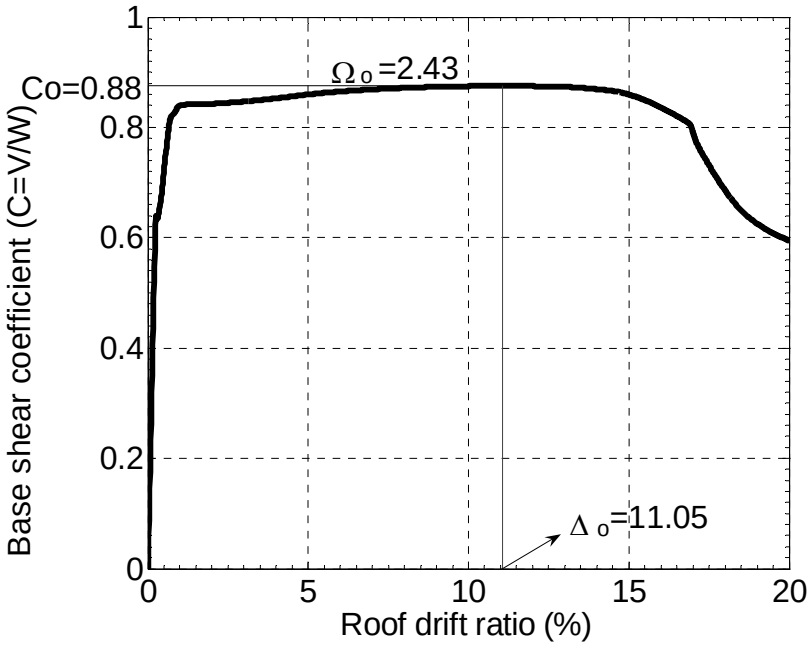

Figure 7.1(a) Pushover curve for the 3-story zipper-braced model building (0~20%).

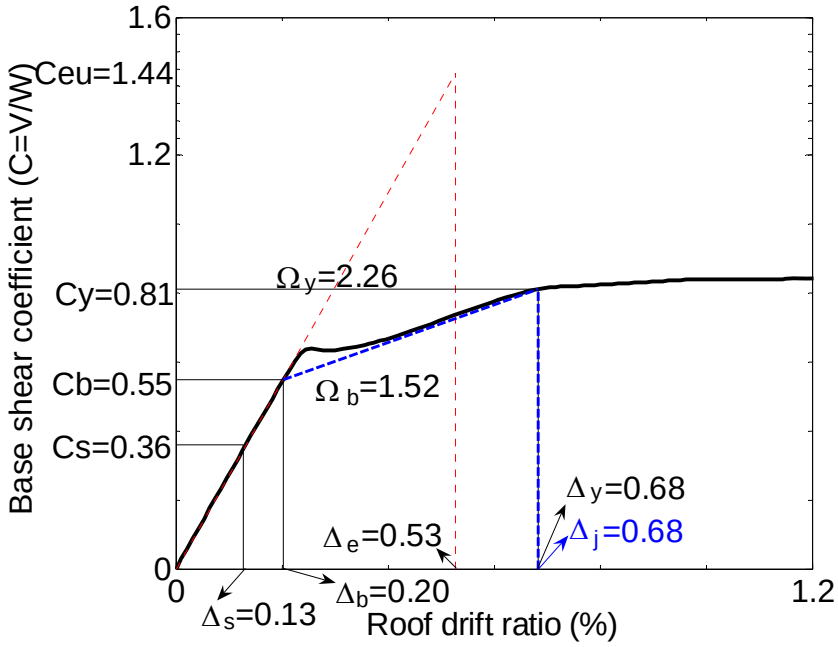

Figure 7.1(b) Pushover curve for the 3-story zipper-braced model building (0~1.2%).

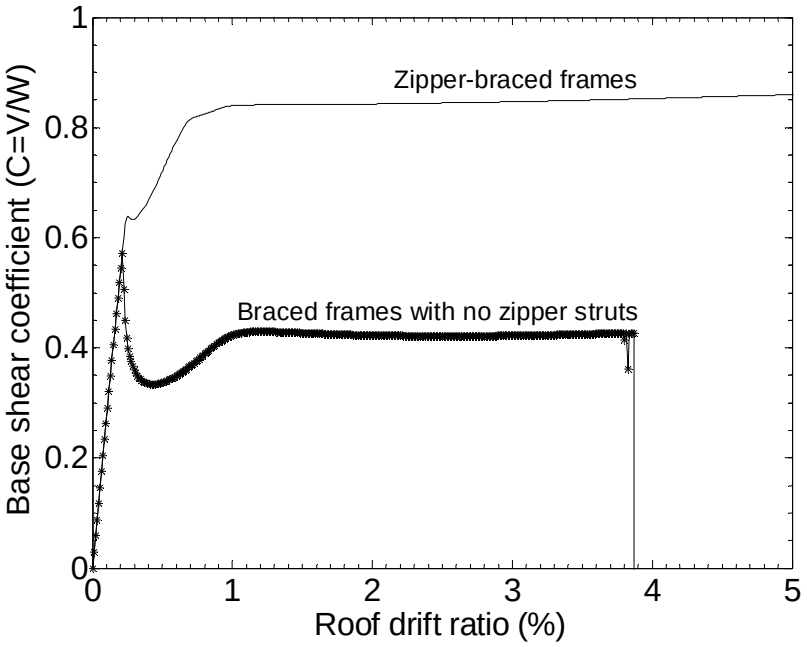

Figure 7.1(c) Pushover curve for the 3-story braced frame with no zipper struts.

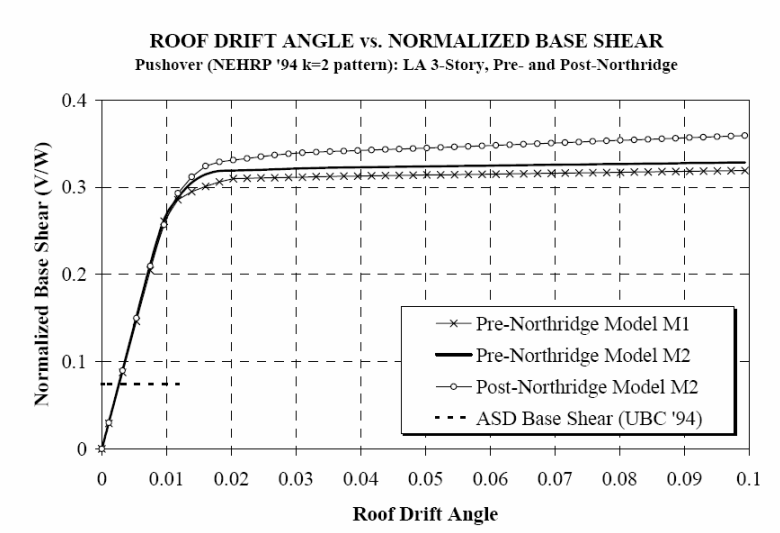

Figure 7.1(d) Pushover curves for SAC LA 3-story moment resisting frames (From FEMA 355C).

For the brace models, the backbone curves for the first-story tension and compression braces are shown in Figure 7.2 and Figure 7.3, respectively. From these figures and comparisons to the experimental tests, it appears that OpenSEES can predict well the buckling strength. However, the simulated post-buckling strength is not reasonable due to the steep drop in strength after the first buckling (See Figure 4.26) and the underestimation of the minimum post-buckling strength, as compared with $0.3P_n$ specified in AISC Seismic Provisions.

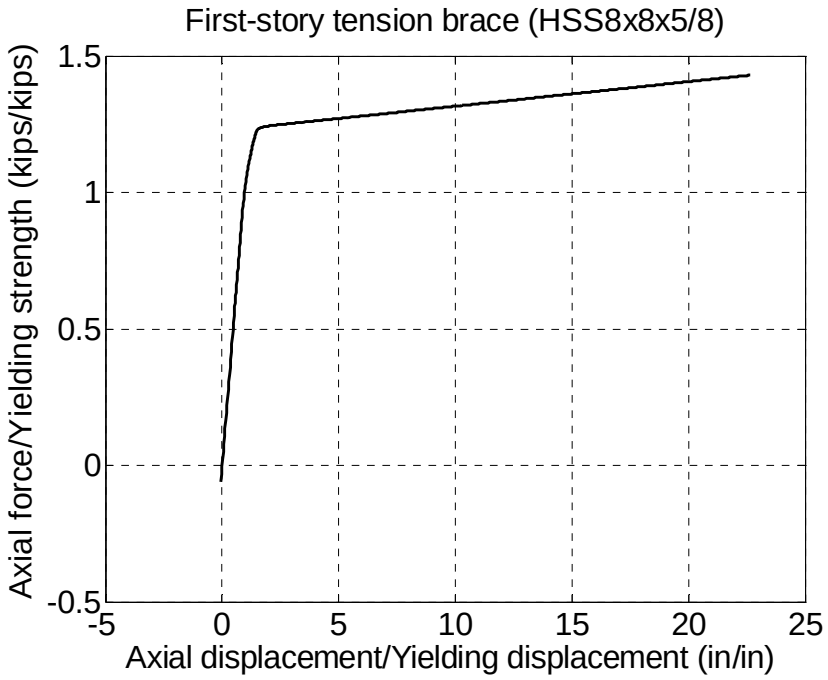

Figure 7.2 Tension brace model for pushover analyses.

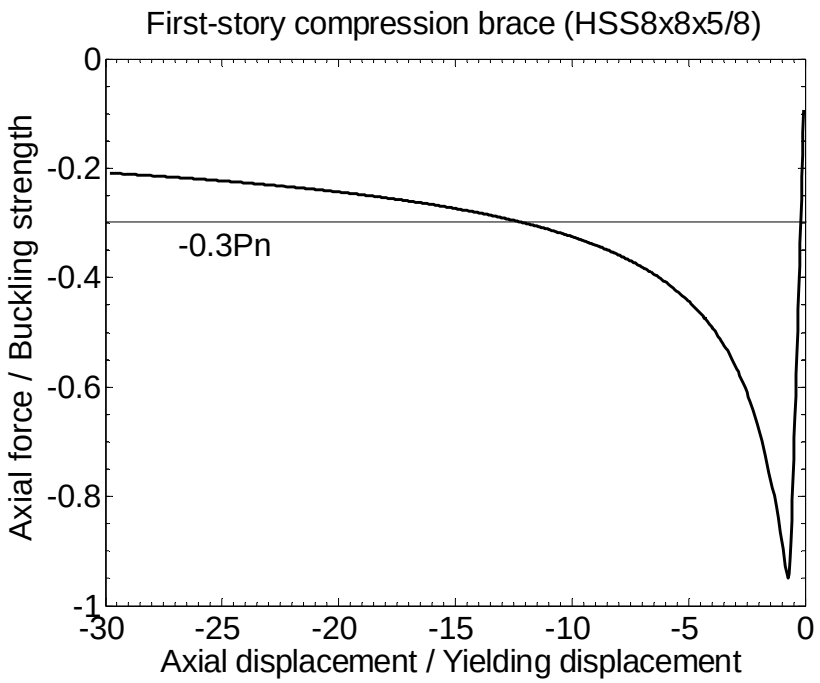

Figure 7.3 Compression brace model for pushover analyses.

7.2.2 Nonlinear Dynamic Analyses

In order to examine the dynamic performance of this building model, nonlinear dynamic analyses were performed using the OpenSEES computer program. The brace, beam, and column models were the same as those used in the pushover analysis of the 3-story zipper frame. An example of the hysteretic behavior of the first-story left brace model when the zipper-braced frame was subjected to the LA22 ground motion is shown in Figure 7.4. P-δ effects were considered using the Corotational Transformation command, and 5% Rayleigh damping was specified in the first and third modes of vibration. The eigenvalue analysis showed that the computed periods of the structure in its first three vibration modes were 0.34, 0.11, and 0.07 sec, respectively. The first three mode shapes are presented in Figure 7.5.

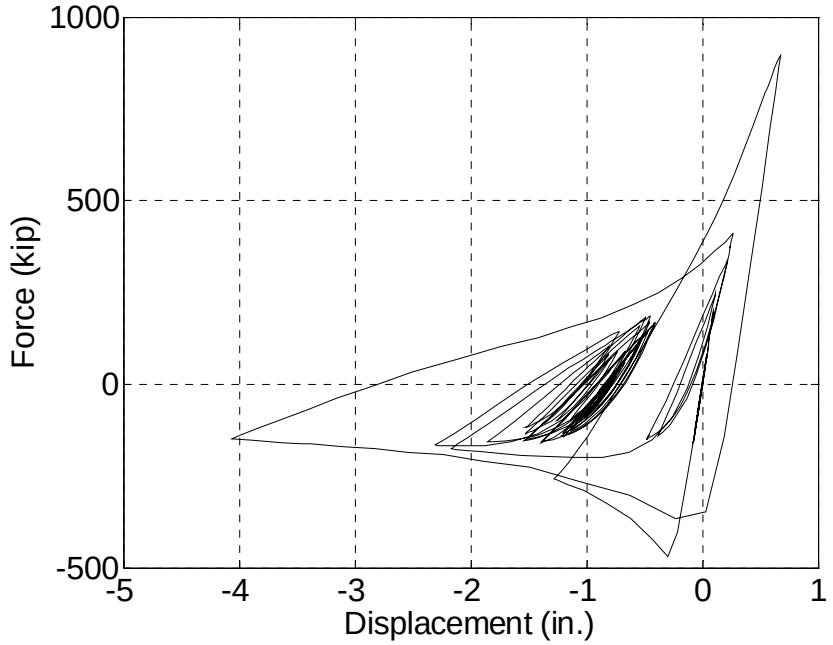

Figure 7.4 Hysteretic behavior of the first-story left brace (LA22).

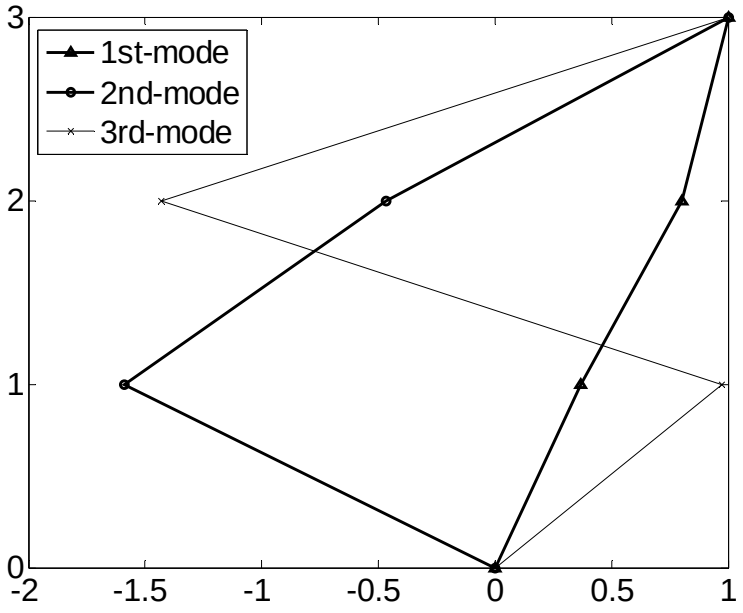

Figure 7.5 First three mode shapes.

In order to verify the appropriateness of the zipper strut forces obtained from the design process (Chapter 6.2), the envelopes of forces in the zipper struts are examined next. The peak tension and compression forces acting in each story zipper strut for each earthquake are listed in Table 7.1. From Sections 6.2.4.1 and 6.2.4.2, the tension design strengths of the second- and third-story zipper struts are 2577 kN (579 kips) and 4717 kN (1060 kips), respectively. Their compression strengths with the effective length of 4m (13 feet) are -1647 kN (-370 kips) and -4673 kN (-1050 kips), respectively. If the maximum peak tension and compression forces among the ensemble of earthquakes, as shown in the bold and italic style in Table 7.1, are normalized by the required strength $T_{req'd}$ for tension and by the design strength ϕP_n for compression, respectively, the envelopes of the normalized zipper strut forces are obtained, as presented in Figure 7.6. This demonstrates that the design procedure provides zipper struts with conservative and well-predicted required strengths.

Table 7.1 Peak tension and compression forces in zipper struts (2% exceedence in 50 years).

	2nd-story zipper strut		3rd-story zipper strut	
	Tension	Compression	Tension	Compression
	(kip)	(kip)	(kip)	(kip)
LA21	***547.1***	***-130.9***	***962.2***	-204.3
LA22	524.0	-100.8	924.0	-119.9
LA23	129.3	-15.4	138.3	0.3
LA24	193.2	-15.1	265.9	0.3
LA25	528.8	-73.0	931.1	0.3
LA26	533.3	-74.8	923.8	-5.6
LA27	363.0	-15.1	567.7	0.3
LA28	515.8	-126.8	919.1	***-238.7***
LA29	295.3	-21.9	459.5	0.3
LA30	470.7	-18.0	786.9	0.3
LA31	525.3	-47.5	952.7	-121.3
LA32	529.5	-119.7	933.7	-163.8
LA33	449.7	-15.2	786.5	0.3
LA34	474.9	-15.4	806.0	0.3
LA35	514.7	-74.1	898.6	-23.8
LA36	504.3	-19.2	889.2	0.3
LA37	296.7	-15.1	484.0	0.3
LA38	296.0	-15.1	445.5	0.3
LA39	307.2	-15.2	544.1	0.3
LA40	148.7	-15.1	163.8	0.3

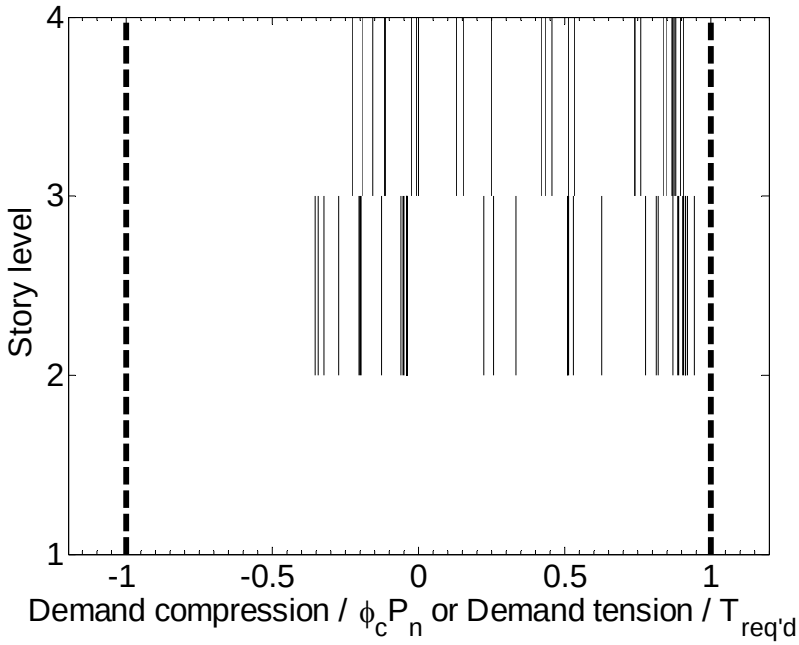

Figure 7.6 Normalized peak tension and compression forces in zipper struts (2% exceedence in 50 years).

The assessment of the performance of the top-story braces was performed in a similar way. The peak tension and compression forces in the top-story braces for each ground motion are listed in Table 7.2. The demand compressive strength for the top-story braces was -4882 kN (-1097 kips), which was less than the required strength -4895 kN (-1100 kips) obtained from the design process (see Section 6.2.4.3). Also, all the required tension forces in the top-story braces were very small.

Table 7.2 Peak forces in the top-story braces (2% exceedence in 50 years).

	Top-story left brace		Top-story right brace	
	Tension	Compression	Tension	Compression
	(kip)	(kip)	(kip)	(kip)
LA21	246.7	-1052.0	154.8	-623.8
LA22	193.5	-1022.6	140.5	-820.2
LA23	152.0	-316.2	155.9	-255.2
LA24	154.8	-413.2	150.2	-305.9
LA25	161.3	-532.8	110.1	-1038.0
LA26	119.6	-694.6	146.2	-1011.8
LA27	101.2	-493.8	139.1	-678.4
LA28	108.2	-591.1	344.5	***-1097.4***
LA29	232.2	-596.8	187.3	-436.3
LA30	190.3	-891.4	229.3	-693.9
LA31	188.8	-1031.0	201.3	-1090.2
LA32	238.4	***-1057.0***	205.0	-806.3
LA33	131.2	-923.7	158.0	-918.7
LA34	149.0	-909.7	160.9	-631.1
LA35	168.5	-766.1	192.1	-974.2
LA36	155.5	-984.8	202.2	-674.8
LA37	118.8	-619.0	142.1	-394.4
LA38	107.5	-571.2	116.9	-284.7
LA39	136.0	-484.2	158.2	-660.2
LA40	134.2	-368.6	170.3	-341.8

Table 7.3 shows the peak interstory drift ratios when the 3-story zipper frame was under the same ensemble of earthquakes with 2% probability of exceedence in 50 years for Los Angeles. The values of the median and 84th percentile employed from here on to represent the statistical values of the peak interstory drift ratios are defined as in the page 5-28 in FEMA 355C. An illustration of the scatter of the story drift demands is provided in Figure 7.7, which shows the median and 84th percentile drift demands together with individual data points for the three-story zipper-braced frame. The median shows a uniform distribution of interstory drifts over the height, and the 84th percentile shows a

similar pattern. Even in the particular case of the earthquake LA21, which caused the maximum peak first-story interstory drift ratio of 3.71 % among the 20 earthquakes, the peak second-story interstory drift ratio approached 2.64 %. These results demonstrate the efficiency of the zipper struts in achieving more uniform story drift distribution over the height.

Table 7.3 Peak interstory drift ratios (2% exceedence in 50 years).

	Peak inter-story drift ratios (%)		
	1st story	2nd story	3rd story
LA21	***3.71***	***2.64***	0.19
LA22	***2.86***	2.21	0.24
LA23	0.36	0.31	0.12
LA24	0.45	0.40	0.13
LA25	1.89	1.05	0.27
LA26	2.04	0.98	0.26
LA27	0.76	0.52	0.18
LA28	2.44	2.25	0.33
LA29	0.59	0.62	0.19
LA30	0.95	0.91	0.20
LA31	1.61	1.65	0.28
LA32	***2.94***	2.17	0.22
LA33	1.08	0.97	0.24
LA34	0.95	0.93	0.17
LA35	1.49	0.91	0.24
LA36	1.20	1.12	0.19
LA37	0.58	0.62	0.15
LA38	0.59	0.56	0.12
LA39	0.66	0.55	0.19
LA40	0.37	0.36	0.13

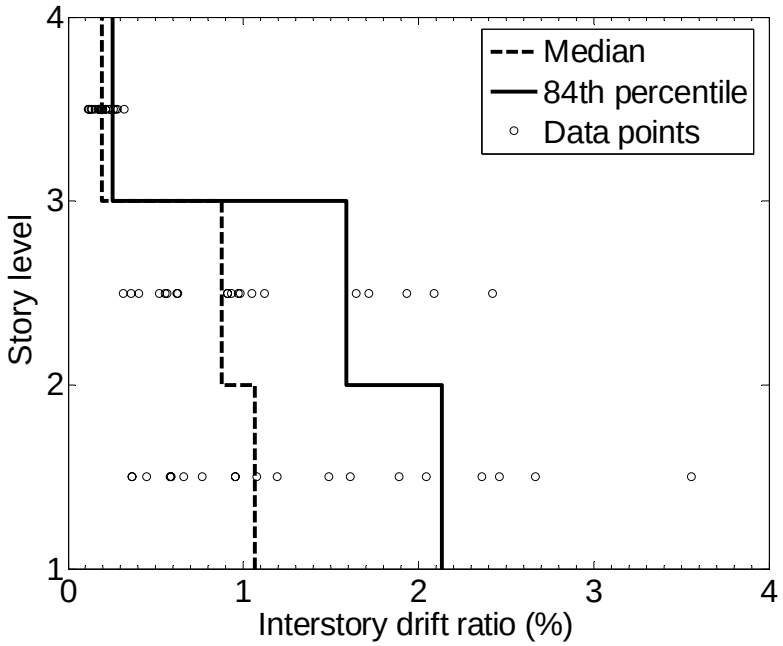

Figure 7.7 Dispersion of story drift for 3-story zipper frame under original ensemble of ground motions (LA21~LA40, 2% exceedence in 50 years).

For this 3-story zipper frame, the allowable interstory drift ratio limit from Section 16.2.4.3 in ASCE 7-05 is 1.875 % (or 125 percent of the allowable intersotry drift ratio of 1.5 % specified in Section 12.12.1 in ASCE 7-05). For comparison to this value, the ensemble of the ground motions (LA21 ~ LA40) were further scaled to match the design spectral response acceleration, *S*, of 1.44g at the structure fundamental period, i.e., *S*(0.34 s) = 1.44 g. The scale factors used and the scaled PGA for each record are presented in Table 7.4. The resulting peak interstory drift ratios for the modified ensemble of accelerations are presented in Table 7.5. The median and 84th percentile values of the peak interstory drift ratios are plotted in Figure 7.8. Both median and 84th percentile demands show a fairly uniform distribution of peak interstory drifts over the height and are within the specified interstory drift ratio limit of 1.875 %. For two particular cases of the earthquakes LA38 and LA40, the adjusted peak ground

accelerations (1.18 and 1.11 g in Table 7.5) were greater than the 2%-in-50-years PGA of 0.9 g for the area in downtown Los Angeles, leading to the exceedence of 1.875 % of interstory drift ratio. Generally, the performance of the interstory drift ratio for the 3-story zipper frame is satisfactory with the 84^{th} percentile demands within the specification limit of 1.875 %.

Table 7.4 Modification of the records for the 3-story zipper frame.

	Scale Factor	PGA (g)
LA21	0.50	0.64
LA22	0.60	0.55
LA23	1.70	0.71
LA24	1.51	0.71
LA25	0.70	0.61
LA26	0.65	0.62
LA27	0.84	0.78
LA28	0.32	0.43
LA29	0.97	0.78
LA30	0.63	0.63
LA31	0.46	0.59
LA32	0.61	0.72
LA33	0.50	0.39
LA34	0.78	0.53
LA35	0.61	0.60
LA36	0.79	0.87
LA37	1.27	0.90
LA38	1.52	***1.18***
LA39	0.92	0.46
LA40	1.78	***1.11***

Table 7.5 Peak inter-story drift ratios when the 3-story zipper frame was under the modified acceleration ensemble.

	Peak inter-story drift ratios (%)		
	1st story	2nd story	3rd story
LA21	0.49	0.43	0.17
LA22	0.63	0.66	0.15
LA23	0.97	0.97	0.16
LA24	1.41	1.29	0.26
LA25	0.84	0.62	0.20
LA26	0.48	0.53	0.19
LA27	0.53	0.49	0.18
LA28	0.60	0.49	0.19
LA29	0.57	0.58	0.18
LA30	0.57	0.53	0.17
LA31	0.48	0.55	0.14
LA32	0.81	0.74	0.17
LA33	0.41	0.48	0.15
LA34	0.71	0.64	0.16
LA35	0.49	0.49	0.16
LA36	0.87	0.89	0.16
LA37	1.32	1.19	0.15
LA38	2.75	1.60	0.13
LA39	0.61	0.52	0.19
LA40	2.11	1.05	0.25

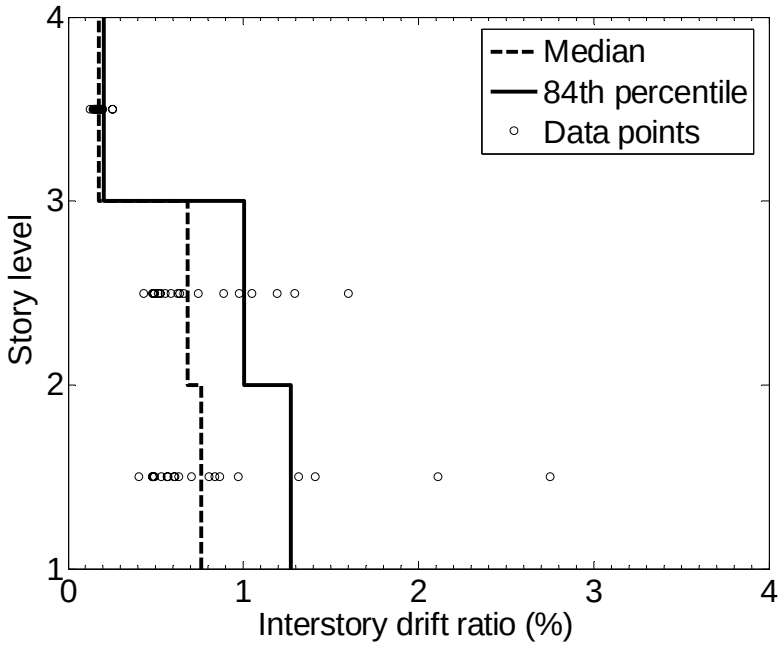

Figure 7.8 Dispersion of story drift for 3-story zipper frame under modified ensemble of ground motions.

7.3 Nine-Story Zipper-Braced Model Building

7.3.1 Pushover Analysis

The basic models used for the beam, column, and zipper strut elements in the analysis of the 9-story structure are the same as those for the 3-story zipper frame model. However, an alternative brace model is utilized for the 9-story frame to enhance the simulation of the post-buckling behavior. In this alternative brace model (brace model 2), the rotational stiffness is increased to 791 m-kN/rad (7000 in-kips/rad), and the elastic modulus of a brace is reduced to 199810 MPa (25000 ksi). The intent of these two modifications is to better match the initial buckling strength and the post-buckling behavior observed from the tests, as can be seen from a comparison in Figures 7.9. As

can be seen, these two modifications result in a simulated behavior that more closely matches that from the test.

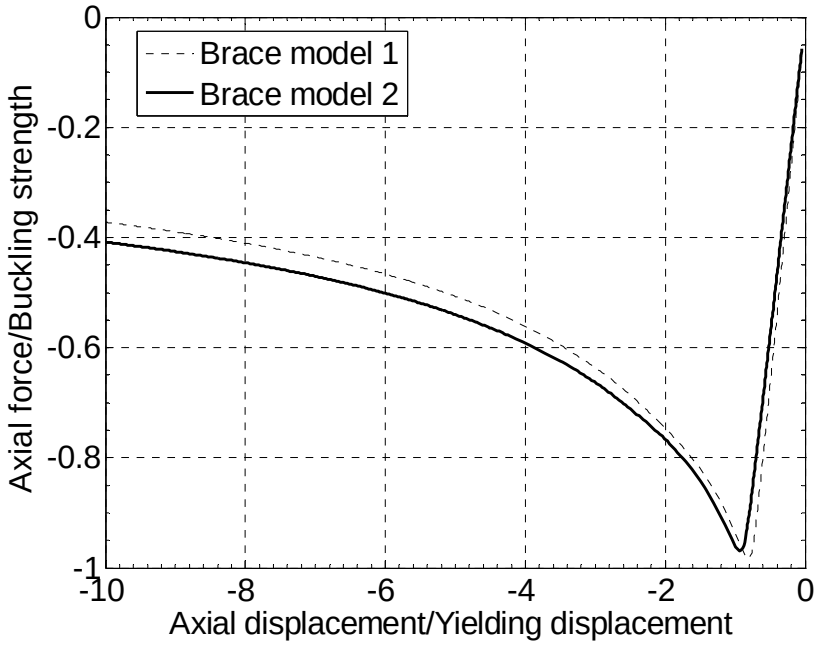

Figure 7.9 Comparison of brace model 1 and brace model 2.

The resulting pushover curve with the roof drift ratio Δ vs. the base shear coefficient C [defined as the base shear divided by the seismic weight 14712 kN (3306 kips) per one-braced bay] is shown in Figures 7.10(a) and (b). As for the 3-story case, Figure 7.10(a) indicates a very ductile behavior that can be approximated by a tri-linear curve [(0% $\sim \Delta_b$=0.41%), ($\Delta_b \sim \Delta_y$=1.53%), ($\Delta_y \sim \Delta_o$=6.77%)]. As shown in Figure 7.10(b), the structure is linearly elastic until the first buckling in one compression brace [3983 kN (895 kips), C_b=0.27]. This is larger than the design seismic base shear of 3008 kN (676 kips, C_s=0.20) by an overstrength factor, Ω_b, of 1.32. The yielding base shear is 5158 kN (1159 kips, C_y=0.35) and the corresponding overstrength Ω_y is 1.71. After yielding in the tension braces, the base shear enters a hardening range and approaches the

ultimate base shear of 5438 kN (1222 kips, C_o=0.37) at a roof drift ratio Δ_o=6.77%. The ultimate overstrength Ω_o is 1.81.

As shown in Figure 7.10(b), the elastic base shear is 10831 kN (2434 kips, C_{eu}=0.74) at the elastic roof drift ratio of Δ_e=1.10 %. The energy demand (E_d) is 2216 m-kN (19609 in-kips). When the roof drift ratio reaches 1.53 %, the energy capacity (E_c) is 2217 m-kN (19614 in-kips), which is slightly greater than the energy demand. This roof drift ratio is almost the same as the yielding roof drift ratio Δ_y=1.53 % and far away from the ultimate roof drift ratio Δ_o=6.77%. If the structure is pushed to the ultimate roof drift ratio, the energy capacity (E_c) is 12536 m-kN (110910 in-kips), which is 5.66 times the energy demand. For the sake of comparison, pushover curves of SAC LA 9-story structures with a moment-resisting system are shown in Figure 7.10(c).

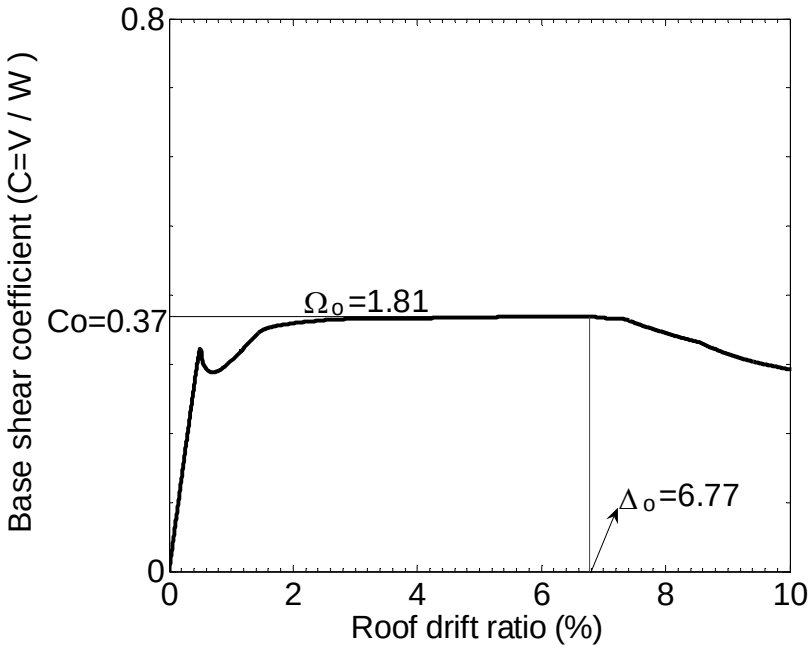

Figure 7.10(a) Pushover curve for the 9-story zipper frame.

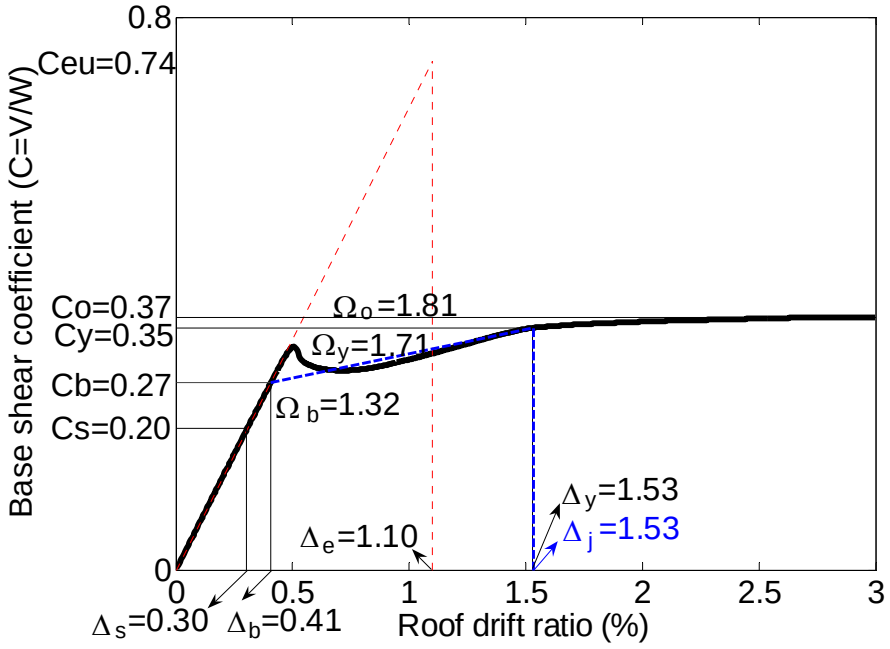

Figure 7.10(b) Pushover curve for the 9-story zipper frame (0 ~ 3%).

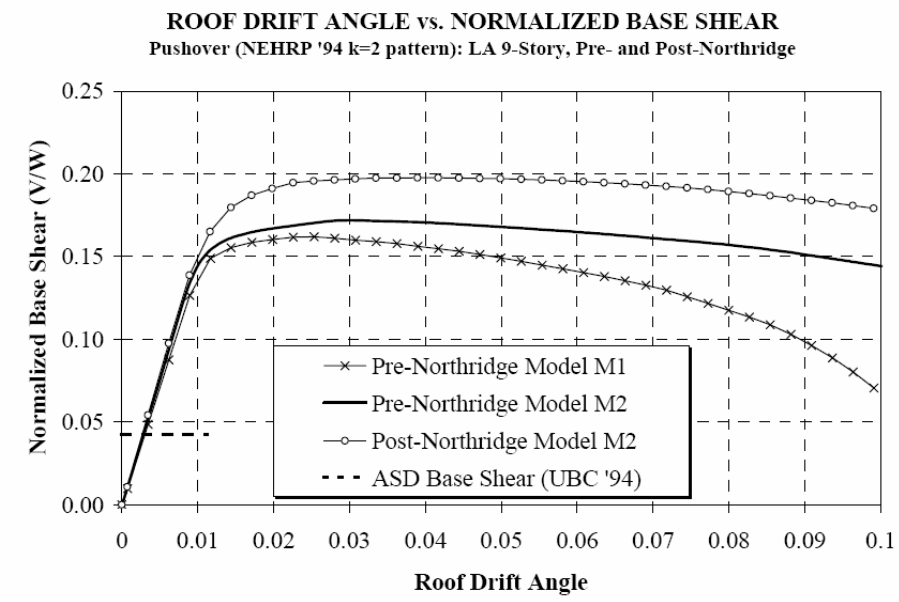

Figure 7.10(c) Pushover curves for SAC LA 9-story moment resisting frames.

7.3.2 Nonlinear Dynamic Analyses

The models of the structural elements are identical to those used in the pushover analysis for the 9-story zipper frame. P-δ effects were considered. However, 5% Rayleigh damping was specified in the first and ninth modes of vibration, ensuring the damping ratios of the other modes were less than 5 %. This damping assumption will probably result in an overestimation of peak interstory drift ratios, leading to a conservative comparison to an allowable interstory drift ratio from the nonlinear time history analyses. Through an eigenvalue analysis, the computed periods of the structure in its first three vibration modes were calculated as 1.09, 0.35, and 0.18 sec, respectively. The corresponding mode shapes are presented in Figure 7.11. The factors of the effective model masses for the first, second, and third modes were 0.76, 0.17, and 0.04, respectively. When only the first two modes were taken into account, the total factor of the effective model mass was 0.93.

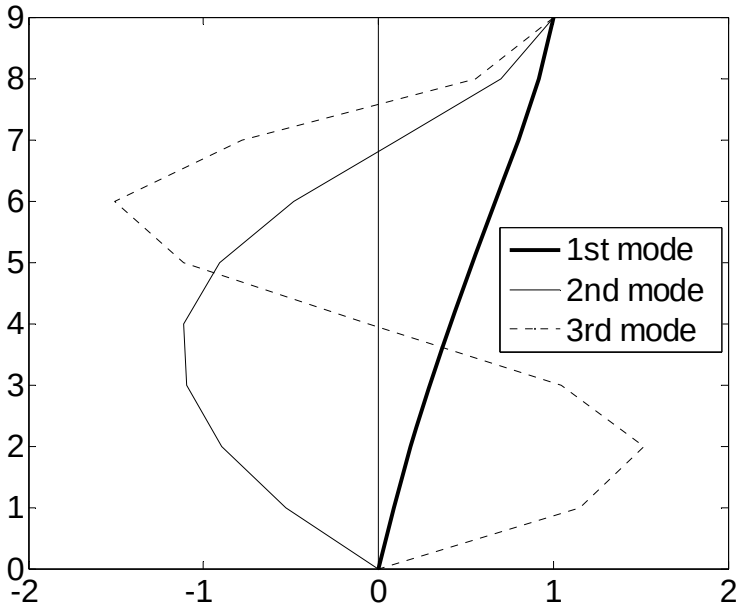

Figure 7.11 First three mode shapes of the 9-story zipper frame.

The reasonableness of the zipper strut forces used for design was verified by comparing the required forces to the envelopes of axial forces in the zipper struts from the nonlinear dynamic analyses. The peak tension and compression forces acting in each story zipper strut for each earthquake are listed in Table 7.6 and Table 7.7. If the maximum peak tension and compression forces among the ensemble of earthquakes, as shown in the bold and italic style in Table 7.6 and Table 7.7, are normalized by the required strength $T_{req'd}$ for tension and by the design strength ϕP_n for compression, respectively, the envelopes of the normalized zipper strut forces are obtained, as presented in Figure 7.12. All ratios of the demand tension force to the required tension force are close to and less than 1, and all ratios of the demand compression force to the design compression strength are much greater than -1. This demonstrates that the design procedure provides zipper struts with conservative and well-predicted required strengths.

Table 7.6 Peak tension forces in the zipper struts when the 9-story zipper frame was under an ensemble of earthquakes, LA21~LA40 (2% exceedence in 50 years).

	Zipper strut in tension (kip)							
	2nd	3rd	4th	5th	6th	7th	8th	9th
LA21	411	866	1154	1363	1776	2138	2418	2538
LA22	255	588	791	923	1021	1486	1797	1971
LA23	137	294	307	309	326	419	597	686
LA24	543	1094	1581	1958	2192	2355	2450	2428
LA25	511	934	1062	1511	2021	2451	2686	2717
LA26	566	1132	1688	2181	2617	3038	3351	3405
LA27	673	1234	1762	2146	2405	2603	2707	2663
LA28	670	1195	1743	1958	2311	2653	3002	3142
LA29	205	429	607	732	714	703	735	740
LA30	581	1122	1474	1682	1640	1509	1673	1680
LA31	338	679	995	1463	1877	2182	2524	2651
LA32	755	1284	1624	1947	2232	2384	2337	2210
LA33	497	1018	1387	1584	1622	1658	1608	1555
LA34	546	1044	1449	1932	2264	2427	2432	2407
LA35	***908***	***1570***	***2221***	***2779***	***3309***	***3743***	***4037***	***4133***
LA36	900	1545	2172	2719	3234	3585	3764	3737
LA37	831	1431	2004	2504	2750	2923	3006	2986
LA38	889	1526	2147	2685	3188	3477	3646	3586
LA39	352	713	1043	1455	1775	1969	2014	2011
LA40	851	1456	2038	2543	2960	3324	3569	3571

Table 7.7 Peak compression forces in the zipper struts when the 9-story zipper frame was under an ensemble of earthquakes, LA21~LA40 (2% exceedence in 50 years).

	Zipper strut in compression (kip)							
	2nd	3rd	4th	5th	6th	7th	8th	9th
LA21	-341	***-542***	***-639***	-416	-105	-87	-83	-13
LA22	-299	-473	-480	-262	-64	-40	-83	-13
LA23	-131	-101	-149	-146	-174	-75	-13	11
LA24	-50	-58	-64	-59	-52	-35	-13	11
LA25	-50	-79	-65	-58	-48	-34	-14	11
LA26	-240	-172	-58	-54	-66	-58	-14	11
LA27	-51	-107	-68	-65	-59	-37	-13	11
LA28	-148	-120	-58	-139	-47	-87	-111	3
LA29	-273	-350	-335	-167	-59	-33	-13	11
LA30	-311	-434	-426	-225	-103	-34	-13	11
LA31	-232	-143	-126	-184	-253	-166	-13	11
LA32	-457	-463	-387	-265	-245	-140	-71	11
LA33	-49	-79	-65	-114	-277	-34	-13	11
LA34	-148	-57	-63	-59	-53	-36	-13	11
LA35	-382	-413	-520	***-810***	***-878***	***-795***	***-744***	***-576***
LA36	-200	-268	-429	-542	-530	-374	-290	-151
LA37	-298	-196	-274	-202	-108	-87	-78	11
LA38	***-428***	-343	-467	-581	-377	-100	-13	11
LA39	-68	-114	-107	-54	-46	-33	-13	11
LA40	-143	-119	-241	-336	-286	-141	-13	11

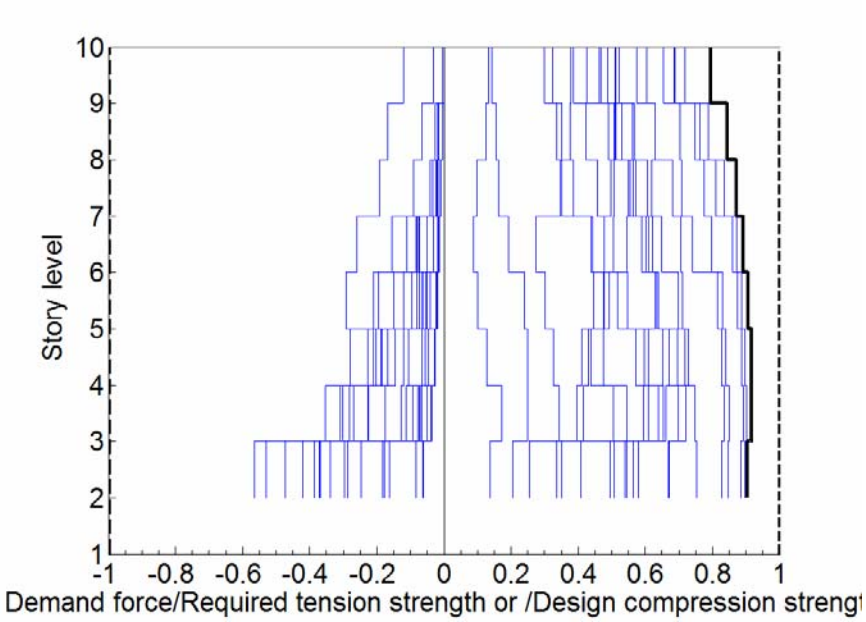

Figure 7.12 Normalized peak tension and compression forces in each story zipper strut when the 9-story zipper frame was under one earthquake of LA21~LA40 (2% exceedence in 50 years).

Similarly, an investigation on the applicability of the design procedure to the top-story braces was performed. The peak tension and compression forces in the top-story braces for each ground motion are listed in Table 7.8. The maximum demand compressive strength for the top-story braces was -15219 kN (-3420 kips), which was less than the required strength 18628 kN (-4186 kips). All the demand tension forces in the top-story braces were very small.

Table 7.8 Peak tension and compression forces in the top-story braces when the 9-story zipper frame was under an ensemble of earthquakes of LA21~LA40 (2% exceedence in 50 years).

	Top-story left brace (kip)		Top-story right brace (kip)	
	Tension	Compression	Tension	Compression
LA21	137	-2083	209	-2187
LA22	136	-1778	69	-1348
LA23	111	-750	137	-475
LA24	90	-1707	108	-2054
LA25	47	-1947	118	-2289
LA26	105	-2425	58	-2837
LA27	54	-1910	157	-2200
LA28	38	-2213	165	-2709
LA29	96	-662	120	-753
LA30	100	-1141	150	-1465
LA31	154	-1852	157	-2330
LA32	100	-1800	104	-1794
LA33	109	-1294	122	-1150
LA34	130	-1693	103	-2085
LA35	271	-2951	562	***-3420***
LA36	163	-2715	164	-3044
LA37	91	-2470	9	-2174
LA38	68	-2935	36	-2616
LA39	6	-1366	94	-1755
LA40	-8	-2552	52	-2951

The resulting peak interstory drift ratios are shown in Table 7.9 and Figure 7.13. The median line shows a uniform distribution of interstory drifts over the height. The maximum median peak interstory drift ratio was about 2.2 %, appearing in the second story. The 84th percentile line shows a similar pattern to the median line. The maximum peak interstory drift ratio in the 84th percentile line was about 4.0 %. For the case of

LA35, which caused the maximum peak first-story interstory drift ratio of 4.45 % among the 20 earthquakes, the second-, third- and forth-story peak interstory drift ratios were higher than the 84^{th} percentile demands with values of 6.33, 6.39, and 5.58 %, respectively. Again, these results demonstrate the efficiency of the zipper struts in achieving more uniform story drift distribution over the height.

Table 7.9 Peak interstory drift ratios when the 9story zipper frame was under an ensemble of earthquakes of LA21~LA40 (2% exceedence in 50 years).

	Peak interstory drift ratios (%)								
	1st	2nd	3rd	4th	5th	6th	7th	8th	9th
LA21	1.17	1.52	1.51	1.88	2.00	***2.95***	***3.41***	***2.54***	0.50
LA22	0.67	0.92	1.09	1.28	1.54	2.12	2.23	1.29	0.46
LA23	0.46	0.59	0.61	0.70	0.73	0.83	0.88	0.72	0.38
LA24	1.55	2.07	1.68	1.55	1.31	1.17	1.04	0.74	0.43
LA25	1.24	1.64	1.79	2.17	1.92	1.74	1.59	1.03	0.51
LA26	1.82	2.49	2.54	2.45	2.26	1.94	1.49	0.92	0.53
LA27	1.73	2.32	1.83	1.61	1.43	1.30	1.16	0.82	0.46
LA28	1.89	2.88	2.49	2.39	1.96	1.87	1.66	1.13	0.56
LA29	0.64	0.82	0.74	0.78	0.85	0.91	0.88	0.68	0.42
LA30	1.28	1.61	1.16	1.06	1.07	1.12	1.01	0.82	0.43
LA31	1.16	1.73	1.87	1.93	1.72	1.70	1.42	1.02	0.51
LA32	1.92	2.49	2.39	2.37	1.63	1.35	1.31	0.88	0.43
LA33	1.17	1.64	1.29	1.09	0.93	0.97	1.30	1.05	0.41
LA34	1.51	2.00	1.86	1.69	1.32	1.15	1.11	0.81	0.45
LA35	***4.45***	***6.33***	***6.39***	***5.58***	***3.53***	2.22	1.99	1.30	***0.69***
LA36	4.31	5.87	5.45	4.24	2.62	1.86	1.61	1.26	0.61
LA37	2.40	3.56	2.93	2.14	1.74	1.59	1.48	1.11	0.42
LA38	3.78	5.39	5.02	3.82	2.28	1.63	1.42	1.18	0.38
LA39	1.15	1.40	1.36	1.38	1.18	1.05	0.99	0.74	0.41
LA40	3.15	4.10	3.59	3.05	2.13	1.65	1.43	0.99	0.58

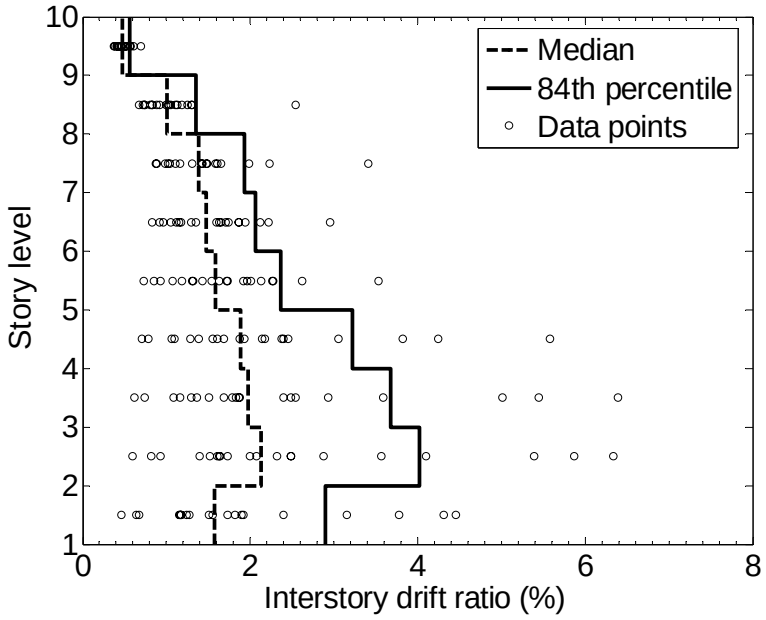

Figure 7.13 Dispersion of story drifts for 9-story zipper frame under original acceleration ensemble (LA21~LA40, 2% exceedence in 50 years).

For this 9-story zipper frame, the allowable interstory drift ratio limit is 1.25 %. The ensemble of the ground motions (LA21 ~ LA40) were further scaled to match the design spectral response acceleration, *S*, of 0.66 g at the structure fundamental period, i.e., *S*(1.09 s) = 0.66 g. The scale factor used and the scaled PGA for each record are presented in Table 7.10. The resulting peak interstory drift ratios for the modified ensemble of accelerations are presented in Table 7.11. The median and 84th percentile drift demands together with the individual data points of the peak interstory drift ratios are plotted in Figure 7.14. The median line shows a uniform distribution of interstory drifts over the height and is within the specified interstory drift ratio limit of 1.25 %. The 84th percentile line presents a similar pattern to the meidan one, but the maximum value appearing at the second story is about 1.55 %, larger than the code limit of 1.25 %. The 84th percentile values in the stories adjacent to the second story are 1.22 %, indicating the

small difference of the peak interstory drift ratios between the adjacent stories. For the case of the LA35 earthquake, which contributed many of the maximum values of the peak interstory drift ratios (Table 7.11), the lower stories had lager peak interstory drift ratios than the upper stories (Figure 7.14), and the maximum peak interstory drift ratio was 2.28 % exceeding the specification limit of 1.25 %. The reason why the second-story peak interstory drift ratio exceeded the code limit is that all the damping ratios with no more than 5% resulted in overestimation of the demands of the peak interstory drift ratios.

Table 7.10 Modification of the records for the 9-story zipper frame.

	Scale Factor	PGA (g)
LA21	0.31	0.40
LA22	0.35	0.32
LA23	1.21	0.51
LA24	0.48	0.23
LA25	0.45	0.39
LA26	0.35	0.33
LA27	0.86	0.79
LA28	0.49	0.65
LA29	1.16	0.94
LA30	0.98	0.97
LA31	0.50	0.64
LA32	0.34	0.40
LA33	0.54	0.43
LA34	0.64	0.44
LA35	0.61	0.60
LA36	0.46	0.51
LA37	0.51	0.36
LA38	0.46	0.35
LA39	0.77	0.39
LA40	0.71	0.44

Table 7.11 Peak interstory drift ratios when the zipper-braced frame was under the modified acceleration ensemble.

	Peak interstory drift ratios (%)								
	1st	2nd	3rd	4th	5th	6th	7th	8th	9th
LA21	0.41	0.57	0.70	0.89	0.97	1.06	1.02	0.79	0.40
LA22	0.41	0.59	0.67	0.81	0.80	0.83	0.82	0.66	0.41
LA23	0.78	1.02	0.92	0.81	0.80	0.93	1.04	***0.82***	0.40
LA24	0.56	0.75	0.78	0.87	0.87	0.87	0.82	0.64	0.41
LA25	0.58	0.75	0.78	0.83	0.84	0.88	0.84	0.66	0.42
LA26	0.46	0.66	0.71	0.80	0.81	0.81	0.76	0.61	0.38
LA27	1.48	1.88	1.56	1.45	1.28	1.14	1.01	0.75	0.43
LA28	1.23	1.52	0.96	0.91	0.88	0.94	1.00	0.75	0.37
LA29	0.68	0.93	0.78	0.84	0.93	1.03	0.98	0.76	***0.43***
LA30	1.23	1.49	1.10	1.02	1.03	1.07	0.97	***0.82***	***0.43***
LA31	0.61	0.81	0.65	0.70	0.70	0.72	0.68	0.57	0.36
LA32	0.59	0.71	0.77	0.88	0.84	0.88	0.92	0.74	0.41
LA33	0.55	0.71	0.64	0.68	0.72	0.75	0.73	0.66	0.38
LA34	0.73	1.03	0.88	0.81	0.66	0.65	0.71	0.63	0.37
LA35	***1.78***	***2.28***	***1.81***	***1.62***	***1.36***	***1.17***	0.98	0.68	***0.43***
LA36	1.19	1.37	1.07	0.95	0.88	0.89	0.90	0.73	***0.43***
LA37	1.01	1.25	1.01	0.94	0.91	0.91	0.87	0.71	0.40
LA38	0.94	1.19	1.07	1.02	0.85	0.77	0.73	0.61	0.34
LA39	0.64	0.85	0.90	0.97	0.92	0.82	0.74	0.60	0.37
LA40	1.41	1.80	1.37	1.26	1.18	1.14	***1.07***	0.79	***0.43***

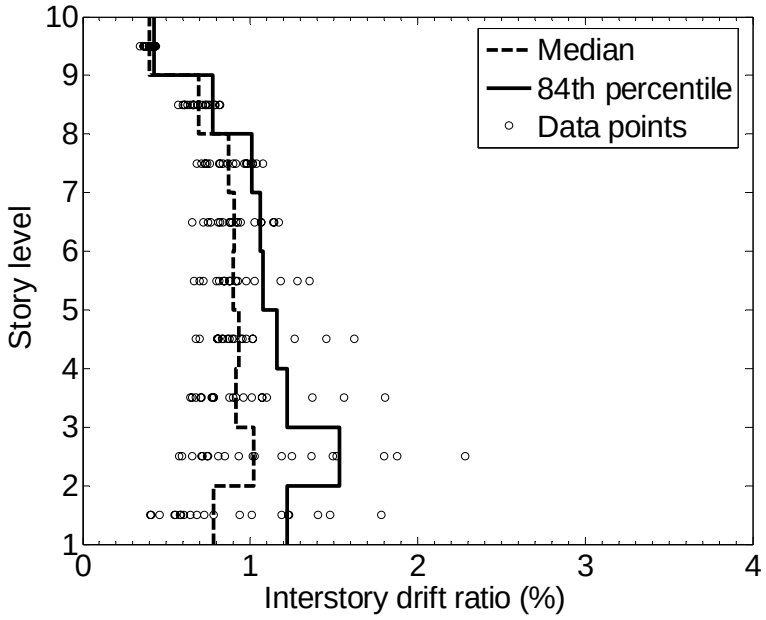

Figure 7.14 Dispersion of story drifts for 9-story zipper frame under modified acceleration ensemble.

7.4 Twenty-Story Zipper-Braced Model Building

7.4.1 Pushover Analysis

In the brace model for the 20-story zipper frame, the elastic modulus of the braces was reduced to 25000 ksi and the rotational stiffness increased up to 3000 in-kips/rad such that the first buckling strengths of the braces were in agreement with the compression capacities of the corresponding bracing members. The pushover curve shown in Figure 7.15(a) presents a slight initial strength degradation due to braces buckling simultaneously, followed by a strength increase and yielding due to the tension braces yielding. The curve can be approximated by a tri-linear curve with three stages [(0% $\sim \Delta_b$=0.83%), ($\Delta_b \sim \Delta_y$=3.41%), ($\Delta_y \sim \Delta_o$=8.47%)]. In stage 1, the structure is linearly elastic until the first buckling in one compression brace. The buckling base shear

is 1896 kN (426 kips, C_b=0.17). This is larger than the design seismic base shear of 1491 kN (335 kips, C_s=0.14) by an overstrength factor, Ω_b, of 1.27. In stage 2, the structural yielding base shear is 2327 kN (523 kips, C_y=0.21) and the corresponding overstrength Ω_y is 1.56. In stage 3, the ultimate base shear is 2608 kN (586 kips, C_o=0.24) at the roof drift ratio of Δ_o=8.47%. The related ultimate overstrength Ω_o is 1.75.

The elastic base shear is 5362 kN (1205 kips, C_{eu}=0.49) at the elastic roof drift ratio of Δ_e=2.34%. The energy demand (E_d) is 5075 m-kN (44903 in-kips). The minimum roof drift ratio for providing a conservative structure is 3.43 % [E_c=5076 m-kN (44906 in-kips)], which is close to the yielding roof drift ratio of Δ_y=3.41% and far away from the ultimate roof drift ratio of Δ_o=8.47%. When the structure is pushed to the ultimate roof drift ratio, the energy capacity E_c reaches 15122 m-kN (133790 in-kips), which is 2.98 times the energy demand. For the sake of comparison, pushover curves of SAC LA 20-story structures with a moment-resisting system are shown in Figure 7.15(b).

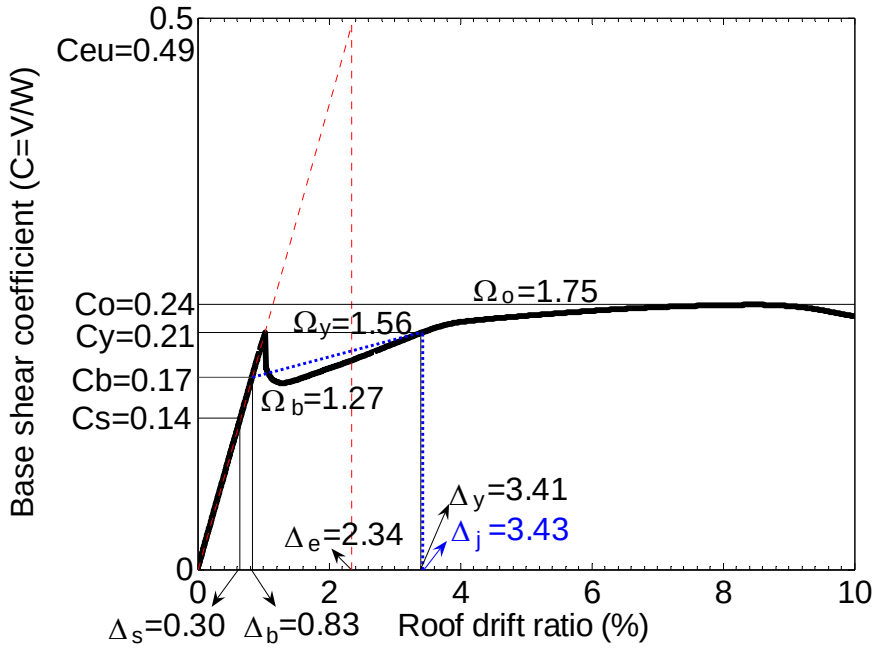

Figure 7.15(a) Pushover curve for the 20-story zipper frame.

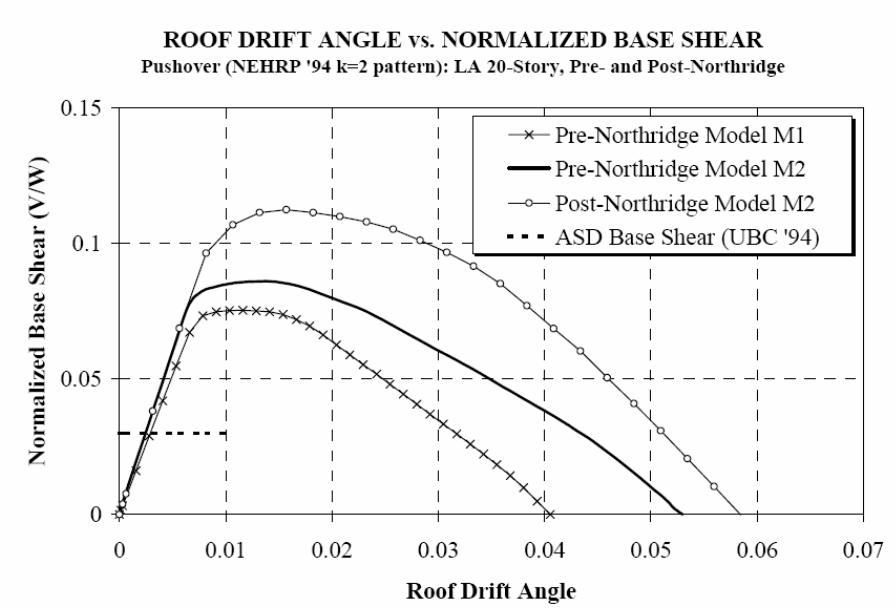

Figure 7.15(b) Pushover curves for SAC LA 20-story moment resisting frames.

7.4.2 Nonlinear Dynamic Analyses

The models of the structural elements used for the nonlinear time history analyses of the 20-story zipper frame are identical to those used in the pushover analysis for the 9-story zipper frame, except for the viscous damping. 5 % Rayleigh damping was specified in the first and twentieth modes of vibration, ensuring that the damping ratios of other modes were less than 5 %. Such a damping arrangement resulted in larger demands of interstory drift ratios, and provided a conservative comparison to the allowable interstory drift ratio specified in the code. The eigenvalue analysis showed that the computed periods of the structure in its first three vibration modes were 2.57, 0.68, and 0.34 sec. The corresponding mode shapes are presented in Figure 7.16. The factors of the effective model masses for the first, second, and third modes were 0.67, 0.21, and 0.06,

respectively. The first three modes need be taken into account, so the total factor of the effective model mass exceeded 90% and was 0.94

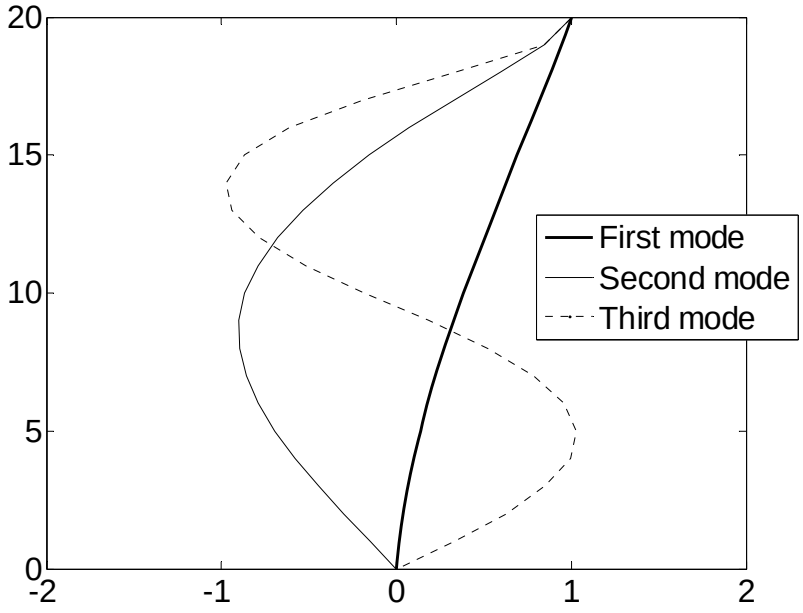

Figure 7.16 First three mode shapes of the 20-story zipper frame.

To verify the required zipper strut forces in the design process, the envelopes of forces in the zipper struts were computed from the nonlinear dynamic analyses. The normalized peak tension and compression forces acting in each story zipper strut for each earthquake are plotted in Figure 7.17. All demands of both tension and compression forces in the zipper struts along the height were less than 1 and greater -1. However, the zipper struts from the 4th to 10th stories required only the tension force demand of 0.6. And the demands decreased to about 0.4 with the height of the structure. This indicates that the design procedure provides zipper struts with a conservative strengths for such a high-rise building. In a general, the first mode will not dominate the behavior of a high-rise building. This implies that not all the compression braces will buckle at the same

time. As a result, the zipper struts did not sustain as much the unbalanced vertical forces as expected in the design procedure.

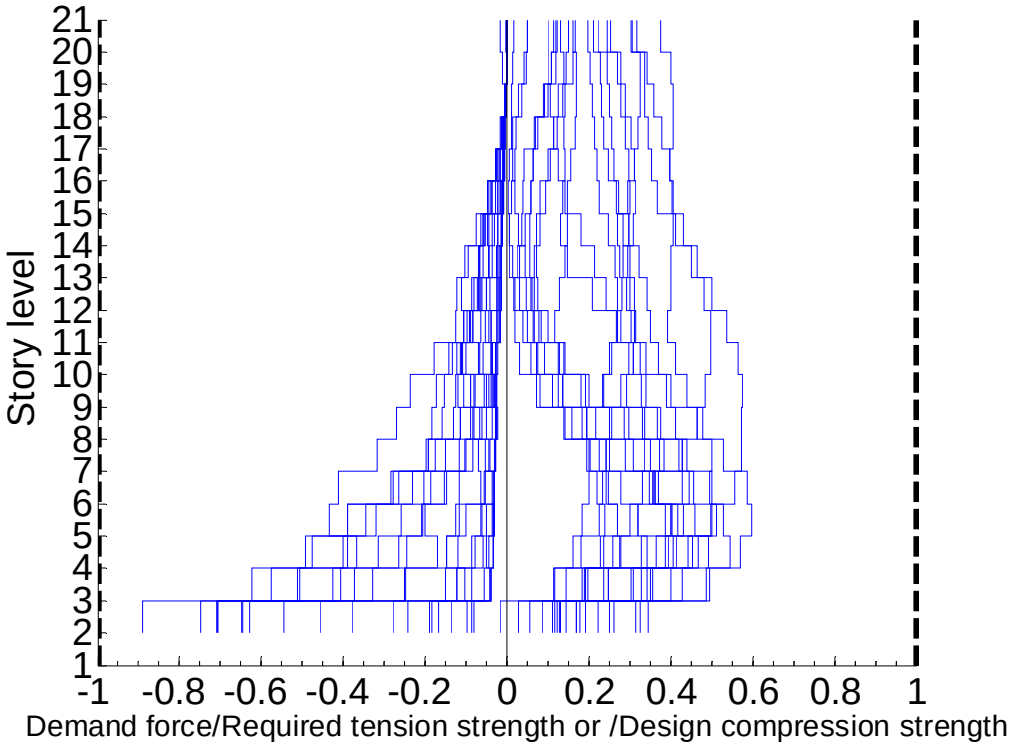

Figure 7.17 Normalized peak tension and compression forces in each story zipper strut when the 20-story zipper frame was under one earthquake of LA21~LA40 (2% exceedence in 50 years).

The investigation on the applicability of the design procedure for the top-story braces shows the peak tension and compression forces in the top-story braces for each ground motion, as listed in Table 7.12. The demand compressive strength for the top-story braces was -10311 kN (-2317 kips), which was much less than the required strength of -26535 kN (-5963 kips).

Table 7.12 Peak tension and compression forces in the top-story braces when the 20-story zipper frame was under an ensemble of earthquakes of LA21~LA40 (2% exceedence in 50 years).

	Top-story left brace (kip)		Top-story right brace (kip)	
	Tension	Compression	Tension	Compression
LA21	21	-880	28	-808
LA22	84	-1193	90	-809
LA23	38	-356	32	-410
LA24	42	-1380	24	-1288
LA25	26	-856	21	-745
LA26	50	-777	19	-1056
LA27	19	-556	33	-690
LA28	34	-972	3	-1040
LA29	33	-396	53	-404
LA30	32	-1118	32	-1281
LA31	49	-749	48	-840
LA32	34	-720	21	-798
LA33	10	-1490	30	-1566
LA34	7	-1424	37	-1488
LA35	37	-1859	35	-1835
LA36	44	-1981	38	-1844
LA37	16	-1310	35	-1215
LA38	6	***-2317***	-8	***-2133***
LA39	30	-200	24	-210
LA40	-4	-1743	1	-1880

The median and 84th percentile drift demands as well as the individual data points of the peak interstory drift ratios are presented in Figure 7.18. Both the median and 84th percentile demands of the peak interstory drift ratios exhibit fairly uniform distribution over the height of the structure. Even through the 20-story zipper frame with the damping ratios of all modes not greater than 5% was subjected to the severe ground motion

ensemble, the maximum peak interstory drift ratio was less than 4 %. The zipper struts mitigated the concentration of deformation on some stories and efficiently completed uniform story distribution over the height.

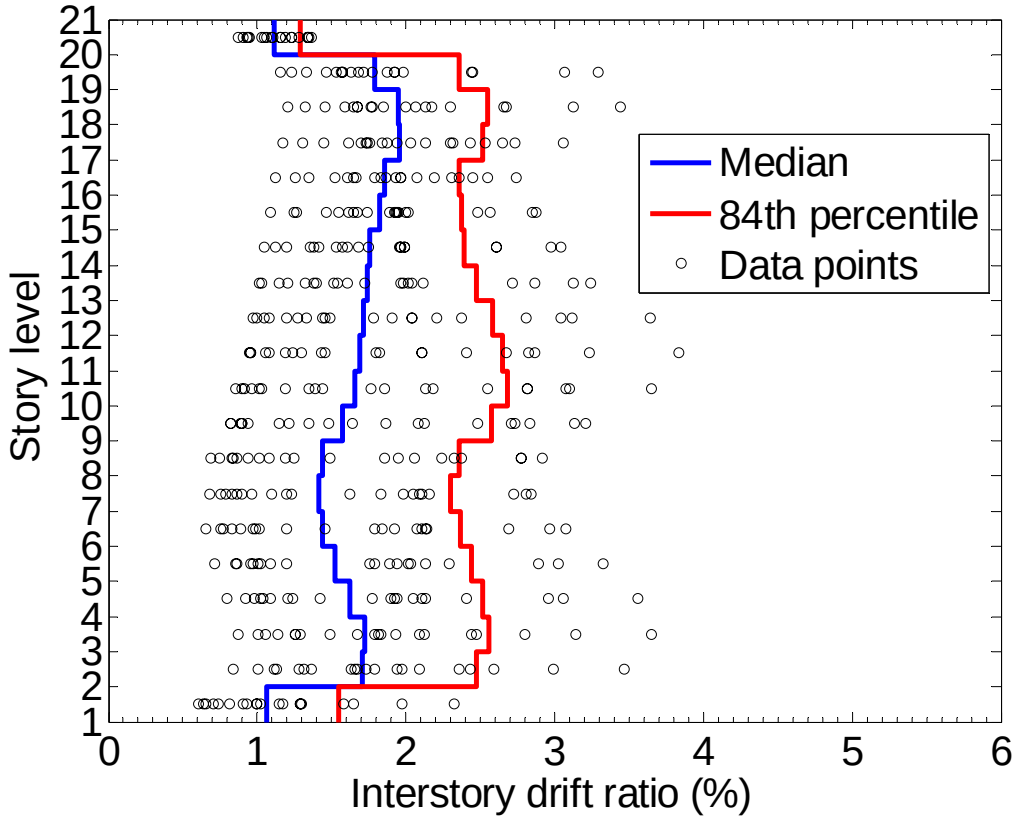

Figure 7.18 Dispersion of story drifts for 20-story zipper frame under original ground motion ensemble (LA21~LA40, 2% exceedence in 50 years).

CHAPTER 8

CONCLUSIONS

8.1 Conclusions

The main hypothesis behind this dissertation is that the suspended zipper frame structural configuration can overcome the instability and full collapse problems of a full-height zipper mechanism and achieve a more uniform distribution of damage over its height without the use of overly stiff beams. The conclusions from the pushover test indicate that:

1. The reduced-scale suspended zipper frame designed in compliance with the capacity design procedure described in Chapter 2.3 exhibited great strength and ductility. It remained stable when pushed to the target roof drift ratio 3.58%, exhibiting a stable tri-linear behavior.
2. The residual strength of the frame (37% of its ultimate strength) was considerable even after one first-story brace fractured and another one had severe compression buckling and tension yielding.
3. The theoretical load path was validated. Once buckling had occurred in the braces, the zipper strut functioned as a tension member, providing support at mid-span of the floor beams and transmitting the unbalanced vertical forces upwards to mobilize the unbuckled braces.
4. The analytical 2D and 3D models can predict the pushover curve of the zipper-braced frame and estimate the maximum deformation of out-of-plane buckling in the braces.

The conclusions from the cyclic tests indicate that:

5. The reduced-scale suspended zipper frame exhibited great strength and capacity to dissipate hysteretic energy and remained stable under the full LA22 ground motion
6. Although the Llolleo (Chile) acceleration was multiplied by 1.5 (the PGA = 1.07 g), the braces did not tear even after numerous cycles of buckling. When the acceleration was multiplied by 2.0, the first-story braces experienced larger deformation, leading to the fatigue damage to the sections at midspan of the braces.

In the analytical verification of the updated design procedure for zipper frames,

7. A code language format for design of zipper frames was proposed to produce zipper-braced frames with a ductile tri-linear response.
8. The design procedure results in zipper struts and top-story braces with reasonable strengths in low- and moderate-rise buildings, and with conservative strengths in high-rise buildings.
9. The studies show considerable effects of higher modes, particularly for the taller structures. This results in an over conservative design as the current design methodology is predicated on a first mode behavior.
10. The statistical values of the peak interstory drift ratios show a uniform distribution over the height in low-, moderate-, and high-rise buildings, demonstrating the efficiency of the zipper struts in achieving more uniform story drift distribution over the height.

8.2 Recommendations for Future Work

Throughout this study several areas which require further work were noticed. These areas are:

1. The effects of higher modes on the sequence of brace yielding and buckling need to be investigated with a structure subjected to dynamic loading.
2. Zipper-braced frames are applicable to high-rise buildings by increasing the number of braced bays in a frame. However, the size of the zipper struts

increases rapidly with the number of stories, presenting practical limitations to the usable height of the system. To make the suspension concept applicable to a tall building, the braced bay can consist of small "units" over the height of the entire structure, each of which is a zipper-braced bay with a few stories. This concept, analogous in some ways to the outrigger truss scheme currently popular for very tall buildings, needs further studies.

3. The applicability of the zipper concept to rehabilitation and strengthening of structures needs to be explored. It may be possible that applications over only portions of an existing structure may prove economical and practical.
4. The use of tension-only zippers, which can be achieved with cables, also needs to be investigated.

APPENDIX A

DETAILS OF TEST FRAME

This appendix contains drawings of the 1/3-scale zipper frame used in the experimental tests conducted as part of this dissertation. Figure A.1 shows the outline of the test frame; Figures A.2 through A.8 show details of the beam-to-column, bracing, and zipper strut connections.

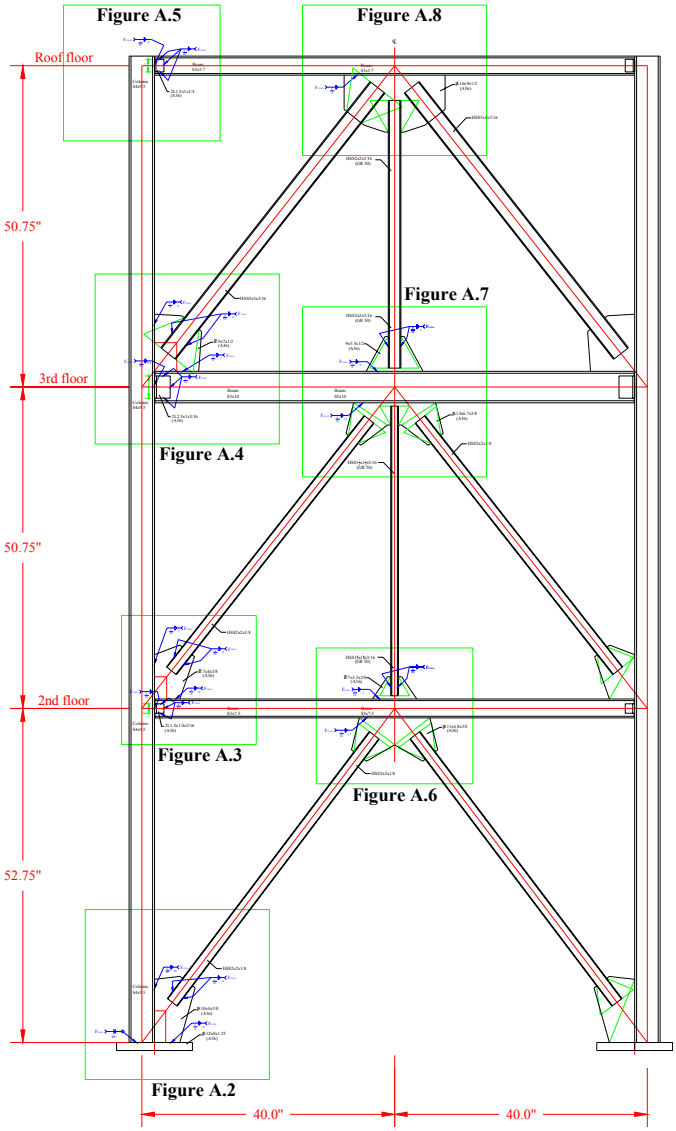

Figure A.1 Elevation view of the 1/3-scale zipper-braced frame.

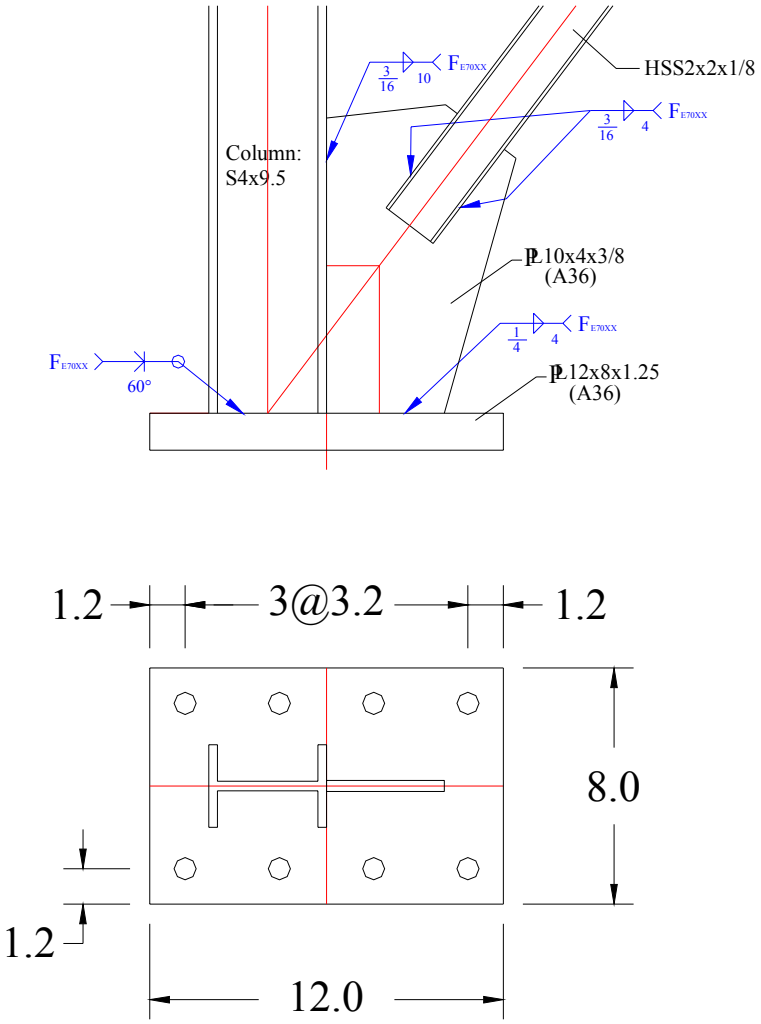

8-3/4 in. diameter A490 anchor rods.
Assume the strenght of the concrete below is 4 ksi.

Figure A.2 Details of the ground-level brace-to-column connection and the column base plate.

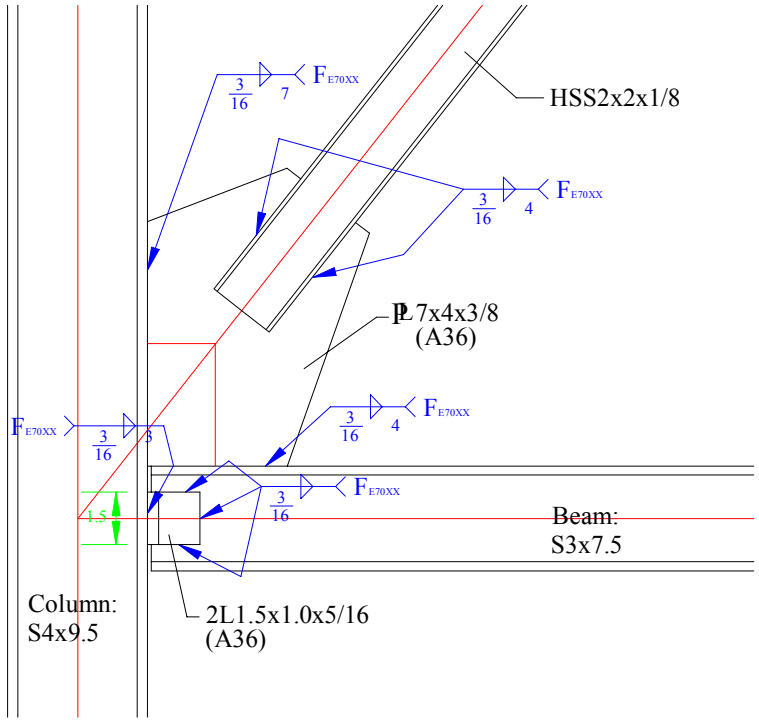

Figure A.3 Details of the 2nd-floor brace-beam-column connection.

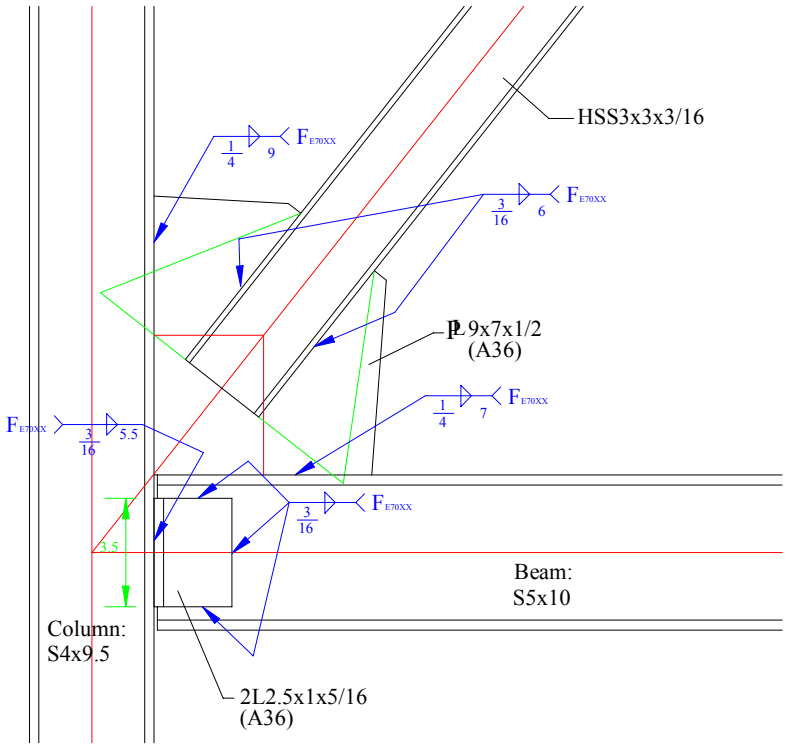

Figure A.4 Details of the 3rd-floor brace-beam-column connection.

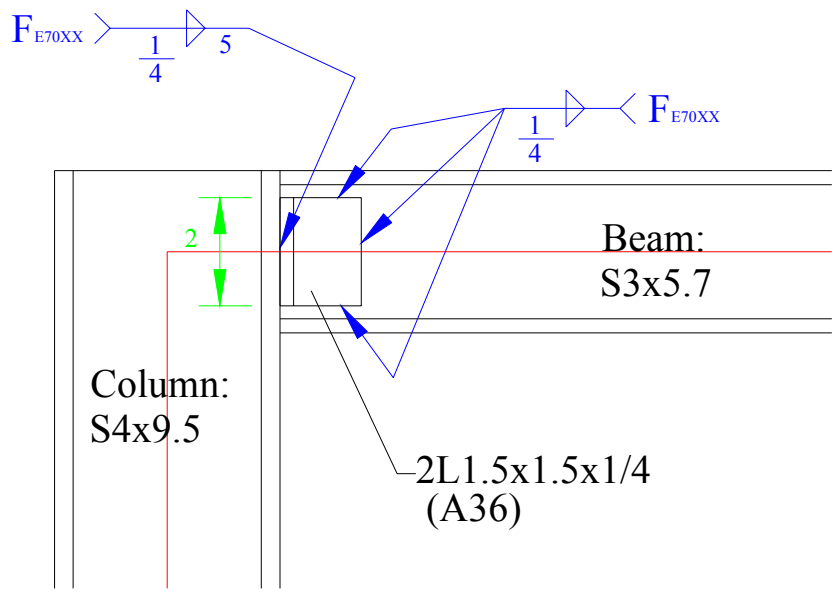

Figure A.5 Details of the Roof-floor beam-to-column connection.

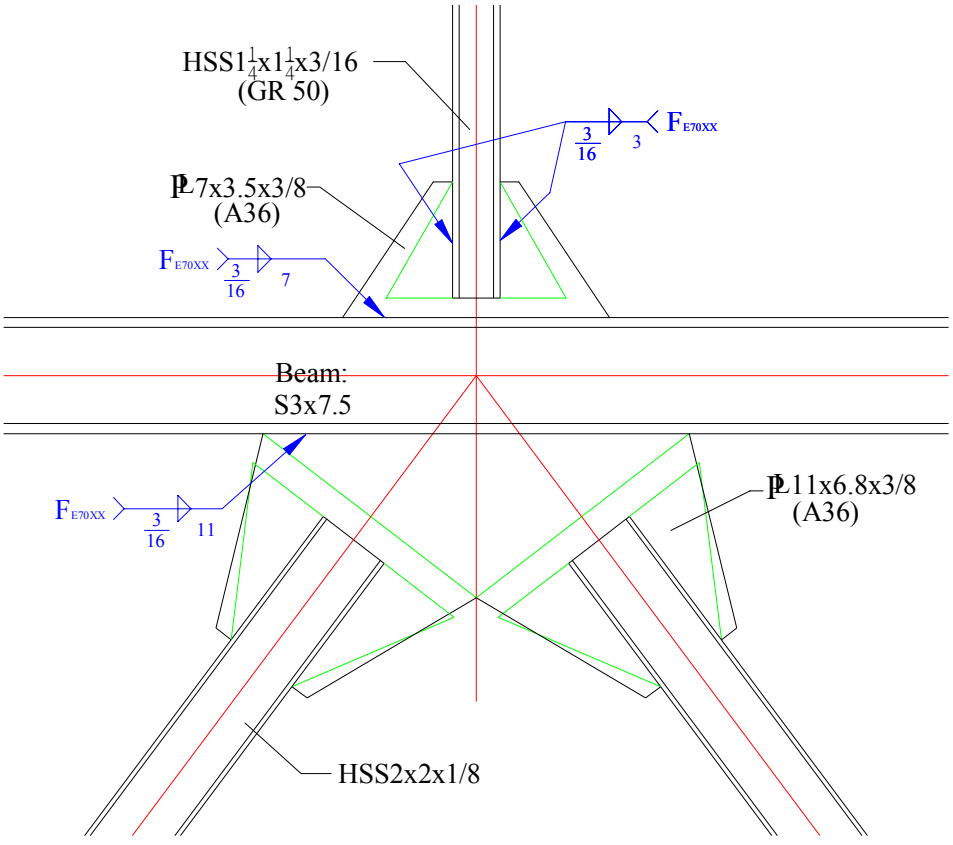

Figure A.6 Details of the 2nd-floor brace-to-beam and zipper strut-to-beam connections.

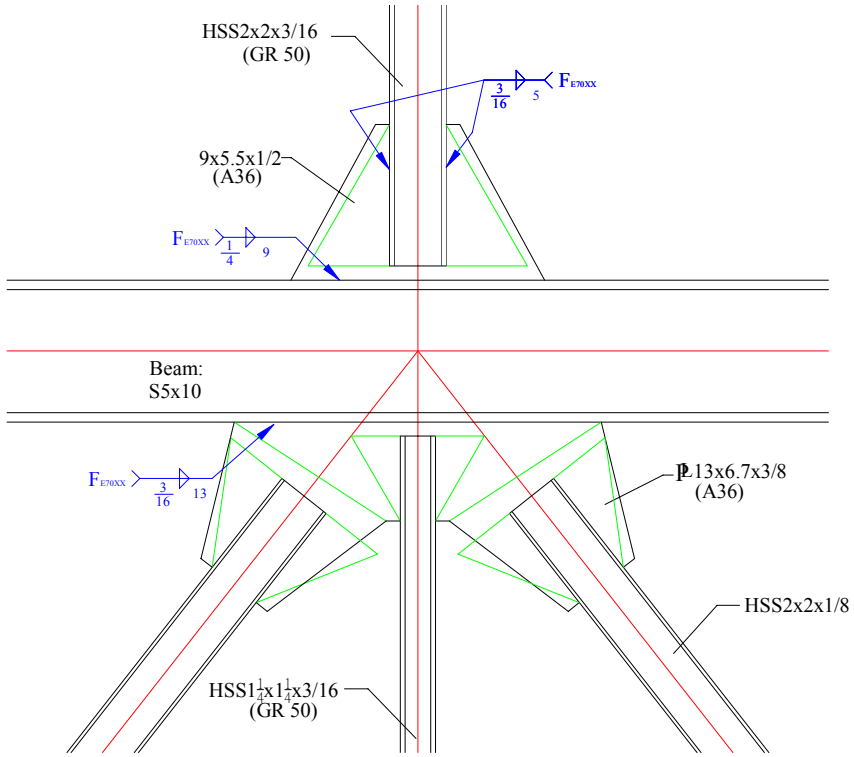

Figure A.7 Details of the 3rd-floor brace-to-beam and zipper strut-to-beam connections.

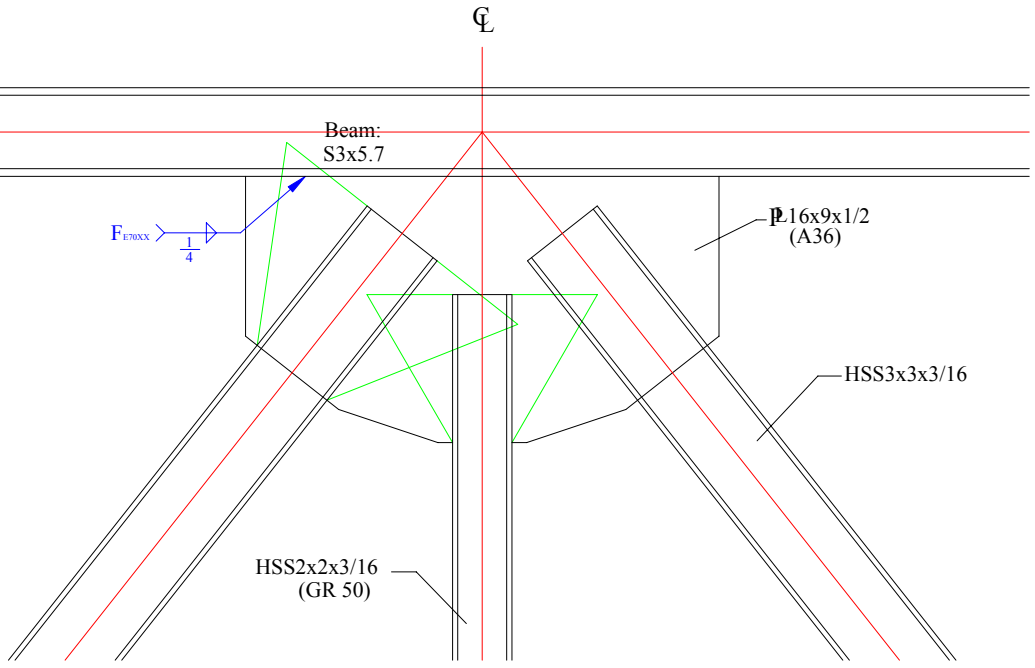

Figure A.8 Details of the Roof-floor brace-beam-zipper strut connection.

APPENDIX B

LIST OF CHANNELS FOR INSTRUMENTATION

Table B.1 shows the card number, channel, tag, bridge configuration, input card, and termination box for each of the instrumentation channels used in all three tests. These channels were connected to an OPTIM data acquisition system, and the location and type of measurement is also shown in the table.

In the tag description for each channel, for the first two letters, SG represents a strain gage and SP means a string pot. The 3rd character (1,2, or 3) stands for the story level. The 4th and 5th letters designate the type of the structural member: CL is a column, BM is a beam, BR is a brace, and ZC is a zipper column. The 6th letter refers to whether the channel is left (L), or right (R). The 7th letter refers to bottom (B), or top (T) section. The 8th letter refers to front (F), or back (B) side and the 9th letter refers again to left (L), or right (R) side. For example, SG1CLLBFL means that the sensor is a strain gage attached in the first-story left column at the bottom section and in the front left side.

There were two types of bridge configuration used for the strain gages in the experiments. One was quarter bridge where one strain gage was connected. Another was full bridge where there were four strain gages connected together.

Table B.1 List of channels.

Card	Channel	Tag	Bridge	Input Card & [Termination]	Location / (Measurements)
Card 1	0	SG1CLLBFL	QB	AD 808QB/350 & [STB808QB (Dummy gages needed)]	1st-story left column / (axial force, moments)
	1	SG1CLLBFR			
	2	SG1CLLBBL			
	3	SG1CLLBBR			
	4	SG1CLLTFL			
	5	SG1CLLTFR			
	6	SG1CLLTBL			
	7	SG1CLLTBR			

Card 2	8	SG1CLRBFL	QB	AD 808QB/350 & [STB808QB (Dummy gages needed)]	1st-story right column / (axial force, moments)
	9	SG1CLRBFR			
	10	SG1CLRBBL			
	11	SG1CLRBBR			
	12	SG1CLRTFL			
	13	SG1CLRTFR			
	14	SG1CLRTBL			
	15	SG1CLRTBR			
Card 3	16	SG1BMLLTF	QB	AD 808QB/350 & [STB808QB (Dummy gages needed)]	2nd-floor left beam / (axial force, moments)
	17	SG1BMLLTB			
	18	SG1BMLLBF			
	19	SG1BMLLBB			
	20	SG1BMLRTF			
	21	SG1BMLRTB			
	22	SG1BMLRBF			
	23	SG1BMLRBB			
Card 4	24	SG1BMRLTF	QB	AD 808QB/350 & [STB808QB (Dummy gages needed)]	2nd-floor right beam / (axial force, moments)
	25	SG1BMRLTB			
	26	SG1BMRLBF			
	27	SG1BMRLBB			
	28	SG1BMRRTF			
	29	SG1BMRRTB			
	30	SG1BMRRBF			
	31	SG1BMRRBB			
Card 5	32	SG1BRL1L	QB	AD-1 808FB-1 & [STB 808FB/120]	1st-story left brace / (axial force, moments)
	33	SG1BRL1R			
	34	SG1BRL1F			
	35	SG1BRL1B			
	36	SG1BRL3L			
	37	SG1BRL3R			
	38	SG1BRL3F			
	39	SG1BRL3B			
Card 6	40	SG1BRR1L	QB	AD-1 808FB-1 & [STB 808FB/120]	1st-story right brace / (axial force, moments)
	41	SG1BRR1R			
	42	SG1BRR1F			
	43	SG1BRR1B			
	44	SG1BRR3L			
	45	SG1BRR3R			
	46	SG1BRR3F			
	47	SG1BRR3B			
Card 7	48	SP1BRLO1		AD-1 808FB-1 & [STB 808FB/350]	1st-story braces / (out-of-plane displacement)
	49	SP1BRLO2			
	50	SP1BRRO1			
	51	SP1BRRO2			

	52				
	53				
	54	SG2ZC2	FB		Zipper struts / (axial forces)
	55	SG3ZC2	FB		
Card 8	56	SG3BRLT	QB	AD 808QB/350 & [STB808QB (Dummy gages needed)]	3-story left brace / (axial force) & 2nd- and 3rd-story left columns (axial forces, moments)
	57	SG3BRLB			
	58	SG2CLLBL			
	59	SG2CLLBR			
	60	SG2CLLTL			
	61	SG2CLLTR			
	62	SG3CLLBL			
	63	SG3CLLBR			
Card 9	64	SG3BRRT	QB	AD 808QB/350 & [STB808QB (Dummy gages needed)]	3-story right brace / (axial force) & 2nd- and 3rd-story right columns (axial forces, moments)
	65	SG3BRRB			
	66	SG2CLRBL			
	67	SG2CLRBR			
	68	SG2CLRTL			
	69	SG2CLRTR			
	70	SG3CLRBL			
	71	SG3CLRBR			
Card 10	72	SG2BMLLT	QB	AD 808QB/350 & [STB808QB (Dummy gages needed)]	3rd-floor beam / (axial forces, moments)
	73	SG2BMLLB			
	74	SG2BMLRT			
	75	SG2BMLRB			
	76	SG2BMRLT			
	77	SG2BMRLB			
	78	SG2BMRRT			
	79	SG2BMRRB			
Card 11	80	SG2BRL1L	QB	AD-1 808FB-1 & [STB 808FB/120]	2nd-story braces / (axial forces, moments)
	81	SG2BRL1R			
	82	SG2BRL1F			
	83	SG2BRL1B			
	84	SG2BRR1L			
	85	SG2BRR1R			
	86	SG2BRR1F			
	87	SG2BRR1B			
Card 12	88	SG2ZC1L	QB	AD-1 808FB-1 & [STB 808FB/120]	2nd-story zipper / (axial force)
	89	SG2ZC1R			
	90	SG2ZC1F			
	91	SG2ZC1B			
	92	SG3ZC1L			3rd-story zipper / (axial force)
	93	SG3ZC1R			
	94	SG3ZC1F			
	95	SG3ZC1B			

Card 13	96	SP1BRL		AD-1 808FB-1 & [STB 808FB/350]	1st- and 2nd-story braces / (axial displacements) & 3 floor drifts
	97	SP1BRR			
	98	SP2BRL			
	99	SP2BRR			
	100	SP1F			
	101	SP2F			
	102	SP3F			
	103				
Card 14	104	Zipper strut 2 (LVDT)		AD-1 808FB-1 & [STB 808CB]	Zipper struts / (axial displacements) & 3 actuators (forces, displacements)
	105	Zipper strut 3 (LVDT)			
	106	Actuator 1 Load			
	107	Actuator 1 Displacement			
	108	Actuator 2 Load			
	109	Actuator 2 Displacement			
	110	Actuator 3 Load			
	111	Actuator 3 Displacement			
Card 15					CB100

B.1 Computation of axial force and moment at one section of a member

To determine the axial force and moment at a section, the data measured by the strain gages at that location were utilized. As shown in Figure B.1(a), an example of the four strain gages attached in the first-story left column at the bottom section (SG1CLLB**FL**, SG1CLLB**FR**, SG1CLLB**BL**, SG1CLLB**BR**), there were four data recorded as ε_{FL}, ε_{FR}, ε_{BL}, and ε_{BR}, respectively. If the assumption is made that a plane remains a plane after a member subjected to an axial force and moment, the strains at Points a, b, and c can be computed as:

$$\varepsilon_L = \frac{\varepsilon_{BL} + \varepsilon_{FL}}{2} \qquad \text{(B.1)}$$

$$\varepsilon_R = \frac{\varepsilon_{BR} + \varepsilon_{FR}}{2} \tag{B.2}$$

$$\varepsilon_{axial} = \frac{\varepsilon_L + \varepsilon_R}{2} \tag{B.3}$$

respectively. The strain distribution along the line ac is shown in Figure B.1(b). It can be viewed as two portions. One is pure axial strain of ε_{axial} which is used to obtain the axial force in the member.

$$P = EA\varepsilon_{axial} \tag{B.4}$$

Another is pure bending strain computed by

$$\varepsilon_{bending} = \varepsilon_R - \varepsilon_{axial} \tag{B.5}$$

The pure bending strain is used to determine a moment applying to that section.

$$M = ES\varepsilon_{bending} \tag{B.6}$$

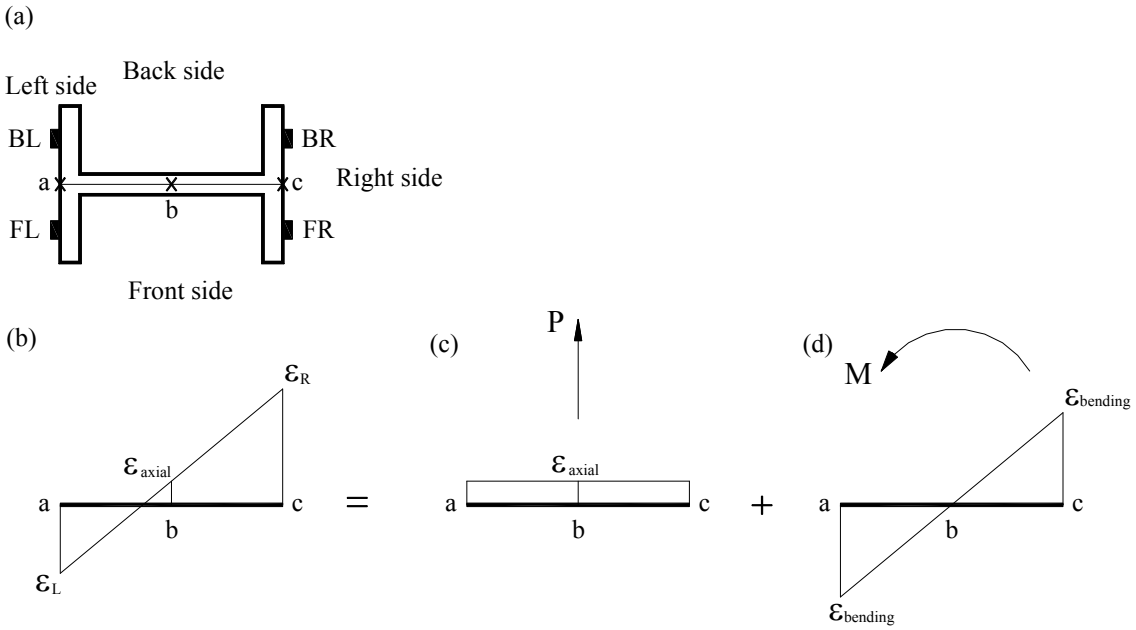

Figure B.1 Schematic illustrating the procedure used to calculate the axial force and moment at a section of a member.

APPENDIX C

BRACE MODELS

This appendix describes two brace models, both of which were implemented in the OpenSEES computer program. The first brace model (BR-Model 1), which was used for the numerical models in this dissertation, utilizes a fiber-based beam column element to simulate the buckling behavior of a brace. A code script describing the implementation of such a brace model is illustrated in Section C.1. Another brace model (BR-Model 2), which was coded by the Author, uses a material model to seamlessly add a phenomenological model for a brace to the OpenSEES modeling framework (Scott and Fenves, 2001). It utilizes the UniaxialMaterial interface to define force-deformation relationships of a brace for an element with similar behavior to that observed in the braces tested in this project. One of three primary source codes for this material model is discussed in Section C.2.1.

C.1 Brace Model 1

The original brace model that was developed for the OpenSEES program by Uriz and Mahin at UC Berkeley had an additional node at midspan of a brace and included a small initial imperfection ($L_w/2000$) to simulate the buckling behavior of a brace under compression. This brace model predicted the monotonic response of the zipper frame model to pushover loading as an approximate bilinear curve, rather than a trilinear skeleton curve. In order to obtain a more accurate simulation for the brace buckling, the model was modified in two ways. First, a larger initial imperfection ratio for the brace was adopted to lower the maximum compression strength of the brace. Second, two rotational springs were added at the end nodes of the brace to increase its maximum compression and minimum post-buckling strengths. The effects of these two parameters

(initial imperfection ratio and rotational stiffness) on the buckling behavior will be investigated in detail later. Figure C.1 shows the schematic configuration of this brace model.

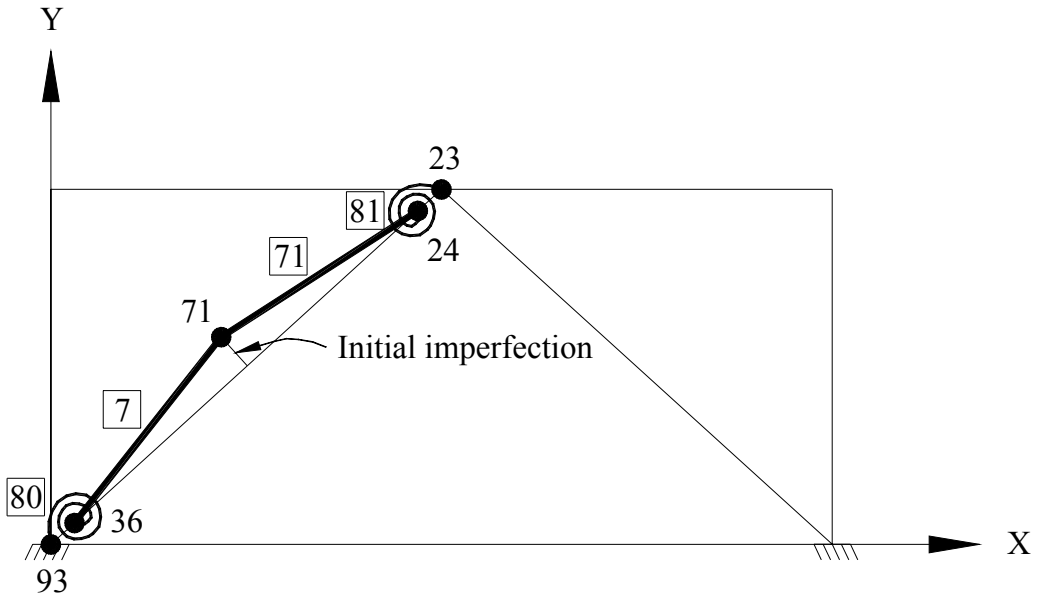

Figure C.1 Schematic graph of a brace model (e.g. the first-story left brace).

A code script for the brace model implemented in the OpenSEES program for the analytical study of the 3-story zipper frame in Chapter 7 is illustrated below. The first-story left brace with two ends at Node 36 and Node 24 was separated by a middle node, Node 71, into two elements numbered as 7 and 71. Two zero-length elements of rotational springs, numbered as 80 and 81, were used to connect the co-location nodes (Nodes 93 and 36 as well as Nodes 23 and 24, respectively). In the following script, six steps are performed to establish a brace model in the OpenSEES program.

```
(1)Define nodes of the brace and the adjacent nodes.
#    tag  X(in)Y(in)
node 36   0    0
```

```
node 93   0    0
node 23  180  156
node 24  180  156
set ratio1L [expr 1./150.]; # Define initial imperfection ratio.
node 71     [expr  90.0 - $ratio1L*156.0] [expr 78.0 + ratio1L*180.0]


(2)Define material properties of the brace and rotational spring.
#                         tag
uniaxialMaterial Steel02  2   Fy E 0.008  18.5 0.925 0.15   0 1 0 1
uniaxialMaterial Elastic  3     700.0  0.0; # rotational springs


(3)Define the fiber section of the brace with HSS8x8x5/8.
#         tag
HSSsection 4   2    8.0   8.0  [expr 5./8.]   20  1   20  1


(4)Construct a Corotational Coordinate.
#                       tag
geomTransf Corotational 2


(5)Define elements of the brace.
#                           tag  ndI  ndJ  nsecs  secID  transfTag

element nonlinearBeamColumn  7   36   71   $np     4        2      -
iter $maxiter $tol
element nonlinearBeamColumn 71   71   24   $np     4        2      -
iter $maxiter $tol


(6)Define elements of the rotational springs.
#                           tag  ndI  ndJ  matID       dof
element  zeroLength         80   93   36  -mat 4 4 3  -dir 1 2 6  -
orient  0.7557   0.6549  0.0     -0.6549   0.7557  0.0
element  zeroLength         81   24   23  -mat 4 4 3  -dir 1 2 6  -
orient  0.7557   0.6549  0.0     -0.6549   0.7557  0.0
```

C.1.1 Effect of Initial Imperfection on the Buckling Behavior of a Brace

Figure C.2 shows monotonic curves for a compression brace with three different initial imperfection ratios ($L_w/100$, $L_w/1000$, $L_w/2000$) and a fixed stiffness of rotational springs [79 m-kN/rad (700 in-kips/rad)]. The curves are normalized to the nominal compression strength (P_n) given by the AISC LRFD manual and to the yielding displacement ($\sigma_y L_w/E$). The results show that the maximum compression strength

decreases as the initial imperfection ratio increases. The case of $L_w/100$ has a peak strength ratio closest to -1 among the three different ratios, with an imperfection of $L_w/150$ (not shown) giving a value very close to -1. It is also important to note that all the three cases generate the same post-buckling strength at a displacement ratio of -20. Their post-buckling strengths are very similar beyond the -10 displacement ratio.

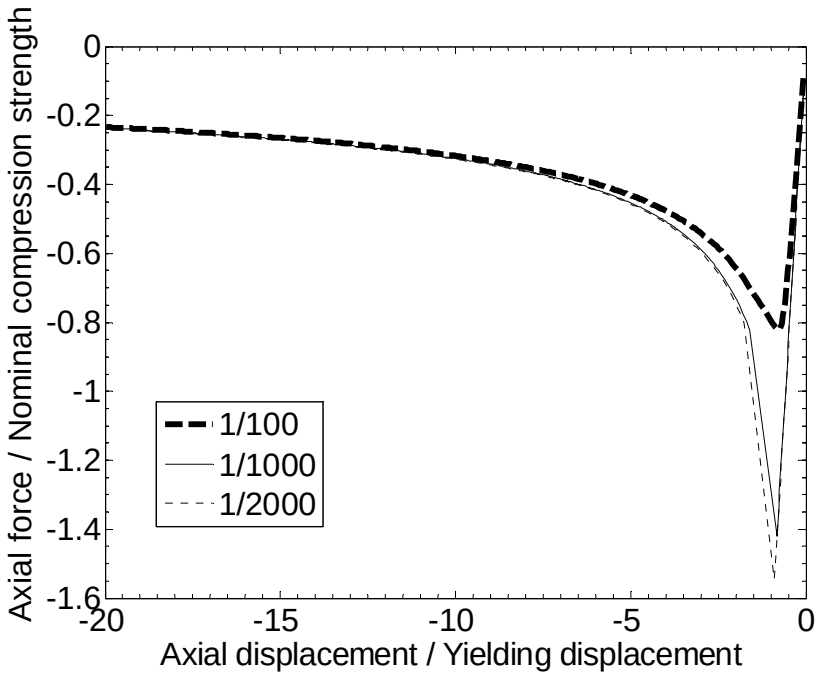

Figure C.2 Effect of initial imperfection.

C.1.2 Effect of Rotational Stiffness on the Buckling Behavior of a Brace

Figure C.3 also shows monotonic curves for a compression brace but with four different values of rotational stiffness [79 m-kN/rad (700 in-kips/rad), 475 m-kN/rad (4200 in-kips/rad), 712 m-kN/rad (6300 in-kips/rad), 1130 m-kN/rad (10000 in-kips/rad)] and a fixed initial imperfection ratio ($L_w/150$). In the peak portion of the curves, the maximum compression strength increases slightly with increasing stiffness of the

rotational spring. However, there is a significant increase in the post buckling strength when a larger value of rotational stiffness is used. Given in the compression strength (P_n) and minimum post-buckling strength ($0.3P_n$ at 10 to 20 times the yielding displacement, AISC Seismic Provisions), the curves with the rotational stiffness of 475 m-kN/rad provides the most accurate results.

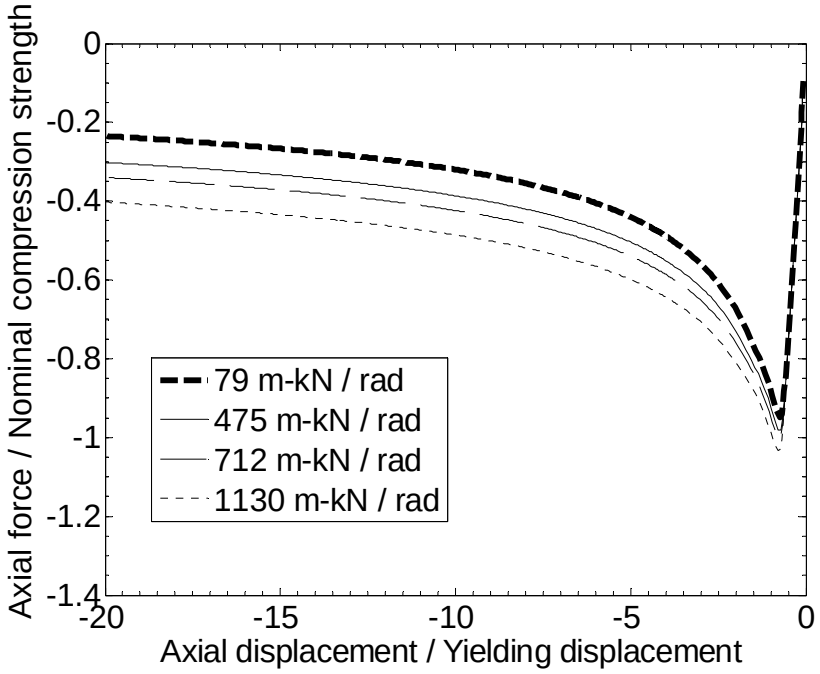

Figure C.3 Effect of rotational stiffness.

C.1.3 Iterative Approach for the Brace Model

The proposed brace model is semi-empirical due to two unknown parameters: (1) the initial imperfect of a brace, and (2) the rotational stiffness of the springs that simulate the restraint provided by the gusset plates. To match the behavior observed in the brace tests at several of the NEES sites involved in this project, a two-step process was followed. First, select a large value for the initial imperfection ratio (say $L_w/500$). Next,

choose a reasonable value for the stiffness of the rotational springs based on an approximation to the actual out-of-plane stiffness for the gusset plate. Then perform the code script and output the hysteretic curve for the brace. Subsequently, adjust the rotational stiffness for the next run and iterate until the numerical maximum compression strength is in agreement with the compressive strength (P_n) of a brace which is computed by using the expected yielding strength and $k=1$. Finally, compare the minimum post-buckling strength with the specified minimum post-buckling strength of $0.3P_n$. If a large difference exists, then reselect a value for initial imperfection and redo the subsequent steps. Note that the final two parameters are merely numerical results obtained by a strategy for the brace model, regardless of the initial imperfection a brace has and the bending capacity of its adjacent gusset plates.

C.2 Brace Model 2

The brace model 2, of which the code (BraceMaterial.cpp) is shown in C.2.1, was created by the Author and used in the early conference papers published by Professor Leon and the Author. For the simulation of bracing members, the 'BraceMaterial' uniaxialMaterial option is used to set up the relationship between the member's axial forces and deformation (See Figure C.4). Also, pinching factors (pinchX 0.5 and pinchY 0.3) are assumed to model the amount of pinching of the deformation and force, respectively, during reloading. A damage factor of 0.02 for damage due to ductility is also selected. As shown in Figure C.5, the post-buckling loops cannot really reflect the true dynamic behavior of a brace once its first buckling has occurred.

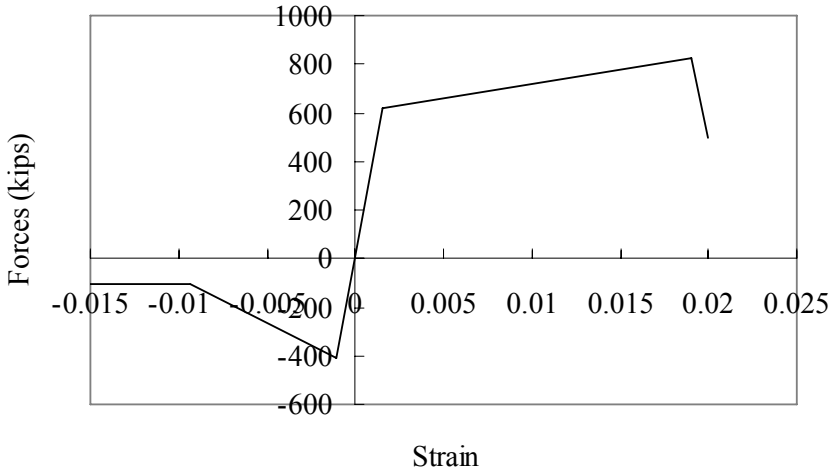

Figure C.4 Backbone for the brace model 2.

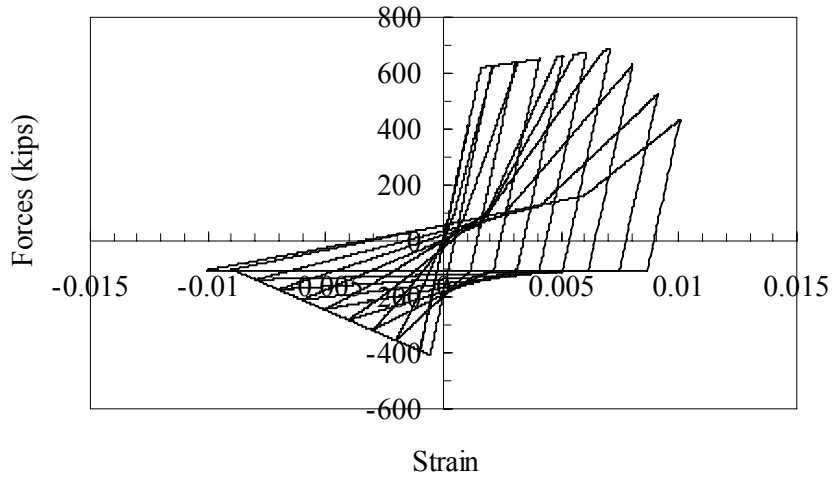

Figure C.5 Hysteretic behavior of the brace model 2.

C.2.1 Source Code for the Brace Model 2

```
/* ****************************************************************** **
**    OpenSees - Open System for Earthquake Engineering Simulation    **
**          Pacific Earthquake Engineering Research Center            **
**                                                                    **
```

```
**                                                                    **
** (C) Copyright 1999, The Regents of the University of California    **
** All Rights Reserved.                                               **
**                                                                    **
** Commercial use of this program without express permission of the   **
** University of California, Berkeley, is strictly prohibited.  See   **
** file 'COPYRIGHT'  in main directory for information on usage and   **
** redistribution,  and for a DISCLAIMER OF ALL WARRANTIES.           **
**                                                                    **
** Developed by:                                                      **
**   Frank McKenna (fmckenna@ce.berkeley.edu)                         **
**   Gregory L. Fenves (fenves@ce.berkeley.edu)                       **
**   Filip C. Filippou (filippou@ce.berkeley.edu)                     **
**            **
**                                                                    **
** ****************************************************************** */

// $Revision: 1.8 $
// $Date: 2002/09/12 19:28:13 $
// $Source: /usr/local/cvs/OpenSees/SRC/material/uniaxial/BraceMaterial.cpp,v $

// Written: Chuang-Sheng Yang (Walter) (gtg189c@mail.gatech.edu)

#include <BraceMaterial.h>
#include <G3Globals.h>
#include <math.h>
#include <float.h>
#include <Channel.h>

BraceMaterial::BraceMaterial(int tag,
                             double m1p, double r1p, double m2p, double r2p, double m3p, double r3p,
                             double m1n, double r1n, double m2n, double r2n, double m3n, double r3n,
                             double px, double py, double d1, double d2, double b):
UniaxialMaterial(tag, MAT_TAG_Brace),
pinchX(px), pinchY(py), damfc1(d1), damfc2(d2), beta(b),
mom1p(m1p), rot1p(r1p), mom2p(m2p), rot2p(r2p), mom3p(m3p), rot3p(r3p),
mom1n(m1n), rot1n(r1n), mom2n(m2n), rot2n(r2n), mom3n(m3n), rot3n(r3n)
{
        bool error = false;

        // Positive backbone parameters
        if (rot1p <= 0.0)
                error = true;

        if (rot2p <= rot1p)
                error = true;

        if (rot3p <= rot2p)
                error = true;

        // Negative backbone parameters
        if (rot1n >= 0.0)
                error = true;

        if (rot2n >= rot1n)
                error = true;
```

```
	if (rot3n >= rot2n)
		error = true;

	if (error)
		g3ErrorHandler->fatal("%s -- input backbone is not unique (one-to-one)",
		"BraceMaterial::BraceMaterial");

	energyA = 0.5 * (rot1p*mom1p + (rot2p-rot1p)*(mom2p+mom1p) + (rot3p-
rot2p)*(mom3p+mom2p) +
		rot1n*mom1n + (rot2n-rot1n)*(mom2n+mom1n) * (rot3n-rot2n)*(mom3n+mom2n));

	// Set envelope slopes
	this->setEnvelope();

	// Initialize history variables
	this->revertToStart();
	this->revertToLastCommit();
}

BraceMaterial::BraceMaterial(int tag,
				double m1p, double r1p, double m2p, double r2p,
				double m1n, double r1n, double m2n, double r2n,
				double px, double py, double d1, double d2, double b):
UniaxialMaterial(tag, MAT_TAG_Brace),
pinchX(px), pinchY(py), damfc1(d1), damfc2(d2), beta(b),
mom1p(m1p), rot1p(r1p), mom3p(m2p), rot3p(r2p),
mom1n(m1n), rot1n(r1n), mom3n(m2n), rot3n(r2n)
{
	bool error = false;

	// Positive backbone parameters
	if (rot1p <= 0.0)
		error = true;

	if (rot3p <= rot1p)
		error = true;

	// Negative backbone parameters
	if (rot1n >= 0.0)
		error = true;

	if (rot3n >= rot1n)
		error = true;

	if (error)
		g3ErrorHandler->fatal("%s -- input backbone is not unique (one-to-one)",
		"BraceMaterial::BraceMaterial");

	energyA = 0.5 * (rot1p*mom1p + (rot3p-rot1p)*(mom3p+mom1p) +
		rot1n*mom1n + (rot3n-rot1n)*(mom3n+mom1n));

	mom2p = 0.5*(mom1p+mom3p);
	mom2n = 0.5*(mom1n+mom3n);

	rot2p = 0.5*(rot1p+rot3p);
```

```
	rot2n = 0.5*(rot1n+rot3n);

	// Set envelope slopes
	this->setEnvelope();

	// Initialize history variables
	this->revertToStart();
	this->revertToLastCommit();
}

BraceMaterial::BraceMaterial():
UniaxialMaterial(0, MAT_TAG_Brace),
pinchX(0.0), pinchY(0.0), damfc1(0.0), damfc2(0.0), beta(0.0),
mom1p(0.0), rot1p(0.0), mom2p(0.0), rot2p(0.0), mom3p(0.0), rot3p(0.0),
mom1n(0.0), rot1n(0.0), mom2n(0.0), rot2n(0.0), mom3n(0.0), rot3n(0.0)
{

}

BraceMaterial::~BraceMaterial()
{
	// Nothing to do
}

int
BraceMaterial::setTrialStrain(double strain, double strainRate)
{
	TrotMax = CrotMax;
	TrotMin = CrotMin;
	TenergyD = CenergyD;
	TrotPu = CrotPu;
	TrotNu = CrotNu;
	TmomNu = CmomNu;
	TmomPu = CmomPu;

	Tstrain = strain;
	double dStrain = Tstrain - Cstrain;

	TloadIndicator = CloadIndicator;
	Tidtime = Cidtime;
	Tidtime1 = Cidtime1;

	if (TloadIndicator == 0)
		TloadIndicator = (dStrain < 0.0) ? 2 : 1;

	if (Tstrain >= CrotMax) {
		TrotMax = Tstrain;
		Ttangent = posEnvlpTangent(Tstrain);
		Tstress = posEnvlpStress(Tstrain);
		TloadIndicator = 1;
	}
	else if (Tstrain <= CrotMin) {
		TrotMin = Tstrain;
		Ttangent = negEnvlpTangent(Tstrain);
		Tstress = negEnvlpStress(Tstrain);
		if (TrotMin <= rot1n && Tidtime == 0) {
```

```
                        Tidtime = 1;
                }
                Tidtime1 = 0;
                TloadIndicator = 2;
        }
        else {
          if (dStrain < 0.0)
            negativeIncrement(dStrain);
          else if (dStrain > 0.0)
            positiveIncrement(dStrain);
        }

        TenergyD = CenergyD + 0.5*(Cstress+Tstress)*dStrain;

        return 0;
}


double
BraceMaterial::getStrain(void)
{
        return Tstrain;
}

double
BraceMaterial::getStress(void)
{
        return Tstress;
}

double
BraceMaterial::getTangent(void)
{
        return Ttangent;
}

void
BraceMaterial::positiveIncrement(double dStrain)
{
//      double kn = pow(CrotMin/rot1n,beta);
        double kn = 1.0;
//      kn = (kn < 1.0) ? 1.0 : 1.0/kn;
//      double kp = pow(CrotMax/rot1p,beta);
        double kp = 1.0;
//      kp = (kp < 1.0) ? 1.0 : 1.0/kp;

//      cout << "Hello: positive Increment" << endl;

        if (TloadIndicator == 2) {
                TloadIndicator = 1;
                if (Cstress <= mom2n) {
                        TrotNu = Cstrain;
                        TmomNu = Cstress;
                        double energy = CenergyD - 0.5*Cstress/(E1n*kn)*Cstress;
                        double damfc = 1.0;
                        if (CrotMin < rot1n) {
```

```
                                damfc += damfc2*energy/energyA;

                                if (Cstrain == CrotMin) {
                                        damfc += damfc1*(CrotMax/rot1p-1.0);
                                }
                        }

                        TrotMax = CrotMax * damfc;
                }
        }

        TloadIndicator = 1;

        TrotMax = (TrotMax > rot1p) ? TrotMax : rot1p;

        double maxmom = posEnvlpStress(TrotMax);
//      double rotlim = negEnvlpRotlim(CrotMin);
//      double rotrel = (rotlim > TrotNu) ? rotlim : TrotNu;
//      rotrel = TrotNu;
//      if (negEnvlpStress(CrotMin) >= 0.0)
//        rotrel = rotlim;

        double rotmp1 = TrotNu + pinchY*(TrotMax-TrotNu);
        double rotmp2 = TrotMax - (1.0-pinchY)*(maxmom-TmomNu)/(E1p*kp);
        double rotch = rotmp1 + (rotmp2-rotmp1)*pinchX;

        double tmpmo1;
        double tmpmo2;

        if (Tstrain < rotch) {
                Ttangent = (maxmom-TmomNu)*pinchY/(rotch-TrotNu);
                tmpmo1 = Cstress + E1p*kp*dStrain;
                tmpmo2 = TmomNu + (Tstrain-TrotNu)*Ttangent;
                if (tmpmo1 < tmpmo2) {
                        Tstress = tmpmo1;
                        Ttangent = E1p*kp;
                }
                else
                        Tstress = tmpmo2;
        }
        else {
                Ttangent = (1.0-pinchY)*(maxmom-TmomNu)/(TrotMax-rotch);
                tmpmo1 = Cstress + E1p*kp*dStrain;
                tmpmo2 = TmomNu + pinchY*(maxmom-TmomNu) + (Tstrain-rotch)*Ttangent;
                if (tmpmo1 < tmpmo2) {
                        Tstress = tmpmo1;
                        Ttangent = E1p*kp;
                }
                else
                        Tstress = tmpmo2;
        }


        if ( Tidtime == 1 && TrotMin > rot2n ) {
                if ( Tstress > mom2n && Tidtime1 == 0 ) {
                        Tidtime1 = 1;
```

```
                }
        }
}

void
BraceMaterial::negativeIncrement(double dStrain)
{
//      double kn = pow(CrotMin/rot1n,beta);
        double kn = 1.0;
//      kn = (kn < 1.0) ? 1.0 : 1.0/kn;
//      double kp = pow(CrotMax/rot1p,beta);
        double kp = 1.0;
//      kp = (kp < 1.0) ? 1.0 : 1.0/kp;

//      cout << "Hello: negative Increment" << endl;

//  cout << "Tidtime: " << Tidtime << endl;

        if ( Tidtime == 1 && TrotMin > rot2n ) {
                double minmom = negEnvlpStress(TrotMin);
                if ( TloadIndicator == 1 ) {
                        TmomPu = Cstress;
                }

                if ( Tidtime1 == 1) {
                        if ( TmomPu >= mom2n ) {
                                if ( Cstress > mom2n ) {
                                        TrotPu = Cstrain - Cstress/(E1p*kp) + mom2n/(E1p*kp);
                                }
                                if ( Tstrain > TrotPu ) {
                                        Ttangent = E1p*kp;
                                        Tstress = Cstress + Ttangent*dStrain;
                                        if ( Tstress <= mom2n ) {
                                                Tstress = mom2n;
                                                Ttangent = E1p*1.0e-9;
                                        }
                                }
                                else {
                                        Ttangent = (minmom-mom2n)/(TrotMin-TrotPu);
                                        Tstress = mom2n + Ttangent*(Tstrain-TrotPu);
                                        if ( Tstress <= minmom ) {
                                                Tstress = minmom;
                                                Ttangent = Ttangent*1.0e-6;
                                                Tidtime1 = 0;
                                        }
                                }
                        }
                        else {
                                if ( Tstrain >= TrotNu ) {
                                        Ttangent = (TmomNu-Cstress)/(TrotNu-Cstrain);
                                        Tstress = Cstress + Ttangent*dStrain;
                                        if ( Tstress <= TmomNu ) {
                                                Tstress = TmomNu;
                                                Ttangent = Ttangent*1.0e-6;
                                        }
                                }
```

```
                                        else {
                                                Ttangent = (minmom-mom2n)/(TrotMin-TrotPu);
                                                Tstress = mom2n + Ttangent*(Tstrain-TrotPu);
                                                if ( Tstress <= minmom ) {
                                                        Tstress = minmom;
                                                        Ttangent = Ttangent*1.0e-6;
                                                        Tidtime1 = 0;
                                                }
                                        }
                                }
                        }
                        else {
                                Ttangent = (minmom-Cstress)/(TrotMin-Cstrain);
                                Tstress = Cstress + Ttangent*dStrain;
                                if ( Tstress <= minmom ) {
                                        Tstress = minmom;
                                        Ttangent = Ttangent*1.0e-6;
                                        Tidtime1 = 0;
                                }
                        }
                }

                TloadIndicator = 2;

                if ( Tidtime == 0 ) {
                        if ( TrotMax > rot1p ) {
                                TrotMin = (TrotMin < rot1n) ? TrotMin : rot1n;
                        }
                        Ttangent = E1p*kp;
                        Tstress = Cstress + Ttangent*dStrain;

                        if ( Tstress <= mom1n ) {
                                TrotPu = Cstrain - Cstress/(E1p*kp);
//                              rot1n = rot1n + TrotPu;
                                rot1n = mom1n/(E1p*kp) + Cstrain - Cstress/(E1p*kp);
                                rot2n = rot1n + (mom2n-mom1n)/E2n;
                                rot3n = rot2n + (mom3n-mom2n)/E3n;
                                Tidtime = 1;
                                TrotMin = Tstrain;

//                              cout << "Tstrain: " << Tstrain << endl;
//                              cout << "rot1n: " << rot1n << endl;
//                              cout << "rot2n: " << rot2n << endl;

                                if (Tstrain > rot1n) {
                                        Tstress = mom1n;
                                        Ttangent = E1p*1.0e-9;
                                }
                                if (Tstrain <= rot1n && Tstrain > rot2n) {
                                        Tstress = mom1n + E2n*(Tstrain-rot1n);
                                        Ttangent = E2n;

//                                      cout << "Tstress: " << Tstress << endl;
                                }
                                if (Tstrain <= rot2n) {
                                        Tstress = mom2n + E3n*(Tstrain-rot2n);
```

```
                                        Ttangent = E3n;
                                }
                        }
                }

                if ( Tidtime >= 1 && TrotMin <= rot2n ) {
                        Ttangent = E1p*kp;
                   Tstress = Cstress + Ttangent*dStrain;
                   if (Tstress <= mom2n) {
                                Tstress = mom2n;
                                Ttangent = E1p*1.0e-9;
                                Tidtime = 2;
                                if ( Tstrain < rot2n ) {
                                        Ttangent = E3n;
                                        Tstress = mom2n + Ttangent*(Tstrain-rot2n);
                                }
                        }
                }

}

int
BraceMaterial::commitState(void)
{
        CrotMax = TrotMax;
        CrotMin = TrotMin;
        CrotPu = TrotPu;
        CrotNu = TrotNu;
        CenergyD = TenergyD;
        CloadIndicator = TloadIndicator;
        Cidtime = Tidtime;
        Cidtime1 = Tidtime1;
        CmomNu = TmomNu;
        CmomPu = TmomPu;

        Cstress = Tstress;
        Cstrain = Tstrain;
        return 0;
}

int
BraceMaterial::revertToLastCommit(void)
{
        TrotMax = CrotMax;
        TrotMin = CrotMin;
        TrotPu = CrotPu;
        TrotNu = CrotNu;
        TenergyD = CenergyD;
        TloadIndicator = CloadIndicator;
        Tidtime = Cidtime;
        Tidtime1 = Cidtime1;
        TmomNu = CmomNu;
        TmomPu = CmomPu;

        Tstress = Cstress;
        Tstrain = Cstrain;
```

```
	return 0;
}

int
BraceMaterial::revertToStart(void)
{
	CrotMax = 0.0;
	CrotMin = 0.0;
	CrotPu = 0.0;
	CrotNu = 0.0;
	CenergyD = 0.0;
	CloadIndicator = 0;
	Cidtime = 0;
	Cidtime1 = 0;
	CmomNu = 0.0;
	CmomPu = 0.0;

	Cstress = 0.0;
	Cstrain = 0.0;

	Tstrain = 0;
	Tstress = 0;
	Ttangent = E1p;

	return 0;
}

UniaxialMaterial*
BraceMaterial::getCopy(void)
{
	BraceMaterial *theCopy = new BraceMaterial (this->getTag(),
		mom1p, rot1p, mom2p, rot2p, mom3p, rot3p,
		mom1n, rot1n, mom2n, rot2n, mom3n, rot3n,
		pinchX, pinchY, damfc1, damfc2, beta);

	theCopy->CrotMax = CrotMax;
	theCopy->CrotMin = CrotMin;
	theCopy->CrotPu = CrotPu;
	theCopy->CrotNu = CrotNu;
	theCopy->CenergyD = CenergyD;
	theCopy->CloadIndicator = CloadIndicator;
	theCopy->Cstress = Cstress;
	theCopy->Cstrain = Cstrain;
	theCopy->Ttangent = Ttangent;
	theCopy->Cidtime = Cidtime;
	theCopy->Cidtime1 = Cidtime1;
	theCopy->CmomNu = CmomNu;
	theCopy->CmomPu = CmomPu;

	return theCopy;
}

int
BraceMaterial::sendSelf(int commitTag, Channel &theChannel)
{
```

```
  int res = 0;

  static Vector data(31);

  data(0) = this->getTag();
  data(1) = mom1p;
  data(2) = rot1p;
  data(3) = mom2p;
  data(4) = rot2p;
  data(5) = mom3p;
  data(6) = rot3p;
  data(7) = mom1n;
  data(8) = rot1n;
  data(9) = mom2n;
  data(10) = rot2n;
  data(11) = mom3n;
  data(12) = rot3n;
  data(13) = pinchX;
  data(14) = pinchY;
  data(15) = damfc1;
  data(16) = damfc2;
  data(17) = beta;
  data(18) = CrotMax;
  data(19) = CrotMin;
  data(20) = CrotPu;
  data(21) = CrotNu;
  data(22) = CenergyD;
  data(23) = CloadIndicator;
  data(24) = Cstress;
  data(25) = Cstrain;
  data(26) = Ttangent;
  data(27) = Cidtime;
  data(28) = Cidtime1;
  data(29) = CmomNu;
  data(30) = CmomPu;

  res = theChannel.sendVector(this->getDbTag(), commitTag, data);
  if (res < 0)
    cerr << "BraceMaterial::sendSelf() - failed to send data\n";


  return res;
}

int
BraceMaterial::recvSelf(int commitTag, Channel &theChannel,
                                FEM_ObjectBroker &theBroker)
{
  int res = 0;

  static Vector data(31);
  res = theChannel.recvVector(this->getDbTag(), commitTag, data);

  if (res < 0) {
     cerr << "BraceMaterial::recvSelf() - failed to receive data\n";
     return res;
```

```
 }
 else {
  this->setTag((int)data(0));
  mom1p = data(1);
  rot1p = data(2);
  mom2p = data(3);
  rot2p = data(4);
  mom3p = data(5);
  rot3p = data(6);
  mom1n = data(7);
  rot1n = data(8);
  mom2n = data(9);
  rot2n = data(10);
  mom3n = data(11);
  rot3n = data(12);
  pinchX = data(13);
  pinchY = data(14);
  damfc1 = data(15);
  damfc2 = data(16);
  beta = data(17);
  CrotMax = data(18);
  CrotMin = data(19);
  CrotPu = data(20);
  CrotNu = data(21);
  CenergyD = data(22);
  CloadIndicator = int(data(23));
  Cstress = data(24);
  Cstrain = data(25);
  Ttangent = data(26);
        Cidtime = int(data(27));
        Cidtime1 = int(data(28));
        CmomNu = data(29);
        CmomPu = data(30);

  // set the trial values
  TrotMax = CrotMax;
  TrotMin = CrotMin;
  TrotPu = CrotPu;
  TrotNu = CrotNu;
  TenergyD = CenergyD;
  TloadIndicator = CloadIndicator;
  Tstress = Cstress;
  Tstrain = Cstrain;
        Tidtime = Cidtime;
        Tidtime1 = Cidtime1;
        TmomNu = CmomNu;
        TmomPu = CmomPu;

 }

 return 0;
}

void
BraceMaterial::Print(ostream &s, int flag)
{
```

```
	s << "Brace Material, tag: " << this->getTag() << endl;
	s << "mom1p: " << mom1p << endl;
	s << "rot1p: " << rot1p << endl;
	s << "E1p: " << E1p << endl;
	s << "mom2p: " << mom2p << endl;
	s << "rot2p: " << rot2p << endl;
	s << "E2p: " << E2p << endl;
	s << "mom3p: " << mom3p << endl;
	s << "rot3p: " << rot3p << endl;
	s << "E3p: " << E3p << endl;

	s << "mom1n: " << mom1n << endl;
	s << "rot1n: " << rot1n << endl;
	s << "E1n: " << E1n << endl;
	s << "mom2n: " << mom2n << endl;
	s << "rot2n: " << rot2n << endl;
	s << "E2n: " << E2n << endl;
	s << "mom3n: " << mom3n << endl;
	s << "rot3n: " << rot3n << endl;
	s << "E3n: " << E3n << endl;

	s << "pinchX: " << pinchX << endl;
	s << "pinchY: " << pinchY << endl;
	s << "damfc1: " << damfc1 << endl;
	s << "damfc2: " << damfc2 << endl;
	s << "energyA: " << energyA << endl;
	s << "beta: " << beta << endl;
}

void
BraceMaterial::setEnvelope(void)
{
	E1p = mom1p/rot1p;
	E2p = (mom2p-mom1p)/(rot2p-rot1p);
	E3p = (mom3p-mom2p)/(rot3p-rot2p);

	E1n = mom1n/rot1n;
	E2n = (mom2n-mom1n)/(rot2n-rot1n);
	E3n = (mom3n-mom2n)/(rot3n-rot2n);
}

double
BraceMaterial::posEnvlpStress(double strain)
{
	if (strain <= 0.0)
		return 0.0;
	else if (strain <= rot1p)
		return E1p*strain;
	else if (strain <= rot2p)
		return mom1p + E2p*(strain-rot1p);
	else if (strain <= rot3p || E3p > 0.0)
		return mom2p + E3p*(strain-rot2p);
	else
		return mom3p;
}
```

```
double
BraceMaterial::negEnvlpStress(double strain)
{
        if (strain >= rot1n)
                return E1n*strain;
        else if (strain >= rot2n)
                return mom1n + E2n*(strain-rot1n);
        else
                return mom2n + E3n*(strain-rot2n);
}

double
BraceMaterial::posEnvlpTangent(double strain)
{
        if (strain < 0.0)
                return E1p*1.0e-9;
        else if (strain <= rot1p)
                return E1p;
        else if (strain <= rot2p)
                return E2p;
        else if (strain <= rot3p || E3p > 0.0)
                return E3p;
        else
                return E1p*1.0e-9;
}

double
BraceMaterial::negEnvlpTangent(double strain)
{
        if (strain >= rot1n)
                return E1n;
        else if (strain >= rot2n)
                return E2n;
        else
                return E3n;
}

double
BraceMaterial::posEnvlpRotlim(double strain)
{
 double strainLimit = POS_INF_STRAIN;

 if (strain <= rot1p)
   return POS_INF_STRAIN;
 if (strain > rot1p && strain <= rot2p && E2p < 0.0)
   strainLimit = rot1p - mom1p/E2p;
 if (strain > rot2p && E3p < 0.0)
   strainLimit = rot2p - mom2p/E3p;

 if (strainLimit == POS_INF_STRAIN)
   return POS_INF_STRAIN;
 else if (posEnvlpStress(strainLimit) > 0)
   return POS_INF_STRAIN;
 else
   return strainLimit;
}
```

```
double
BraceMaterial::negEnvlpRotlim(double strain)
{
 double strainLimit = NEG_INF_STRAIN;

 if (strain >= rot1n)
  return NEG_INF_STRAIN;
 if (strain < rot1n && strain >= rot2n && E2n < 0.0)
  strainLimit = rot1n - mom1n/E2n;
 if (strain < rot2n && E3n < 0.0)
  strainLimit = rot2n - mom2n/E3n;

 if (strainLimit == NEG_INF_STRAIN)
  return NEG_INF_STRAIN;
 else if (negEnvlpStress(strainLimit) < 0)
  return NEG_INF_STRAIN;
 else
  return strainLimit;
}
```

APPENDIX D

COLLABORATIVE NATURE OF THE WORK

This work was part of a project designed to showcase the capabilities of the Network for Earthquake Engineering Simulation (NEES, Figure D.1), an initiative of the National Science Foundation to fundamentally change the way engineering research is conducted. The NEES Collaboratory is a collection of 15 facilities around the United States that provide unique testing capabilities both as individual laboratories but more importantly in coordinated fashion linking both experimental and analytical platforms. The laboratories are linked through NEESGrid, an Internet-based platform that intends to provide seamless interaction between data acquisition and load control systems running experiments and analytical platforms that couple the experiments to simulations through substructuring techniques. A simple example of this type of application is a recent project for testing a large RC bridge (Figure D.2). For this test, two of the three piers on the bridge were tested experimentally, one at the University of Illinois and one at Lehigh University, with the third pier and the deck being modeled in OpenSEES and Zeus-NL simulations being run from another site at the University of Illinois. The model also benefited from input on soil-structure interaction from centrifuge testes previously carried out at RPI.

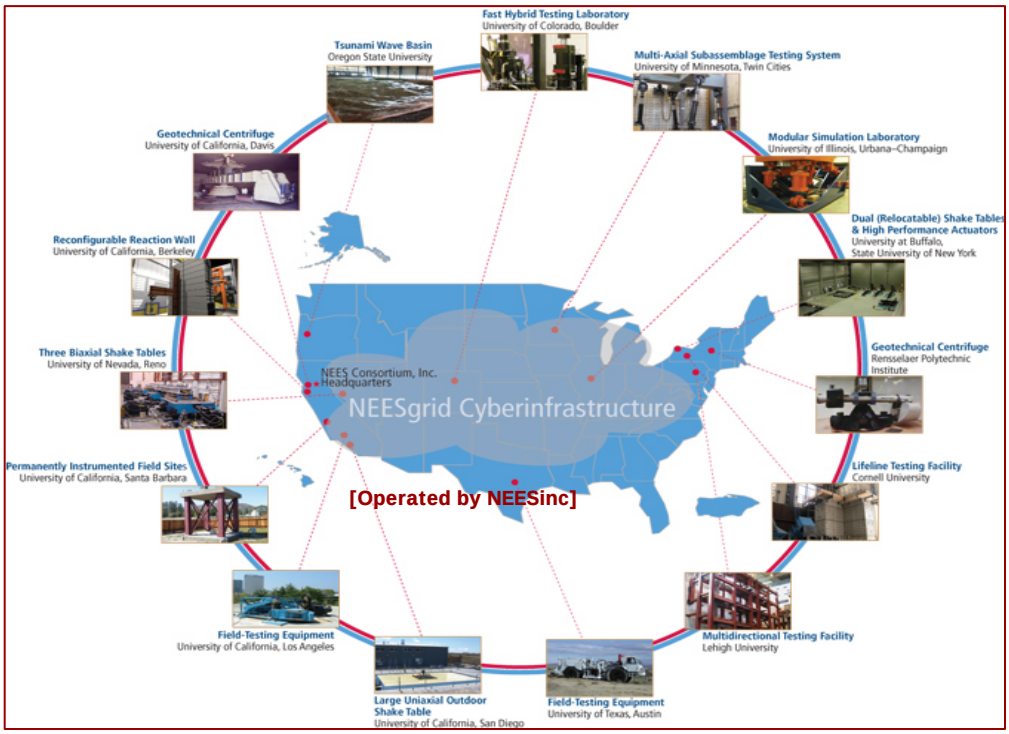

Figure D.1 NEES Experimental Infrastructure.

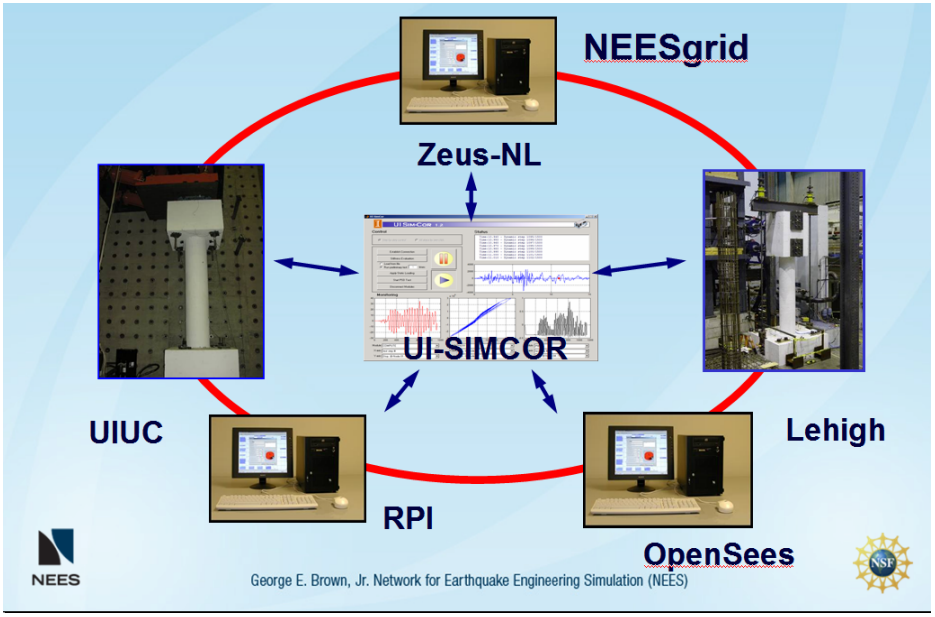

Figure D.2 Multi-Site Simulation System.

The test described in the paragraph above represents some level of maturity for the NEES Collaboratory. The research described herein was funded four years ago as part of an initial attempt at showcasing the potential of the system. The premise of the project was to choose a challenging, innovative structural system to assess the possibilities of doing real-time and quasi-real time cooperative work among several research facilities. As shown in Figure D.3, the original intent was to run a test in the shake table at the University at Buffalo (UB) and take its output in real time to drive a quasi-static test at Georgia Tech and hybrid simulations between the University of Colorado (CU) and the University of California at Berkeley (UCB). Because the implementation of a number of information technologies (IT) infrastructure features of NEES was severely delayed, this ambitious program could not be achieved. The initial tests were run on the shake table at Buffalo, and the actual table motions from this test extracted and used as the input to OpenSEES analyses of the model structure. Those analyses then output the displacements at the floor levels that were used for the quasi-static tests at Georgia Tech. Similar procedures were followed for the individual brace tests and the hybrid simulations run between CU and UCB. Because of the slight differences in modeling between the different sites, not all the results are directly comparable. In general, good coordination between the sites was observed, particularly in the time from the planning of the initial tests at Buffalo to the end of the testing at Georgia Tech (October 2004 to March 2005). Through the use of email, WEBEX, and other similar tools, extensive interaction took place between the sites. Much of that interaction is not explicitly described in this thesis except as it directly impacted the work described herein. The results of the joint aspects of the research are presented in a recently submitted article (Yang et al. 2006); the dissertation for the four students involved in this collaboration project are completely separate and independent contributions with little or no duplication between them.

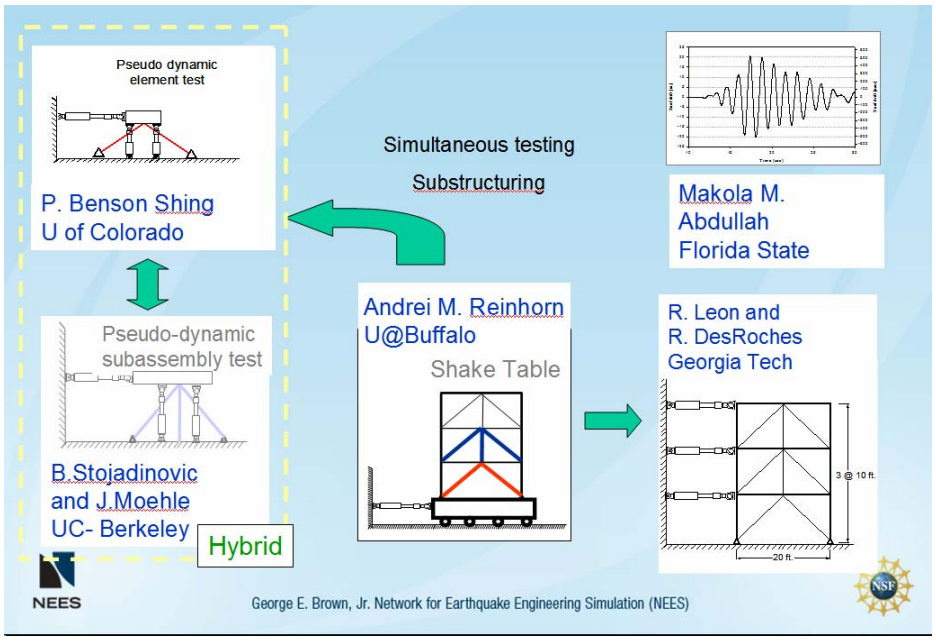

Figure D.3 Zipper Project Research Approach.

REFERENCES

AISC, 2003. Seismic Provisions for Structural Steel Buildings.

AISC, 2005. Seismic Provisions for Structural Steel Buildings.

AISC, 2002. Steel Construction Manual.

AISC, 2006. Steel Construction Manual.

ASCE, 2005. Minimum Design Loads for Buildings and Other Structures.

Aslani, F., and Goel, S. C. 1991, "Stitch Spacing and Local Buckling in Seismic Resistant Double Angle Bracing Members," Journal of Structural Engineering, Vol. 177, No. 8, (August), ASCE, Reston, VA.

Bruneau, M., Uang, C.-M., and Whittaker, A. 1998. Ductile Design of Steel Structures. McGraw-Hill.

Chopra, Anil K., & Goel, Rakesh K. 1998. "A modal pushover analysis procedure for estimating seismic demands for buildings," Earthquake Engng. Struct. Dyn. 2002; 31: 561-582.

Fell, B. V., Myers, A. T., Deierlien, G., Kanvinde, A., "Testing and simulation of ultra-low cycle fatigue and fracture in steel structures," 8th National Conference on Earthquake Engineering, San Francisco, April 2006.

FEMA 355C, 2000, State of the Art Report on Systems Performance of Steel Moment Frames Subject to Earthquake Ground Shaking, prepared by the SAC Joint Venture for the Federal Emergency Management Agency, Washington, DC.

Goel, S. C., 1992c, "Earthquake Resistant Design of Ductile Braced Steel Structures," Stability and Ductility of Steel Structures under Cyclic Loading, pp. 297-308, CRC Press, Boca Raton, FL.

Goel, S. C. and Lee, S., 1992, "A Fracture Criterion for Concrete-Filled Tubular Bracing Members Under Cyclic Loading," Proceedings of the 1992 ASCE Structures Congress, pp. 922-925, ASCE, Reston, VA.

Hassan, O. and Goel, S. C., 1991, Report UMCE91-1 Seismic Behavior and Design of Concentrically Braced Steel Structures, The University of Michigan Department of Civil and Environmental Engineering, Ann Arbor, MI.

Kanvinde, A., Deierlien, G., 2005, "Large scale tests and micromechanics-based simulation of ultra-low cycle fatigue and fracture in steel structures, http://cee.engr.ucdavis.edu/faculty/kanvinde/NEESPage/default.htm

Khatib, I.F., Mahin, S.A., and Pister, K.S. 1988. Seismic Behavior of Concentrically Braced Steel Frames. Report No. UCB/EERC-88/01. Berkeley: Earthquake Engineering Research Center. University of California.

Lee, S. and Goel, S. C. 1987, Report No. UMCE 87-11 Seismic Behavior of Hollow and Concrete-Filled Square Tubular Bracing Members, University of Michigan Department of Civil Engineering, Ann Arbor, MI.

PEER, "Open System for Earthquake Engineering Simulation," http://opensees.berkeley.edu/OpenSees/OpenSees.html

Somerville, P.G., Smith, N., Punyamurthula, S., & Sun, J. 1997. Development of Ground Motion Time Histories for Phase 2 of the FEMA/SAC Steel Project. SAC Background Document, Report No. SAC/BD 97/04.

Tang, X. and Goel, S. C., 1989, "Brace Fractures and Analysis of Phase I Structure," Journal of Structural Engineering, Vol. 115, No. 8, (August), pp. 1960-1976, ASCE, Reston, VA.

Tang, X., and Goel, S. C. 1987. Seismic Analysis and Design Considerations of Braced Steel Structures. Report No. UMCE 87-4. June. Ann Arbor: Department of Civil Engineering. The University of Michigan.

Tremblay, R. & Tirca, L. 2003. Behavior and Design of Multi-Story Zipper Concentrically Braced Steel Frames for the Mitigation of Soft-Story Response.

Uriz, Patxi & Mahin, Stephen 2004. Summary of test results for UC Berkeley special concentric braced frame specimen No. 1(SCBF-1). http://www.ce.berkeley.edu/~patxi/SCBF/publications/PrelimSCBFtestResults.pdf